Introduction to Wave Turbulence Formalisms for Incoherent Optical Waves

Antonio Picozzi, Josselin Garnier, Gang Xu, and Sergio Rica

Abstract We provide an introduction to different wave turbulence formalisms describing the propagation of partially incoherent optical waves in nonlinear media. We consider the nonlinear Schrödinger equation as a representative model accounting for a nonlocal or a noninstantaneous nonlinearity, as well as higher-order dispersion effects. We discuss the wave turbulence kinetic equation describing, e.g., wave condensation or wave thermalization through supercontinuum generation; the Vlasov formalism describing incoherent modulational instabilities and the formation of large scale incoherent localized structures in analogy with long-range gravitational systems; and the weak Langmuir turbulence formalism describing spectral incoherent solitons, as well as spectral shock or collapse singularities. Finally, recent developments and some open questions are discussed, in particular in relation with a wave turbulence formulation of laser systems and different mechanisms of breakdown of thermalization.

A. Picozzi (✉)
Laboratoire Interdisciplinaire Carnot de Bourgogne, Université de Bourgogne Franche-Comté, 9 Av. A. Savary, 21078 Dijon, France
e-mail: Antonio.Picozzi@u-bourgogne.fr

J. Garnier
Laboratoire de Probabilités et Modèles Aléatoires, University Paris Diderot, 75205 Paris Cedex 13, France
e-mail: garnier@math.univ-paris-diderot.fr

G. Xu
PhLAM/IRCICA, CNRS-Université Lille 1, UMR 8523/USR 3380, F-59655 Villeneuve d'Ascq, France
e-mail: gang.xu@ircica.univ-lille1.fr

S. Rica
Facultad de Ingeniería y Ciencias, Universidad Adolfo Ibáñez, Avda. Diagonal las Torres 2640, Peñalolén, Santiago, Chile
e-mail: sergio.rica@uai.cl

M. Onorato et al. (eds.), *Rogue and Shock Waves in Nonlinear Dispersive Media*,
Lecture Notes in Physics 926, DOI 10.1007/978-3-319-39214-1_8

1 Introduction

1.1 From Incoherent Solitons to Wave Turbulence

The coherence properties of partially incoherent optical waves propagating in nonlinear media have been studied since the advent of nonlinear optics in the 1960s, because of the natural poor degree of coherence of laser sources available at that time. However, it is only recently that the dynamics of incoherent nonlinear optical waves received a renewed interest. The main motive for this renewal of interest is essentially due to the first experimental demonstration of incoherent solitons in photorefractive crystals [1, 2]. The formation of an incoherent soliton results from the *spatial self-trapping* of incoherent light that propagates in a highly noninstantaneous response nonlinear medium [3, 4]. This effect is possible because of the noninstantaneous photorefractive nonlinearity that averages the field fluctuations provided that its response time, τ_R, is much longer than the correlation time t_c that characterizes the incoherent beam fluctuations, i.e., $t_c \ll \tau_R$. The remarkable simplicity of experiments realized in photorefractive crystals has led to a fruitful investigation of the dynamics of incoherent nonlinear waves. Several theoretical approaches have been developed to describe such experiments [5–8], which have been subsequently shown to be formally equivalent one to each other [9, 10].

The field of incoherent optical solitons has become a blooming area of research, as illustrated by several important achievements, e.g., the existence of incoherent dark solitons [11, 12], the modulational instability of incoherent waves [13–15], incoherent solitons in resonant interactions [16, 17], in liquid crystals [18], in nonlocal nonlinear media [19, 20], in spin waves [21], or spectral incoherent solitons in optical fibers [22, 23]. Nowadays, statistical nonlinear optics constitutes a growing field of research covering various topics of modern optics, e.g., supercontinuum generation [24], filamentation [25], random lasers [26], or extreme rogue wave events emerging from optical turbulence [27–29].

From a broader perspective, statistical nonlinear optics is fundamentally related to fully developed turbulence [30, 31], a subject which still constitutes one of the most challenging problems of theoretical physics [32, 33]. In its broad sense, the kinetic wave theory provides a nonequilibrium thermodynamic description of developed turbulence. We schematically report in Fig. 1a qualitative and intuitive physical insight into the analogy which underlies the kinetic wave approach and the kinetic theory relevant for a gas system. The wave turbulence theory occupies a rather special place on the road-map of modern science, at the interface between applied mathematics, fluid dynamics, statistical physics and engineering. It has potential applications and implications in a diverse range of subjects including oceanography, plasma physics and condensed matter physics. This chapter is aimed at introducing the wave turbulence theory as an appropriate theoretical framework to describe the propagation of incoherent optical waves.

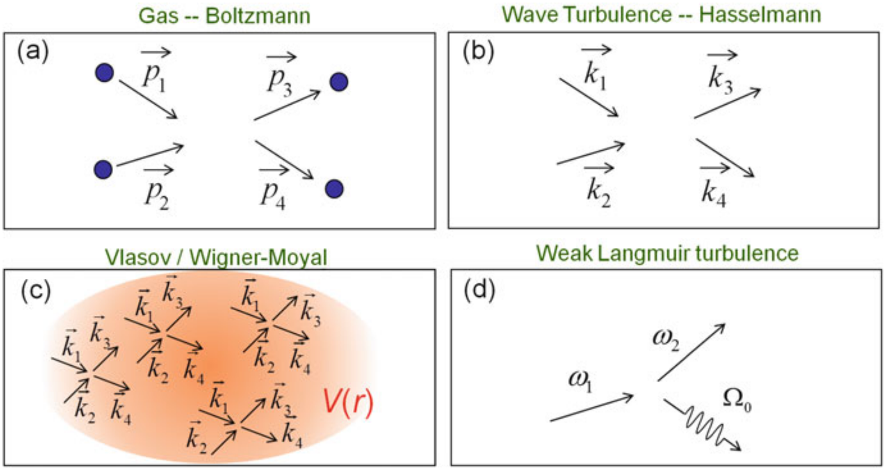

Fig. 1 Analogy between a system of classical particles and the propagation of an incoherent optical wave in a cubic nonlinear medium. (**a**) As described by the kinetic gas theory (Boltzmann kinetic equation), collisions between particles are responsible for an irreversible evolution of the gas towards thermodynamic equilibrium. (**b**) In complete analogy, the (Hasselmann) WT kinetic equation and the underlying four-wave mixing describe an irreversible evolution of the incoherent optical wave toward the thermodynamic Rayleigh-Jeans equilibrium state. (**c**) When the incoherent optical wave exhibits an inhomogeneous statistics, the four-wave interaction no longer takes place locally, i.e., the quasi-particles feel the presence of an effective self-consistent potential, $V(r)$, which prevents them from relaxing to thermal equilibrium. The dynamics of the incoherent optical wave turns out to be described by a Vlasov-like kinetic equation. (**d**) In the presence of a noninstantaneous nonlinear interaction, the causality condition inherent to the response function changes the physical picture: the nonlinear interaction involves a material excitation (e.g., molecular vibration in the example of Raman scattering). The dynamics of the incoherent optical wave turns out to be described by a kinetic equation analogous to the weak Langmuir turbulence equation. Note however that a highly noninstantaneous nonlinear response is no longer described by the weak Langmuir turbulence equation, but instead by the 'long-range' Vlasov-like equation (see Fig. 3)

In the following we provide a panoramic overview of the subjects covered by this chapter. Note that these topics have been usually discussed separately in the literature within different contexts.

1.1.1 Wave Turbulence Formulation: Thermalization and Condensation

Consider the nonlinear propagation of a partially coherent optical wave characterized by fluctuations that are statistically homogeneous in space (note that caution should be exercised when separating the description of statistically homogeneous and inhomogeneous random waves, since a homogeneous statistical wave can become inhomogeneous as a result of the incoherent MI (see Sect. 4), or the instability of the Zakharov-Kolmogorov spectrum [34]). In complete analogy with a system of classical particles, the incoherent optical field evolves, owing to nonlinearity, towards a thermodynamic equilibrium state, as schematically illustrated in Fig. 1a,b. A detailed theoretical description of the process of dynamical thermalization constitutes a difficult problem. However, a considerable simplification occurs when wave propagation is essentially dominated by linear dispersive effects, so that a weakly nonlinear description of the field becomes possible [30, 32, 33]. The weak- (or wave-)turbulence (WT) theory has been the subject of lot of investigations in the context of plasma physics [35], in which it is often referred to the so-called "random phase-approximation" approach [30, 35–39]. This approach may be considered as a convenient way of interpreting the results of the more rigorous technique based on a multi-scale expansion of the cumulants of the nonlinear field, as originally formulated in [40–42]. This theory has been reviewed in [43], and studied in more details through the analysis of the probability distribution function of the random field in [33]. In a loose sense, the so-called 'random phase approximation' may be considered as justified when phase information becomes irrelevant to the wave interaction due to the strong tendency of the waves to decohere. The random phases can thus be averaged out to obtain a weak turbulence description of the incoherent wave interaction, which is formally based on irreversible kinetic equations [30]. It results that, in spite of the formal reversibility of the equation governing wave propagation, the kinetic equation describes an irreversible evolution of the field to thermodynamic equilibrium. This equilibrium state refers to the fundamental Rayleigh-Jeans spectrum, whose tails are characterized by an equipartition of energy among the Fourier modes. The mathematical statement of such irreversible process relies on the H-theorem of entropy growth, whose origin is analogous to the Boltzmann's H-theorem relevant for gas kinetics. Note that the terminology 'wave turbulence' is often employed in the literature to denote the study of wave systems governed by this type of irreversible kinetic equations, whose structure is analogous to the Boltzmann kinetic formulation (see, e.g., [30, 33, 39]). However, in many cases in this review the terminology 'wave turbulence' will be employed in a broader sense, which also includes different forms of nonequilibrium kinetic formalisms, such as the Vlasov or the weak Langmuir turbulence descriptions of a wave system (see Fig. 1). We remark that besides this *nonequilibrium* kinetic approach, the equilibrium properties of a random nonlinear wave may be studied on the basis of *equilibrium* statistical mechanics by computing appropriate partition functions [44–49].

In this chapter we will discuss different processes of optical wave thermalization on the basis of the WT theory, as well as some mechanisms responsible for its inhibition. In particular, the phenomenon of supercontinuum generation can be interpreted, under certain conditions, as a consequence of the natural thermalization of the optical field toward the thermodynamic equilibrium state [50–52]. Furthermore, wave thermalization can be characterized by a self-organization process, in the sense that it is thermodynamically advantageous for the system to generate a large-scale coherent structure in order to reach the most disordered equilibrium state. A remarkable example of this counterintuitive phenomenon is provided by wave condensation [53–57], whose thermodynamic equilibrium properties are analogous to those of quantum Bose-Einstein condensation. Classical wave condensation can be interpreted as a redistribution of energy among different modes, in which the (kinetic) energy is transferred to small scales fluctuations, while an inverse process increases the power (i.e., number of 'particles') into the lowest allowed mode, thus leading to the emergence of a large scale coherent structure.

We note in this respect that the phenomenon of condensation has been recently extended to optical cavities in different circumstances [58–65], which raises important questions, such as e.g., the relation between laser operation and the phenomenon of Bose-Einstein condensation (see Sect. 5 below) [66]. From a different perspective, when a wave system is driven away from equilibrium by an external source, it no longer relaxes towards the Rayleigh-Jeans equilibrium distribution. A typical physical example of forced system can be the excitation of hydrodynamic surface waves by the wind. This corresponds to the generic problem of developed turbulence. In general, it refers to a system in which the frequency-scales of forcing and damping differ significantly. The nonlinear interaction leads to an energy redistribution among the frequencies (modes). A fundamental problem is to find the stationary spectrum of the system, i.e., the law of energy distribution over the different scales. The WT theory provides an answer to this vast issue under the assumption that the nonlinear interaction is weak—the so-called Kolmogorov-Zakharov spectra of turbulence [30]. An experiment aimed at observing these nonequilibrium stationary turbulent states in the context of optics has been reported in [67] (see [68] for a complete review). Beyond optics, we refer the interested reader to different comprehensive reviews concerning this vast area of research [30, 32, 33, 39, 43].

1.1.2 Vlasov and Wigner-Moyal Formulations: Incoherent Solitons

When the nonlinear material is characterized by a nonlocal or a highly-noninstantaneous response, the dynamics of the incoherent wave turns out to be essentially governed by an effective nonlinear potential $V(r)$. This potential is *self-consistent* in the sense that it depends itself on the averaged intensity distribution of the random field, as schematically illustrated in Fig. 1c. Actually, the mechanism underlying the formation of an incoherent soliton state finds its origin in the existence of such self-consistent potential, which is responsible for a spatial self-trapping of the incoherent optical beam. From this point of view, the very nature of incoherent optical solitons is analogous to the random phase solitons predicted in plasma physics a long time ago in the framework of the Vlasov equation [69–71]. This analogy with nonlinear plasma waves has been also exploited in optics in different circumstances [72–74], in particular in the framework of the Wigner-Moyal formalism [8, 75], or to interpret the existence of a threshold in the incoherent modulational instability as a consequence of the phenomenon of Landau damping [8].

Incoherent spatial solitons can be also supported by a nonlocal spatial nonlinearity, instead of the traditional noninstantaneous nonlinearity inherent to the photorefractive experiments. A nonlocal wave interaction means that the response of the nonlinearity at a particular point is not determined solely by the wave intensity at that point, but also depends on the wave intensity in the neighborhood of this point. Nonlocality thus constitutes a generic property of a large number of nonlinear wave systems [76–83], and the dynamics of nonlocal nonlinear waves has been widely investigated in this last decade [84–88]. In particular, in the highly nonlocal limit, i.e., in the limit where the range of the nonlocal response is much larger than the size of the beam, the propagation equation reduces to a linear and local equation with an effective guiding potential given by the nonlocal response function. The optical beam can thus be guided by the nonlocal response of the material, a process originally termed 'accessible soliton' [78, 79, 88, 89]. In this highly nonlocal limit, it has been shown both theoretically and experimentally that a speckled beam can be guided and trapped by the effective waveguide induced by the nonlocal response [19, 90].

More recently, the long-term evolution of a modulationally unstable homogeneous wave has been studied in the presence of a nonlocal response [20]. Contrarily to the expected soliton turbulence process where a coherent soliton is eventually generated in the midst of thermalized small-scale fluctuations [46, 91–93], a highly nonlocal response is responsible for an *incoherent soliton turbulence* process [20]. It is characterized by the spontaneous formation of an incoherent soliton structure starting from an initially homogeneous plane-wave. A WT approach of the problem revealed that this type of incoherent solitons can be described in detail in the framework of a long-range Vlasov equation, which is shown to provide an accurate statistical description of the nonlocal random wave even in the *highly nonlinear regime* of interaction. We note that this Vlasov equation differs from the traditional Vlasov equation considered for the study of incoherent modulational instability and incoherent solitons in plasmas [70, 71, 94], hydrodynamics [95] and optics [8, 73, 74, 96]. The structure of this Vlasov equation is in fact analogous to that recently used to describe systems of particles with long-range interactions [97]. For this reason we will term this equation 'long-range Vlasov' equation. It is important to underline that the long-range nature of a highly nonlocal nonlinear response prevents the wave system from reaching thermal equilibrium [20]. This fact can be interpreted intuitively in analogy with gravitational long-range systems and the Vlasov-like description of the dynamics of formation and interaction of galaxies in the Universe [97].

1.1.3 Weak Langmuir Turbulence Formulation: Spectral Incoherent Solitons and Incoherent Shocks

When the incoherent wave propagates in a nonlinear medium whose non-instantaneous response time cannot be neglected (e.g., Raman effect in optical fibers), the dynamics turns out to be strongly affected by the causality property inherent to the nonlinear response function (see Fig. 1). The kinetic wave theory reveals in this case that the appropriate description is provided by a formalism analogous to that used to describe weak Langmuir turbulence in plasmas [22, 98]. A major prediction of the theory is the existence of spectral incoherent solitons [22, 23, 99]. This incoherent soliton is of a fundamental different nature than the incoherent solitons discussed here above. In particular, it does not exhibit a confinement in the spatiotemporal domain, but exclusively in the frequency domain. For this reason this incoherent structure has been termed 'spectral incoherent soliton'. Indeed, because the optical field exhibits a stationary statistics, the soliton behavior only manifests in the spectral domain. Then contrarily to the expected thermalization process, the incoherent wave self-organizes into these incoherent soliton structures, which can thus be regarded as nonequilibrium and nonstationary stable states of the incoherent field.

As discussed here above, the existence of a highly nonlocal response changes the dynamics of spatially incoherent nonlinear waves in a profound way. A natural question is to see how a highly noninstantaneous nonlinear response can change the dynamics of temporally incoherent waves. In this temporal long-range regime, the spectral dynamics of the field can exhibit incoherent shock waves [100]. They manifest themselves as an unstable singular behavior of the spectrum of incoherent waves, i.e., 'spectral wave-breaking'. Note that shock waves play an important role in many different branches of physics [101]. However, it should be underlined that, at variance with conventional coherent shock waves, which require the strong nonlinear regime, incoherent shocks develop into the highly incoherent regime of propagation, in which linear dispersive effects dominate nonlinear effects. The weakly nonlinear kinetic approach then reveals that these incoherent shocks are described, as a rule, by singular integro-differential kinetic equations, which involve the Hilbert transform as singular operator. In this way, the theory reveals unexpected links with the 3D vorticity equation in incompressible fluids [102], or the integrable Benjamin-Ono equation [103, 104], which was originally derived in hydrodynamics to model internal waves in stratified fluids [105, 106].

1.1.4 Breakdown of Thermalization and the FPU Problem

The relationship between formal reversibility and actual dynamics can be rather complex for infinite dimensional Hamiltonian systems like classical optical waves. In integrable systems, one may expect that the dynamics is essentially periodic in time, reflecting the underlying regular phase-space structure of nested tori. This recurrent behavior is broken in nonintegrable systems, where the dynamics is in general governed by an irreversible process of diffusion in phase space. The essential properties of this irreversible evolution to equilibrium can be described by the wave turbulence theory.

It is instructive to discuss the phenomenology of nonlinear wave thermalization from a broader perspective. We recall in this respect the fundamental assumption of statistical mechanics that a closed system with many degrees of freedom ergodically samples all equal energy points in phase space. In order to analyze the limits of this assumption, Fermi, Pasta and Ulam (FPU) considered in the 1950s a one-dimensional chains of particles with anharmonic forces between them [107]. They argued that, owing to the nonlinear coupling, an initial state in which the energy is in the first few lowest modes would eventually relax to a state of thermal equilibrium where the energy is equidistributed among all modes on the average. However they observed that, instead of leading to the thermalization of the system, the energy transfer process involves only a few modes and exhibits a reversible behavior, in the sense that after a sufficiently (long) time the system nearly goes back to its initial state. This recurrent behavior could not be interpreted in terms of Poincaré recurrences, a feature which motivated an intense research activity. Fundamental mathematical and physical discoveries, like the Kolmogorov-Arnold-Moser theorem and the formulation of the soliton concept, have led to a better understanding of the Fermi-Pasta-Ulam problem, although it is by no means completely understood [107, 108].

We should note that, in spite of the large number of theoretical studies, experimental demonstrations of FPU recurrences have been reported in very few systems. In particular, the FPU recurrences associated to modulational instability of the NLS equation have been experimentally studied in deep water waves [109], and, more recently, in optical wave systems [110, 111]. In relation with the FPU problem, we will comment some mechanisms which inhibit the irreversible process of optical wave thermalization toward the Rayleigh-Jeans distribution, as described in detail by the WT kinetic equation. In particular, the WT theory reveals the existence of local invariants in frequency space, which lead to a novel family of equilibrium states of a different nature than the expected thermodynamic (Rayleigh-Jeans) equilibrium states [112, 113].

1.2 Organization of the Chapter

The chapter is structured in three different parts aimed at introducing the three different formalisms discussed above. We will start with the Vlasov formalism in Sect. 2, which describes in particular incoherent MI and incoherent solitons. Next we will consider the weak Langmuir turbulence formalism in Sect. 3, which describes spectral incoherent solitons, as well as spectral shocks and collapse singularities. In Sect. 4 we will consider the wave turbulence kinetic equation, which will be discussed in the framework of optical wave thermalization and condensation. Finally some generalizations concerning the wave turbulence formulation of laser systems and the breakdown of thermalization, as well as some open problems will be discussed in the last Sect. 5.

2 Vlasov Formalism

In this Section we study the transverse spatial evolution of a partially coherent wave that propagates in a nonlocal nonlinear medium. We consider the case where the random wave exhibits fluctuations that are statistically inhomogeneous in space. As illustrated schematically in Fig. 2, the dynamics of the incoherent wave is described by different forms of the Vlasov equation, whose self-consistent potential depends on the degree of nonlocality.

2.1 Nonlocal Nonlinear Response

2.1.1 NLS Model

A nonlocal nonlinear response of the medium is found in several wave systems such as, e.g., dipolar Bose-Einstein condensates [76], atomic vapors [77], nematic liquid crystals [78, 79, 114], photorefractive media [82], thermal susceptibilities [80, 81, 115], and plasmas physics [83]. For this reason the impact of nonlocality on the dynamics of nonlocal nonlinear waves has been widely investigated [88], in

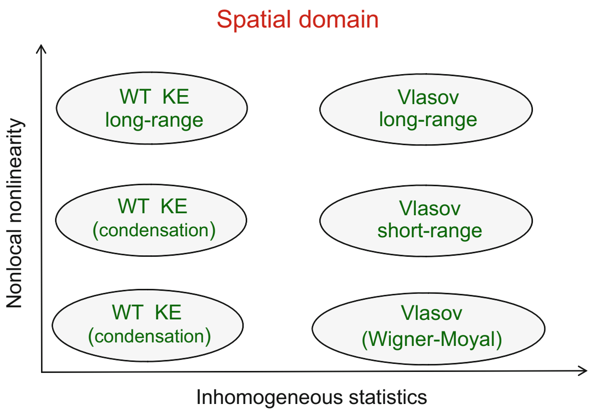

Fig. 2 Schematic illustration of the validity of the fundamental kinetic equations in the framework of a spatially nonlocal nonlinear response—the *vertical arrow* denotes the amount of nonlocality of the nonlinear interaction, while the *horizontal arrow* represents the amount of inhomogeneous statistics of the incoherent wave. When the incoherent wave is characterized by fluctuations that are statistically homogeneous in space, the relevant kinetic description is provided by the wave turbulence kinetic equation ('WT KE'), which describes in particular the processes of optical wave thermalization or condensation (see Sect. 4). When the incoherent wave exhibits an inhomogeneous statistics, the relevant kinetic description is provided by different variants of the Vlasov equation, whose self-consistent potential depends on the amount of nonlocality in the system (see Sect. 2). The Vlasov equation describes in particular the phenomena of incoherent modulational instability and the formation of incoherent soliton states

particular through the analysis of MI [84], of dark solitons [87], or the inhibition of collapse in multi-dimensional systems [85, 86].

We consider here the standard form of the nonlocal NLS model equation describing wave propagation in nonlinear media that exhibit a nonlocal response

$$i\partial_z\psi + \alpha\nabla^2\psi + \gamma\psi \int U(\boldsymbol{x}-\boldsymbol{x}')\, |\psi|^2(\boldsymbol{x}',z)\, d\boldsymbol{x}' = 0, \tag{1}$$

where $\boldsymbol{x}$ denotes the position in the transverse plane of dimension d and ∇^2 denotes the corresponding transverse Laplacian ($\nabla^2 = \partial_x^2$ for $d = 1$, $\nabla^2 = \partial_x^2 + \partial_y^2$ for $d = 2$). The nonlocal response function $U(\boldsymbol{x})$ is a real and even function normalized in such a way that $\int U(\boldsymbol{x})\, d\boldsymbol{x} = 1$, so that in the limit of a local response [$U(\boldsymbol{x}) = \delta(\boldsymbol{x})$, $\delta(\boldsymbol{x})$ being the Dirac function], Eq. (1) recovers the standard local NLS equation. The parameters $\alpha = 1/(2k_L)$ and γ refer to the linear and nonlinear coefficients, respectively, where $k_L = n2\pi/\lambda_L$, n being the linear refractive index of the material and λ_L the wavelength of the laser source. A positive (negative) value of γ corresponds to a focusing (defocusing) nonlinear interaction. Besides the momentum, Eq. (1) conserves the power (or number of particles) $\mathscr{N} = \int |\psi(\boldsymbol{x})|^2 d\boldsymbol{x}$, and the Hamiltonian $\mathscr{H} = \mathscr{E} + \mathscr{U}$, where

$$\mathscr{E}(z) = \alpha \int |\nabla\psi(\boldsymbol{x},z)|^2\, d\boldsymbol{x} \tag{2}$$

denotes the linear (kinetic) contribution, and

$$\mathscr{U}(z) = -\frac{\gamma}{2} \iint |\psi(\boldsymbol{x},z)|^2\, U(\boldsymbol{x}-\boldsymbol{x}')\, |\psi(\boldsymbol{x}',z)|^2\, d\boldsymbol{x}\, d\boldsymbol{x}' \tag{3}$$

the nonlinear contribution to the total energy $\mathscr{H}$. We denote by σ the spatial extension of $U(\boldsymbol{x})$, which characterizes the amount of nonlocality in the system. This length scale has to be compared with the healing length $\Lambda = \sqrt{\alpha/(|\gamma|\rho)}$, where $\rho = \mathscr{N}/L^d$ is the density of power (intensity), L being the size of the periodic box in the numerical simulations. We recall that Λ denotes the typical wavelength excited by the modulational instability of a homogeneous background in the limit of a local nonlinearity, $\sigma \to 0$. An other important length scale is the typical length Δ that characterizes the homogeneity of the statistics. It reflects the typical length scale over which the fluctuations of the incoherent wave can be considered as homogeneous in space.

2.1.2 Homogeneous vs Inhomogeneous Statistics

The kinetic equation consists of an equation describing the evolution of the spectrum of the field during its propagation in the nonlinear medium. Note that, in the particular case in which diffraction effects can be neglected ($\alpha = 0$), an expression for the evolution of the second order correlation function can be obtained in explicit form, see [116, 117].

As schematically described through Figs. 2, 3, the structure of a kinetic equation depends on the nature of the statistics of the random wave. The statistics is said to be homogeneous (or stationary in the temporal domain), if the correlation function $B(\boldsymbol{x_1}, \boldsymbol{x_2}, z) = \langle \psi(\boldsymbol{x_1}, z)\psi^*(\boldsymbol{x_2}, z)\rangle$ only depends on the distance $|\boldsymbol{x_1} - \boldsymbol{x_2}|$. In the following, the brackets $\langle . \rangle$ denote an average over the realizations of the initial noise of the random wave $\psi(\boldsymbol{x}, z = 0)$.

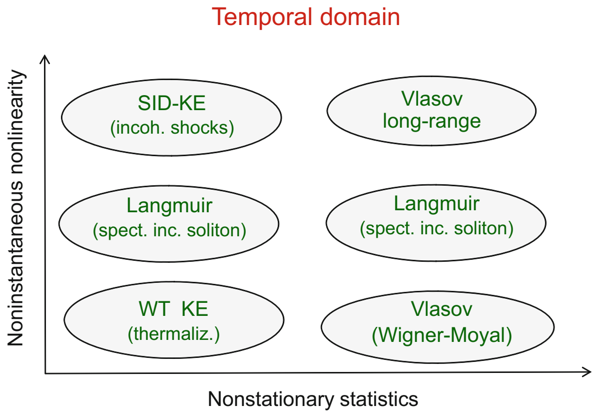

Fig. 3 Schematic illustration of the validity of the fundamental kinetic equations in the framework of a temporally noninstantaneous nonlinear response—the *vertical arrow* denotes the amount of noninstantaneous response of the nonlinearity, while the *horizontal arrow* represents the amount of non-stationary statistics of the incoherent wave. The diagram for the temporal domain reported here is similar to that reported in the spatial domain in Fig. 2. The essential difference between the spatial and the temporal domain relies on the fact that in the temporal domain the response function is constrained by the causality condition. It turns out that when the finite response time of the nonlinearity cannot be neglected, the relevant kinetic description is provided by an equation analogous to the weak Langmuir turbulence equation (see Sect. 3), which describes for instance non-localized spectral incoherent solitons. In the presence of a highly noninstantaneous nonlinear response and a stationary statistics of the incoherent wave, the weak Langmuir turbulence reduces to singular integro-differential kinetic equations ('SID-KE'), e.g., Benjamin-Ono equation, which describe spectral singularities such as dispersive shock waves and collapse behaviors. Conversely, when the wave exhibits a non-stationary statistics still in the presence of a highly noninstantaneous response, the dynamics is ruled by a 'temporal long-range' Vlasov equation, whose self-consistent potential is constrained by the causality condition of the noninstantaneous response function, which breaks the Hamiltonian structure of the Vlasov equation (see Sect. 2.4). The WT kinetic equation ('WT KE') turns out to be relevant for an instantaneous nonlinear response and a statistically stationary incoherent wave, as will be discussed in the framework of supercontinuum generation in Sect. 5.2

2.2 Short-Range Vlasov Equation

We follow the standard procedure to derive an equation for the evolution of the autocorrelation function of the field, $B(\boldsymbol{x}, \boldsymbol{\xi}, z) = \langle \psi(\boldsymbol{x} + \boldsymbol{\xi}/2, z)\psi^*(\boldsymbol{x} - \boldsymbol{\xi}/2, z)\rangle$, with

$$\boldsymbol{x} = (\boldsymbol{x}_1 + \boldsymbol{x}_2)/2, \ \boldsymbol{\xi} = \boldsymbol{x}_1 - \boldsymbol{x}_2. \tag{4}$$

Because of the nonlinear character of the NLS equation, the evolution of the second-order moment of the wave depends on the fourth-order moment. In the same way, the equation for the fourth-order moment depends on the sixth-order moment, and so on. One obtains in this way an infinite hierarchy of moment equations, in which the nth order moment depends on the $(n + 2)$th order moment of the field. This makes the equations impossible to solve unless some way can be found to truncate the hierarchy. This refers to the fundamental problem of achieving a closure of the infinite hierarchy of the moment equations [30, 32, 33, 43]. A simple way to achieve a closure of the hierarchy is to assume that the field has Gaussian statistics. This approximation is justified in the weakly nonlinear regime, $L_d/L_{nl} \ll 1$ (or $|\mathscr{U}/\mathscr{E}| \ll 1$), where $L_d = \lambda_c^2/\alpha$ is the diffraction length, λ_c being the coherence length, and $L_{nl} = 1/(|\gamma|\rho)$ is the characteristic length of nonlinear interaction.

Exploiting the property of factorizability of moments of Gaussian fields, one obtains the following closed equation for the evolution of the autocorrelation function

$$i\partial_z B(\boldsymbol{x}, \boldsymbol{\xi}, z) = -2\alpha\nabla_{\boldsymbol{x}}.\nabla_{\boldsymbol{\xi}} B(\boldsymbol{x}, \boldsymbol{\xi}, z) - \gamma P(\boldsymbol{x}, \boldsymbol{\xi}, z) - \gamma Q(\boldsymbol{x}, \boldsymbol{\xi}, z), \tag{5}$$

where

$$P(\boldsymbol{x}, \boldsymbol{\xi}) = B(\boldsymbol{x}, \boldsymbol{\xi}) \int U(\boldsymbol{y})\big[N(\boldsymbol{x} - \boldsymbol{y} + \boldsymbol{\xi}/2) - N(\boldsymbol{x} - \boldsymbol{y} - \boldsymbol{\xi}/2)\big]d\boldsymbol{y} \tag{6}$$

$$\begin{aligned} Q(\boldsymbol{x}, \boldsymbol{\xi}) = \int U(\boldsymbol{y})\big[&B(\boldsymbol{x} - \boldsymbol{y}/2 + \boldsymbol{\xi}/2, \boldsymbol{y})B(\boldsymbol{x} - \boldsymbol{y}/2, \boldsymbol{\xi} - \boldsymbol{y}) + \\ &- B(\boldsymbol{x} - \boldsymbol{y}/2, \boldsymbol{\xi} + \boldsymbol{y})B(\boldsymbol{x} - \boldsymbol{y}/2 - \boldsymbol{\xi}/2, -\boldsymbol{y})\big]d\boldsymbol{y}, \end{aligned} \tag{7}$$

and

$$N(\boldsymbol{x}, z) \equiv B(\boldsymbol{x}, \boldsymbol{\xi} = 0, z) = \left\langle |\psi|^2 \right\rangle(\boldsymbol{x}, z) \tag{8}$$

denotes the averaged power of the field, which depends on the spatial variable $\boldsymbol{x}$ because the statistics of the field is *a priori* inhomogeneous. Note that we have omitted the z-label in Eqs. (6), (7).

Equations (5)–(7) is quite involved. To provide an insight into its physics we assume that the incoherent wave exhibits a quasi-homogeneous statistics, that is to say λ_c (i.e. the length scale of the random fluctuations) is much smaller than the length scale of homogeneous statistics Δ (i.e. typically the size of the incoherent beam), $\varepsilon = \lambda_c/\Delta \ll 1$. We assume that the range of the response function is of the same order as the healing length, $\sigma \sim \Lambda$. Defining the local spectrum of the wave as the Wigner-like transform of the autocorrelation function,

$$n_{\boldsymbol{k}}(\boldsymbol{x}, z) = \int B(\boldsymbol{x}, \boldsymbol{\xi}, z) \, \exp(-i\boldsymbol{k}.\boldsymbol{\xi}) \, d\boldsymbol{\xi}, \tag{9}$$

and performing a multiscale expansion of the solution

$$B(\boldsymbol{x}, \boldsymbol{\xi}, z) = B^{(0)}\big(\varepsilon\boldsymbol{x}, \boldsymbol{\xi}, \varepsilon z\big) + O(\varepsilon), \tag{10}$$

we obtain in the first-order in ε the following Vlasov-like kinetic equation [118]

$$\partial_z n_{\boldsymbol{k}}(\boldsymbol{x}, z) + \partial_{\boldsymbol{k}}\tilde{\omega}_{\boldsymbol{k}}(\boldsymbol{x}, z).\partial_{\boldsymbol{x}} n_{\boldsymbol{k}}(\boldsymbol{x}, z) - \partial_{\boldsymbol{x}}\tilde{\omega}_{\boldsymbol{k}}(\boldsymbol{x}, z).\partial_{\boldsymbol{k}} n_{\boldsymbol{k}}(\boldsymbol{x}, z) = 0. \tag{11}$$

The generalized dispersion relation reads

$$\tilde{\omega}_{\boldsymbol{k}}(\boldsymbol{x}, z) = \omega(\boldsymbol{k}) + V_{\boldsymbol{k}}(\boldsymbol{x}, z), \tag{12}$$

where $\omega(\boldsymbol{k}) = \alpha k^2$ is the linear dispersion relation of the NLS equation (1), and the self-consistent potential reads

$$V_{\boldsymbol{k}}(\boldsymbol{x}, z) = -\frac{\gamma}{(2\pi)^d} \int (1 + \tilde{U}_{\boldsymbol{k}-\boldsymbol{k}'}) \, n_{\boldsymbol{k}'}(\boldsymbol{x}, z) \, d\boldsymbol{k}', \tag{13}$$

where $\tilde{U}(\boldsymbol{k}) = \int U(\boldsymbol{x}) \exp(-i\boldsymbol{k}.\boldsymbol{x}) \, d\boldsymbol{x}$ is the Fourier transform of $U(\boldsymbol{x})$ [$\tilde{U}(\boldsymbol{k})$ being real and even] and

$$N(\boldsymbol{x}, z) = \frac{1}{(2\pi)^d} \int n_{\boldsymbol{k}}(\boldsymbol{x}, z) \, d\boldsymbol{k} \tag{14}$$

is the averaged spatial intensity profile of the wave [see Eq. (8)].

2.2.1 Properties of the Vlasov Equation

Several important properties of the Vlasov equation (11) result from its Poisson bracket structure. More specifically, the Vlasov equation can be recast in Hamiltonian form by means of the following Liouville's equation

$$d_z n_{\boldsymbol{k}}(z, \boldsymbol{x}) \equiv \partial_z n + \dot{\boldsymbol{x}}.\partial_{\boldsymbol{x}} n + \dot{\boldsymbol{k}}.\partial_{\boldsymbol{k}} n = 0, \tag{15}$$

where the variables $\boldsymbol{k}$ and $\boldsymbol{x}$ appear as canonical conjugate variables,

$$\dot{\boldsymbol{k}} = \partial_z \boldsymbol{k} = -\partial_{\boldsymbol{x}} \tilde{\omega}, \tag{16}$$

$$\dot{\boldsymbol{x}} = \partial_z \boldsymbol{x} = \partial_{\boldsymbol{k}} \tilde{\omega}, \tag{17}$$

where the generalized dispersion relation (12) plays the role of an effective Hamiltonian.

The Vlasov equation is a formally reversible equation, i.e., it is invariant under the transformation $(z, \boldsymbol{k}) \rightarrow (-z, -\boldsymbol{k})$. Moreover, it conserves the number of particles, $\mathscr{N} = (2\pi)^{-d} \iint n_{\boldsymbol{k}}(\boldsymbol{x}, z)\, d\boldsymbol{x} d\boldsymbol{k}$, the momentum $\mathscr{P} = (2\pi)^{-d} \iint \boldsymbol{k}\, n_{\boldsymbol{k}}(\boldsymbol{x}, z)\, d\boldsymbol{x} d\boldsymbol{k}$, and the Hamiltonian

$$\mathscr{H} = \frac{1}{(2\pi)^d} \iint \omega(\boldsymbol{k})\, n_{\boldsymbol{k}}(\boldsymbol{x})\, d\boldsymbol{x} d\boldsymbol{k} - \frac{\gamma}{2(2\pi)^{2d}} \iiint n_{\boldsymbol{k}_1}(\boldsymbol{x})\, \tilde{U}_{\boldsymbol{k}_1 - \boldsymbol{k}_2}\, n_{\boldsymbol{k}_2}(\boldsymbol{x}) d\boldsymbol{x} d\boldsymbol{k}_1 d\boldsymbol{k}_2. \tag{18}$$

In addition, the Vlasov equations (11)–(13) also conserves the so-called Casimirs, $\mathscr{M} = \iint f[n]\, d\boldsymbol{x} d\boldsymbol{k}$, where $f[n]$ is an arbitrary functional of the distribution $n_{\boldsymbol{k}}(\boldsymbol{x}, z)$.

2.3 *Long-Range Vlasov Equation*

2.3.1 Long-Range Response

Let us now consider a long-range nonlocal nonlinear response, $\sigma/\Lambda \gg 1$. Note that in this case the random field exhibits fluctuations whose spatial inhomogeneities are of the same order as the range of the nonlocal potential, $\sigma \sim \Delta$. The derivation of the long-range Vlasov equation is obtained by following a procedure similar to that for the short-range case ($\sigma \sim \Lambda$), except that we have to introduce the following scaling for the nonlocal potential

$$U(\boldsymbol{x}) = \varepsilon^d U^{(0)}(\varepsilon \boldsymbol{x}). \tag{19}$$

Note that the pre-factor ε^d is required by the normalization condition, $\int U(\boldsymbol{x}) d\boldsymbol{x} = \int U^{(0)}(\varepsilon \boldsymbol{x})\, d(\varepsilon^d \boldsymbol{x}) = 1$. Following the multiscale expansion technique [118], one can derive the Vlasov-like kinetic Eq. (11), with the effective dispersion relation

$$\tilde{\omega}_{\boldsymbol{k}}(\boldsymbol{x}, z) = \omega(\boldsymbol{k}) + V(\boldsymbol{x}, z), \tag{20}$$

and the long-range self-consistent potential

$$V(\boldsymbol{x}, z) = -\gamma \int U(\boldsymbol{x} - \boldsymbol{x}')\, N(\boldsymbol{x}', z)\, d\boldsymbol{x}'. \tag{21}$$

This effective potential then appears as a convolution of the nonlocal response with the intensity profile of the incoherent wave. Contrarily to the short-range potential, it does not depend on the spatial frequency $\boldsymbol{k}$. The long-range Vlasov equation conserves the number of particles, $\mathscr{N} = (2\pi)^{-d} \iint n_{\boldsymbol{k}}(\boldsymbol{x}, z)\, d\boldsymbol{x} d\boldsymbol{k}$, the momentum $\mathscr{P} = (2\pi)^{-d} \iint \boldsymbol{k}\, n_{\boldsymbol{k}}(\boldsymbol{x}, z)\, d\boldsymbol{x}\, d\boldsymbol{k}$, the Hamiltonian

$$\mathscr{H} = \frac{1}{(2\pi)^d} \iint \omega(\boldsymbol{k})\, n_{\boldsymbol{k}}(\boldsymbol{x}, z)\, d\boldsymbol{x} d\boldsymbol{k} + \frac{1}{2} \int V(\boldsymbol{x}, z) N(\boldsymbol{x}, z)\, d\boldsymbol{x}, \tag{22}$$

as well as the Casimirs, $\mathscr{M} = \iint f[n]\, d\boldsymbol{x} d\boldsymbol{k}$, where $f[n]$ is an arbitrary functional of the distribution $n_{\boldsymbol{k}}(\boldsymbol{x}, z)$.

2.3.2 Validity of the Long-Range Vlasov Equation

It is important to underline that, thanks to the long-range nonlocal response, the system exhibits a self-averaging property of the nonlinear response,

$$\int U(\boldsymbol{x} - \boldsymbol{x}')|\psi(\boldsymbol{x}', z)|^2 d\boldsymbol{x}' \simeq \int U(\boldsymbol{x} - \boldsymbol{x}') N(\boldsymbol{x}', z) d\boldsymbol{x}'.$$

Substitution of this property into the nonlocal NLS equation (1) thus leads to a closure of the hierarchy of the moment equations. More specifically, using statistical arguments similar as those in [96], one can show that, owing to the highly nonlocal response, the statistics of the incoherent wave turns out to be Gaussian. Then contrarily to a conventional Vlasov equation, whose validity is constrained by the assumptions of (1) weakly nonlinear interaction and (2) quasi-homogeneous statistics, the long-range Vlasov equation provides an *exact* statistical description of the random wave $\psi(\boldsymbol{x}, z)$ in the highly nonlocal regime, $\varepsilon \ll 1$. This property is corroborated by the fact that the Vlasov equation considered here is formally analogous to the Vlasov equation considered to study long-range interacting systems [97, 119]. In this context, it has been rigorously proven that, in the limit of an infinite number of particles, the dynamics of *mean-field Hamiltonian systems* is governed by the long-range Vlasov equation [97]. Note however that the term 'long-range' used in [97] refers to a response function whose integral diverges, $\int U(\boldsymbol{x})\, d\boldsymbol{x} = +\infty$, while the response functions considered here refer to exponential or Gaussian shaped functions typically encountered in optical materials (see e.g., [88]). We finally note that the validity of the long-range Vlasov equation in the strongly nonlinear regime has been recently confirmed by direct numerical simulations in a recent work in which collective large scale incoherent shocks have been reported [120].

2.3.3 Incoherent Modulational Instability

Modulational (or Benjamin-Feir) Instability (MI) refers to the phenomenon in which an initially plane- (or continuous-) wave tends to break up spontaneously into periodic modulations while it propagates through a nonlinear medium. In the frequency domain, this phenomenon can be interpreted as a phase-matched partially degenerate four-wave mixing process in which an intense pump wave yields energy to a pair of weak sideband waves. In the following we shall see that an incoherent field that exhibits a homogeneous statistics may become modulationally unstable with respect to the growth of weakly statistical inhomogeneities, i.e., the incoherent field thus becomes statistically inhomogeneous [13–15, 94].

The phenomenon of incoherent MI has been the subject of a detailed investigation in the optical context with an inertial nonlinear response [8, 13, 118]. We present here the phenomenon of incoherent MI in the framework of the long-range Vlasov formalism. For the sake of simplicity, we limit the incoherent MI analysis to the one-dimensional case. We assume that the incident field exhibits a homogeneous statistics, except for small perturbations that depend on x and z. Note that any homogeneous stationary distribution, n_k^0, is a solution of the Vlasov equation, that is, $\partial_z n_k^0 = 0$. We perturb this stationary solution according to $n_k(x,z) = n_k^0 + \delta n_k(x,z)$, with $|\delta n_k(x,z)| \ll n_k^0$, and linearize the Vlasov equation

$$\partial_z \delta n_k(x,z) + 2\alpha k \partial_x \delta n_k(x,z) + \frac{\gamma}{2\pi}\partial_k n_k^0 \int dx' \partial_x U(x-x') \int dk \delta n_k(x',z) = 0 \tag{23}$$

This equation can be solved by a Fourier-Laplace transform,

$$\tilde{\delta n}_k(K,\lambda) = \int_0^\infty dz \int_{-\infty}^{+\infty} dx \, \exp(-\lambda z - iKx)\, \delta n_k(x,z),$$

which gives the dispersion relation

$$-1 = \frac{\gamma}{\pi}\alpha K^2 \tilde{U}(K) \int_{-\infty}^{+\infty} \frac{n_k^0}{(i\lambda - 2\alpha K k)^2}\, dk, \tag{24}$$

where $\tilde{U}(K) = \int U(x) \exp(-iKx)\, dx$. Assuming that the initial spectrum is Lorentzian-shaped, $n_k^0 = 2N_0 \Delta k/(k^2 + (\Delta k)^2)$ [i.e., $(2\pi)^{-1} \int n_k^0 dk = N_0$], Eq. (24) gives

$$\lambda(K) = -2\alpha \Delta k |K| + |K| \sqrt{2\alpha\gamma N_0 \tilde{U}(K)}, \tag{25}$$

where the incoherent MI gain reads $g_{\mathrm{MI}}(K) = 2\Re[\lambda(K)]$.

First of all, we can note that incoherent MI requires a focusing nonlinearity, $\gamma > 0$, as for the usual coherent MI. However, contrary to coherent MI, a focusing nonlinearity is not a sufficient condition for the occurrence of incoherent MI. Indeed,

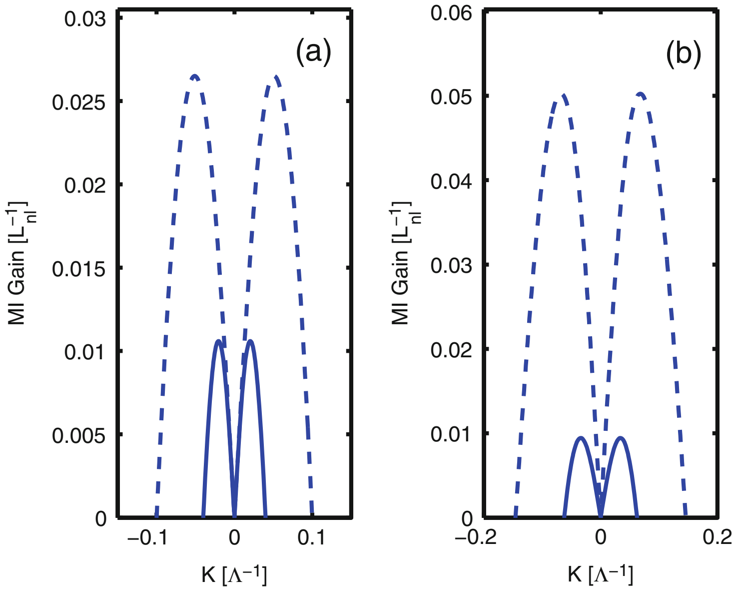

Fig. 4 Spatial incoherent MI: Plots of the MI gain given by Eq. (25), $g_{\rm MI}(K) = 2\Re[\lambda(K)]$, for an exponential response function, $U(x) = \exp(-|x|/\sigma)/(2\sigma)$: (**a**) $\sigma = 10\Lambda$ (*dashed*), $\sigma = 25\Lambda$ (*continuous*), for $\Delta k = 0.5\Lambda^{-1}$. (**b**) $\Delta k = 0.4\Lambda^{-1}$ (*dashed*), $\Delta k = 0.6\Lambda^{-1}$ (*continuous*), for $\sigma = 10\Lambda$

we remark in the MI gain expression (25) the existence of a damping term, which introduces a threshold for incoherent MI [8, 13, 74]. Note that, the existence of a threshold for incoherent MI was shown to be formally related to an effective Landau damping [8]. In this way, the stabilizing effect of the partial coherence does not refer to a genuine dissipative damping, but rather a self-action effect analogous to Landau damping of electron plasma waves that causes a redistribution of the spectrum $n_k(x, z)$. This effective damping significantly reduces the MI gain and the optimal MI frequency, $K_{\rm MI}$, as illustrated in Fig. 4.

It is interesting to note that in the limit of a local response ($\tilde{U}(K) = 1$), Eq. (25) reduces to a straight line. This leads to an unphysical result: the MI gain increases with the modulation frequency K. This pathology stems from the fact that the derivation of the Vlasov equation with a local nonlinearity is constrained by the assumption of *quasi-homogeneous statistics*. However, as discussed above in Sect. 2.3.1, the assumption of quasi-homogeneous statistics is automatically satisfied in the presence of a long-range nonlocality. Accordingly, the incoherent MI gain curve (25) is bell-shaped, with a maximum growth-rate at some optimal frequency, $K_{\rm MI}$.

2.3.4 Incoherent Solitons

The Vlasov equation describes the evolution of the averaged spectrum of a random wave. Hence, a spatially localized and stationary solution of the Vlasov equation describes an incoherent soliton state. The mechanism underlying the formation of an incoherent soliton is schematically explained in Fig. 5. We consider here the case of bright solitons with a focusing nonlinearity ($\gamma > 0$), and again we limit the study to the pure one-dimensional situation. Let us consider the stationary Vlasov equation

$$2\alpha k\, \partial_x n_k^{st}(x) - \partial_x V(x)\, \partial_k n_k^{st}(x) = 0. \tag{26}$$

where the self-consistent potential is given by $V(x) = -\gamma \int U(x-x')\, N(x')\, dx'$ [see Eq. (21)]. Let us now recall an important observation originally pointed out in the seminal paper [69], namely the fact that the solution to Eq. (26) can be expressed as an arbitrary function of the effective Hamiltonian, $h = \alpha k^2 + V(x)$. To find an explicit analytical solution to Eq. (26), we make use of this observation by following the procedure outlined in [70]. In this work, Hasegawa obtained an analytical soliton solution of the Vlasov equation in the limit of a *local nonlinear interaction*, $U(x) = \delta(x)$. This solution has been recently generalized to a nonlocal interaction in [20]. The idea of the method is to argue that the 'particles' that constitute the soliton are trapped by the self-consistent potential $V(x)$ provided that their energy is negative, $h \leq 0$. This determines a specific interval of momenta for the trapped particles, $-k_c \leq k \leq k_c$, where $k_c = \sqrt{-V/\alpha}$ (note that $V < 0$ in the focusing regime, see Fig. 5). According to Eq. (14), the intensity profile of the soliton solution thus reads $N(x) = (2\pi)^{-1} \int_{-k_c}^{+k_c} n_k^{st}(x)\, dk$. By means of a simple change of variables, this

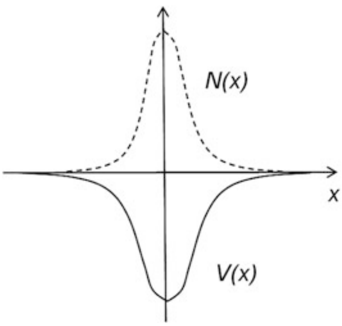

Fig. 5 Schematic representation of the self-trapping mechanism underlying the formation of an incoherent soliton solution of the Vlasov equation. A soliton forms when the optical beam induces an attractive potential $V(x) < 0$ (waveguide) owing to a focusing nonlinearity ($\gamma > 0$). In turn, the optical beam is guided in its own induced potential $V(x)$

integral can thus be expressed in the form of a Fredholm equation

$$N = \frac{1}{2\pi} \int_V^0 \frac{n^{st}(h)}{\sqrt{h - V}} dh. \tag{27}$$

A solution to this equation can be obtained under the assumption that $U(x)$ and $N(x)$ are Gaussian-shaped [20]. Assuming $U(x) = (2\pi\sigma^2)^{-1/2} \exp[-x^2/(2\sigma^2)]$ and $N(x) = \mathcal{N}(2\pi\sigma_N^2)^{-1/2} \exp[-x^2/(2\sigma_N^2)]$, and making use of the Laplace convolution theorem, we have

$$n_k^{st}(x) = Q_\eta \left[c_\eta N^\eta(x) - \beta k^2\right]^{\frac{1}{\eta} - \frac{1}{2}}, \tag{28}$$

where

$$Q_\eta = \frac{2\pi\beta^{\frac{1}{2}} \Gamma(\eta^{-1} + 1)}{\Gamma(\eta^{-1} + 1/2)\Gamma(1/2)c_\eta^{1/\eta}}, \tag{29}$$

$\Gamma(x)$ being the Gamma function, and

$$c_\eta = \frac{(2\pi)^{\frac{\eta}{2} - \frac{1}{2}} \gamma \sigma_N^\eta}{\mathcal{N}^{\eta-1} \sqrt{\sigma^2 + \sigma_N^2}}, \tag{30}$$

with

$$\eta = \frac{1}{1 + (\sigma/\sigma_N)^2}. \tag{31}$$

This analytical solution is self-consistent, in the sense that it verifies the condition (27), and it is straightforward to check by direct substitution that it is indeed a solution of (27).

The fact that the above solution generalizes the solution obtained by Hasegawa [70] becomes apparent by remarking that Eq. (28) can be expressed as

$$n^{st}(h) \sim (-h)^{\frac{1}{\eta} - \frac{1}{2}}. \tag{32}$$

In the limit of a local potential, $U(x) = \delta(x)$, the parameter $\eta \to 1$, and (32) recovers the solution $n^{st}(h) \sim \sqrt{-h}$ [70]. Note however that for a local nonlinearity [70], the analytical solution is valid for *any* form of the intensity distribution, $N(x)$, a property that was subsequently interpreted in the framework of a ray-optics approach [121]. Conversely, for a nonlocal nonlinearity, the analytical solution (28)–(31) refers to a Gaussian-shaped intensity profile.

2.3.5 Vlasov Simulations: Incoherent Soliton Turbulence

The phenomena of incoherent MI and subsequent incoherent soliton formation can be visualized by means of a direct numerical integration of the long-range Vlasov equations (11), (21). This is illustrated in Fig. 6, which reports the evolution of the spectrum of the incoherent wave during its propagation. The simulation starts from a homogeneous spectrum, $n_k(x, z = 0) \simeq n_k^0$, which is periodically perturbed to seed the incoherent MI. Because of the nonlinear Hamiltonian flow, particles following different orbits travel at different angular speeds, a process known as 'phase-mixing'. Each MI-modulation thus starts spiralling in the phase-space (x, k), which leads to the formation of four localized incoherent structures, which are

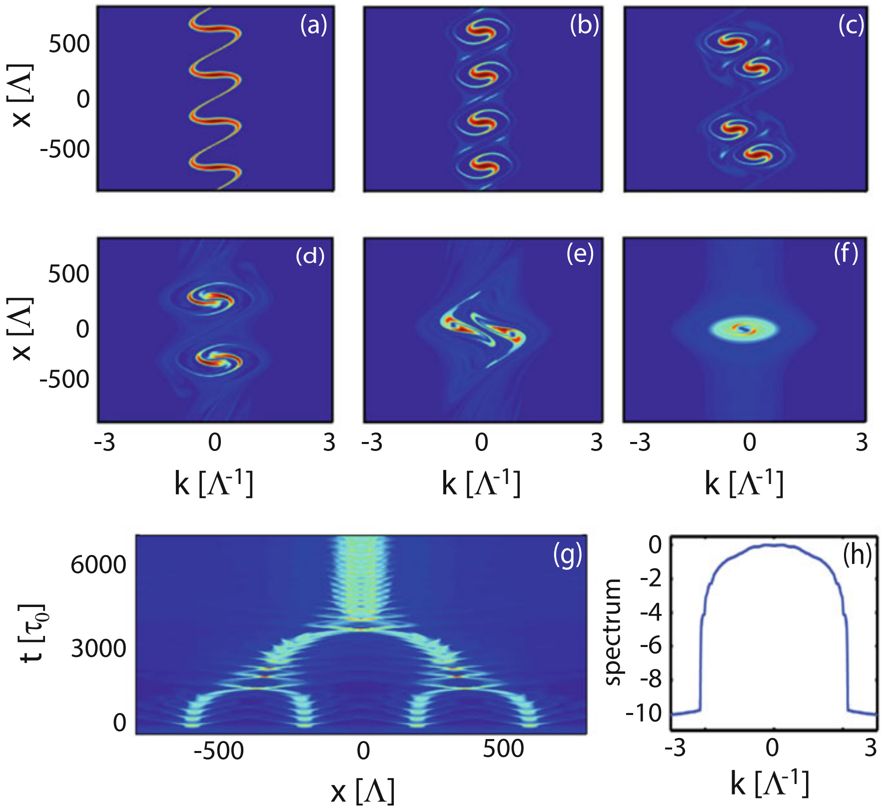

Fig. 6 Incoherent soliton turbulence: Numerical simulation of the long-range Vlasov equations (11), (21), showing the evolution of the local spectrum, $n_k(x)$, during the propagation. The initial homogeneous spectrum exhibits incoherent MI: the four modulations excited by the initial condition lead to the generation of four incoherent structures, which slowly coalesce into two, and then into one incoherent soliton state. (**a**) $z = 300$, (**b**) $z = 1000$, (**c**) $z = 1500$, (**d**) $z = 3000$, (**e**) $z = 4000$, (**f**) $z = 10^4$ (in units of L_{nl}), $\sigma = 10^2 \Lambda$. (**g**) Corresponding evolution of the spatial intensity profile, $N(x, z)$. (**h**) Corresponding spectrum $S(k, z_0)$ at $z_0 = 700 L_{nl}$. *Source*: from [20]

mutually attracted and coalesce into two, and eventually into a single incoherent structure. Note that this process is analogous to the soliton turbulence scenario that occurs for *coherent* solitons [91]. The phase-mixing then leads to a smoothing and homogenization of the perturbations on the incoherent structure, which thus slowly tend to relax toward a stationary incoherent soliton state. Note that the asymptotic evolution of inhomogeneous Vlasov states is a long standing mathematical problem [122].

2.4 Temporal Version: Non Hamiltonian Long-Range Vlasov Equation

We remark that, as discussed above through Fig. 3, the long-range Vlasov formalism also plays a role in the temporal domain in the presence of a highly noninstantaneous nonlinear response (temporal nonlocality). Because of the causality condition inherent to the response function in the temporal domain, the Vlasov equation no longer exhibit a Hamiltonian structure [118]. The corresponding Vlasov formalism predicts different interesting behaviors, such as the existence of incoherent solitons in the normal dispersion regime, in contrast to conventional solitons which are known to require anomalous dispersion. For a review on the long-range Vlasov formalism in the temporal domain, see [118].

3 Weak Langmuir Turbulence Formalism

In this Section we study the temporal evolution of a partially coherent wave that propagates in a nonlinear medium characterized by a noninstantaneous response. As discussed in Sect. 1 through Fig. 3, a delayed nonlinearity leads to a kinetic description which is formally analogous to the weak Langmuir turbulence kinetic equation, irrespective of the nature of the fluctuations that may be either stationary or non-stationary. In the presence of a temporal long-range response and a stationary statistics of the incoherent wave, the weak Langmuir turbulence formalism reduces to a family of singular integro-differential kinetic equations (e.g., Benjamin-Ono equation) that describe incoherent dispersive shock waves and incoherent collapse singularities in the spectral evolution of the random wave.

3.1 Noninstantaneous Nonlinear Response

A typical example of noninstantaneous nonlinear response in one dimensional systems is provided by the Raman effect in optical fibers [123]. We consider the standard 1D NLS equation accounting for a noninstantaneous nonlinear response function

$$i\partial_z\psi + \beta\partial_{tt}\psi + \gamma\psi \int_{-\infty}^{+\infty} R(t-t')\, |\psi|^2(t',z)\, dt' = 0, \tag{33}$$

where the response function $R(t)$ is constrained by the causality condition. In the following we use the convention that $t > 0$ corresponds to the leading edge of the pulse, so that the causal response will be on the trailing edge of a pulse, i.e., $R(t) = 0$ for $t > 0$. We will write the response function in the form $R(t) = H(-t)\bar{R}(-t)$, where $\bar{R}(t)$ is a smooth function from $[0,\infty)$ to $(-\infty,\infty)$, while the Heaviside function $H(-t)$ guarantees the causality property. As we will see, this convention will allow us to easily compare the dynamics of temporal and spatial incoherent solitons. Because of the causality property, the real and imaginary parts of the Fourier transform of the response function

$$\tilde{R}(\omega) = \tilde{U}(\omega) + i\,g(\omega), \tag{34}$$

are related by the Kramers-Krönig relations. We recall that $\tilde{U}(\omega)$ is even, while the gain spectrum $g(\omega)$ is odd. The causality condition breaks the Hamiltonian structure of the NLS equation, so that Eq. (33) only conserves the total power ('number of particles') of the wave $\mathcal{N} = \int |\psi|^2(t,z)\, dt$. The typical temporal range of the response function $R(t)$ denotes the response time, τ_R. Note that $\beta = -\frac{1}{2}\partial^2_\omega k(\omega)$ in Eq. (33), so that $\beta > 0$ ($\beta < 0$) denotes the regime of anomalous (normal) dispersion.

3.2 Short-Range Interaction: Spectral Incoherent Solitons

The dynamics is ruled by the comparison of the response time, τ_R, with the 'healing time', $\tau_0 = \sqrt{|\beta| L_{nl}}$. We remind that the weakly nonlinear regime of interaction refers to the regime in which linear dispersive effects dominate nonlinear effects, i.e., $L_d/L_{nl} \ll 1$ where $L_d = t_c^2/|\beta|$ and $L_{nl} = 1/(|\gamma|\rho)$ refer to the dispersive and nonlinear characteristic lengths respectively, t_c being the correlation time of the partially coherent wave. We consider here the case of a noninstantaneous nonlinearity characterized by a short-range response time, i.e., $\tau_R \sim \tau_0$. In this regime, it can be shown that the kinetic equation governing the evolution of the incoherent wave takes a form analogous to the WT Langmuir kinetic equation [22, 118]:

$$\partial_z n_\omega(z) = \frac{\gamma}{\pi}\, n_\omega(z) \int_{-\infty}^{+\infty} g(\omega-\omega')\, n_{\omega'}(z)\, d\omega', \tag{35}$$

where we have implicitly assumed that the incoherent wave exhibits fluctuation that are statistically stationary (homogeneous) in time—a generalized WT Langmuir equation can be obtained for a non-stationary statistics [118]. We first note that this equation does not account for dispersion effects (it does not involve the parameter β), although the role of dispersion in its derivation is essential in order to verify the criterion of weakly nonlinear interaction, $L_d/L_{nl} \ll 1$. The fact that the dynamics ruled by the WT Langmuir equation does not depend on the sign of the dispersion coefficient has been verified by direct numerical simulations of the NLS Eq. (33) [99]. The kinetic Eq. (35) conserves the power of the field $N = \frac{1}{2\pi}\int n_\omega(z)\,d\omega$. Moreover, as discussed above for the Vlasov equation, the WT Langmuir equation (35) is a formally reversible equation [it is invariant under the transformation $(z,\omega) \to (-z,-\omega)$], a feature which is consistent with the fact that it also conserves the non-equilibrium entropy $S = \frac{1}{2\pi}\int \log[n_\omega(z)]\,d\omega$.

The WT Langmuir equation admits solitary wave solutions [22, 74, 98, 99]. This may be anticipated by remarking that, as a result of the convolution product in (35), the odd spectral gain curve $g(\omega)$ amplifies the low-frequency components of the wave at the expense of the high-frequency components, thus leading to a global red-shift of the spectrum. We remind that these incoherent solitons are termed 'spectral' because they can only be identified in the spectral domain, since in the temporal domain the field exhibits stochastic fluctuations at any time, t.

3.2.1 Numerical Simulations

Typical spectral incoherent soliton behaviors are reported in Fig. 7. The initial condition is an incoherent wave characterized by a Gaussian spectrum with δ-correlated random spectral phases, so that the initial wave exhibits stationary fluctuations. The Gaussian spectrum is superposed on a background of small noise of averaged intensity $n_0 = 10^{-5}$. This is important in order to sustain a steady soliton propagation, otherwise the soliton undergoes a slow adiabatic reshaping so as to adapt its shape to the local value of the noise background. The relative intensity of the background noise with respect to the average power of the wave plays an important role in the dynamics of discrete spectral incoherent solitons. Indeed, the *continuous* spectral incoherent soliton is known to become narrower (i.e., of higher amplitude) as the intensity of the background noise decreases. Accordingly, a transition from a continuous to a discrete spectral incoherent soliton behavior occurs as the relative intensity of the background noise is decreased: as the spectral soliton becomes narrower than ω_R, the leading edge of the tail of the spectrum will be preferentially amplified, thus leading to the formation of a discrete spectral incoherent soliton. In order to test the validity of the WT Langmuir theory, we reported in Fig. 7 a direct comparison with NLS simulations. We underline that an excellent agreement has been obtained between the simulations of the NLS equation and the WT Langmuir equation, without using any adjustable parameter [99].

Note that if the background noise level increases in a significant way and becomes of the same order as the amplitude of the spectral soliton, the incoherent

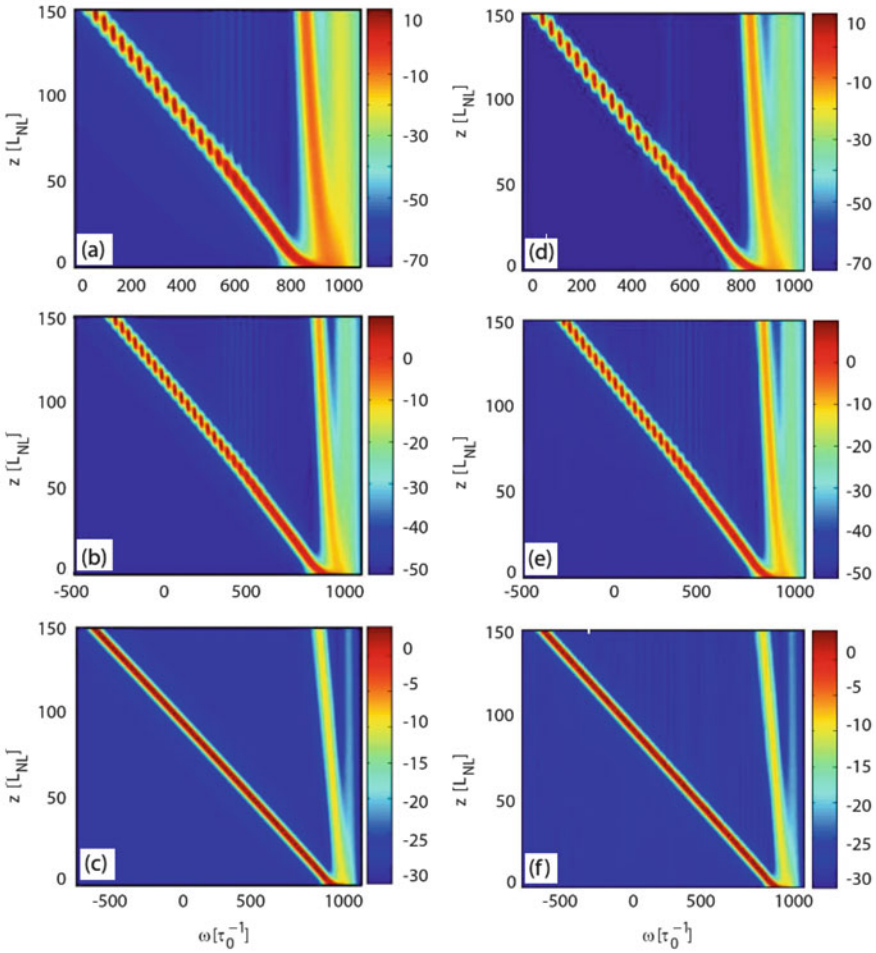

Fig. 7 Spectral incoherent solitons: Transition from discrete to continuous solitons. *Left column* (**a**)–(**c**): Evolution of the non-averaged spectrum of the optical field, $|\tilde{\psi}|^2(z,\omega)$ (in dB-scale), obtained by integrating numerically the NLS equation (33) for three different values of the noise background, $n_0 = 10^{-7}$ (**a**), $n_0 = 10^{-5}$ (**b**), $n_0 = 10^{-3}$ (**c**). *Right column* (**d**)–(**f**): Corresponding evolution of the averaged spectrum, $n(z,\omega)$ (in dB-scale), obtained by solving the Langmuir WT equation (35): The comparison reveals a quantitative agreement, without using adjustable parameters. We considered the typical Raman-like gain spectrum, $g(\omega)$ ($\beta\gamma < 0$). *Source*: from [99]

wave enters a novel regime [124]. This regime is characterized by an oscillatory dynamics of the incoherent spectrum which develops within a spectral cone during the propagation. Such spectral dynamics exhibits a significant spectral blue shift, which is in contrast with the expected Raman-like spectral red shift.

3.2.2 Analytical Soliton Solution

The WT Langmuir kinetic equation (35) admits analytical soliton solutions [74, 118, 125]. More precisely, it is possible to compute the width and velocity of the soliton given its peak amplitude n_m in the regime $n_m \gg n_0$, where n_0 denotes the spectral amplitude of the background noise. We introduce the antiderivative of the spectral gain $G(\omega) = -\int_\omega^\infty g(\omega')d\omega'$. The gain spectrum $g(\omega)$ is characterized by its typical gain amplitude g_i and its typical spectral width ω_i. Regardless of the details of the gain curve $g(\omega)$, g_i and ω_i can be assessed by two characteristic quantities, namely the gain slope at the origin $\partial_\omega g(0)$ and the total amount of gain $G(0) = -\int_0^\infty g(\omega)d\omega$. A dimensional analysis allows to express g_i and ω_i in terms of these two quantities, $g_\mathrm{i} = \frac{1}{\sqrt{2}}(-\partial_\omega g(0))^{1/2}\big[-\int_0^\infty g(\omega)d\omega\big]^{1/2}$, $\omega_\mathrm{i} = \sqrt{2}\big[-\int_0^\infty g(\omega)d\omega\big]^{1/2}/\big[-\partial_\omega g(0)\big]^{1/2}$. With these definitions, the function $G(\omega)$ can be written in the following normalized form $G(\omega) = g_\mathrm{i}\omega_\mathrm{i}h(\omega/\omega_\mathrm{i})$, where the dimensionless function $h(x)$ verifies $h(0) = 1$, $h'(0) = 0$, and $h''(0) = -2$. Proceeding as in [125], the profile of the soliton in the regime $n_m \gg n_0$ is of the form [74], $\log\left(\frac{n_\omega(z)}{n_0}\right) = \log\left(\frac{n_m}{n_0}\right)h\left(\frac{\omega - Vz}{\omega_\mathrm{i}}\right)$, or equivalently:

$$n_\omega(z) - n_0 = \big(n_m - n_0\big)\exp\left[-\log\left(\frac{n_m}{n_0}\right)\frac{(\omega - Vz)^2}{\omega_\mathrm{i}^2}\right], \tag{36}$$

where the velocity of the soliton is

$$V = -\frac{n_m - n_0}{\log^{3/2}\left(\frac{n_m}{n_0}\right)}\frac{\gamma g_\mathrm{i}\omega_\mathrm{i}^2}{\sqrt{\pi}}, \tag{37}$$

and its full width at half maximum is $\omega_{\mathrm{sol}} = 2\omega_\mathrm{i}\log^{1/2}(2)/\log^{1/2}(n_m/n_0)$.

Spectral incoherent solitons have been recently generalized in the framework of the generalized NLS equation accounting for the self-steepening term and a frequency dependence of the nonlinear Kerr coefficient [126]. Such nonlinear dispersive effects are shown to strongly affect the dynamics of the incoherent wave. A generalized WT Langmuir kinetic equation is derived and its predictions have been found in quantitative agreement with the numerical simulations of the NLS equation, without adjustable parameters [126].

The structure of discrete spectral incoherent solitons can also be interpreted with an analytical soliton solution of the *discretized* WT Langmuir equation derived in [127]. In this way, discrete frequency bands of the soliton are modelled as coupled Dirac δ-functions in frequency space (δ-peak model). However, the simulations show that, when injected as initial condition into the WT Langmuir equation with a Raman-like gain spectrum, the analytical soliton solution rapidly relaxes during the propagation toward a discrete spectral incoherent solution [99]. This property reveals the incoherent nature of discrete spectral incoherent solitons.

We finally note that the emergence of continuous and discrete spectral incoherent solitons has been identified experimentally owing to the Raman effect in photonic crystal fibers in the context of supercontinuum generation, a feature discussed in detail in [23].

3.3 Long-Range Interaction: Spectral Singularities

In this section we present the procedure which allows one to derive appropriate reduced kinetic equations from the WT Langmuir equation in the long-range limit, i.e., the limit of a highly noninstantaneous nonlinear response, $\tau_R \gg \tau_0$. As discussed here above, the causality condition leads to a gain spectrum $g(\omega)$ that decays algebraically at infinity, a property which introduces singularities into the convolution operator of the WT Langmuir equation (35). The mathematical procedure consists in accurately addressing these singularities, see [100]. It reveals that, as a general rule, a singular integro-differential operator arises systematically in the derivation of the reduced kinetic equation [100, 128]. The resulting singular integro-differential kinetic equation then originates in the causality property of the nonlinear response function.

These singular integro-differential kinetic equations find a direct application in the description of dispersive shock waves, i.e., shock waves whose singularity is regularized by dispersion effects instead of dissipative (viscous) effects [101]. Dispersive shock waves have been constructed mathematically [129] and observed in ion acoustic waves [130] long ago, though it is only recently that they emerged as a general signature of singular fluid-type behavior, in particular in Bose-Einstein condensates [131, 132] and nonlinear optics [80, 81, 133, 134].

These previous studies on dispersive shock waves have been discussed for coherent, i.e., deterministic, amplitudes of the waves. Through the analysis of the WT Langmuir equation, we will see that incoherent waves can exhibit dispersive shock waves of a different nature that their coherent counterpart. They manifest themselves as a wave breaking process ("gradient catastrophe") in the spectral dynamics of the incoherent field [100]. Contrary to conventional shocks which are known to require a strong nonlinear regime, these incoherent shocks develop into the weakly nonlinear regime. This WT kinetic approach also reveals unexpected links with the 3D vorticity equation in incompressible fluids [102], or the integrable Benjamin-Ono equation [103], which was originally derived in hydrodynamics.

3.3.1 Damped Harmonic Oscillator Response: Spectral Dispersive Shock Waves

The derivation of singular integro-differential kinetic equations has been developed for a general form of the response function (see the Supplemental of [100]). Here we illustrate the theory by considering two physically relevant examples of response functions, which, respectively, induce and inhibit the formation of incoherent shock waves.

Let us first consider the example of the damped harmonic oscillator response, $\bar{R}(t) = \frac{1+\eta^2}{\eta\tau_R}\sin(\eta t/\tau_R)\exp(-t/\tau_R)$. Figure 8 reports a typical evolution of the spectrum of the incoherent wave obtained by numerical simulations of the NLS equation (33). Here we considered the highly incoherent limit, $\Delta\omega \gg \Delta\omega_g$ ($t_c \ll \tau_R$). We see that the low frequency part of the spectrum exhibits a self-steepening process, whose wave-breaking is ultimately regularized by the development of large amplitude and rapid spectral oscillations typical of a dispersive shock wave. This behavior has been described by deriving a singular integro-differential kinetic equation from the WT Langmuir equation in the long-range regime ($\tau_R \gg \tau_0$):

$$\tau_R^2\partial_z n_\omega = \gamma(1+\eta^2)\Big(n_\omega\partial_\omega n_\omega - \frac{1}{\tau_R}n_\omega\mathscr{H}\partial_\omega^2 n_\omega\Big), \tag{38}$$

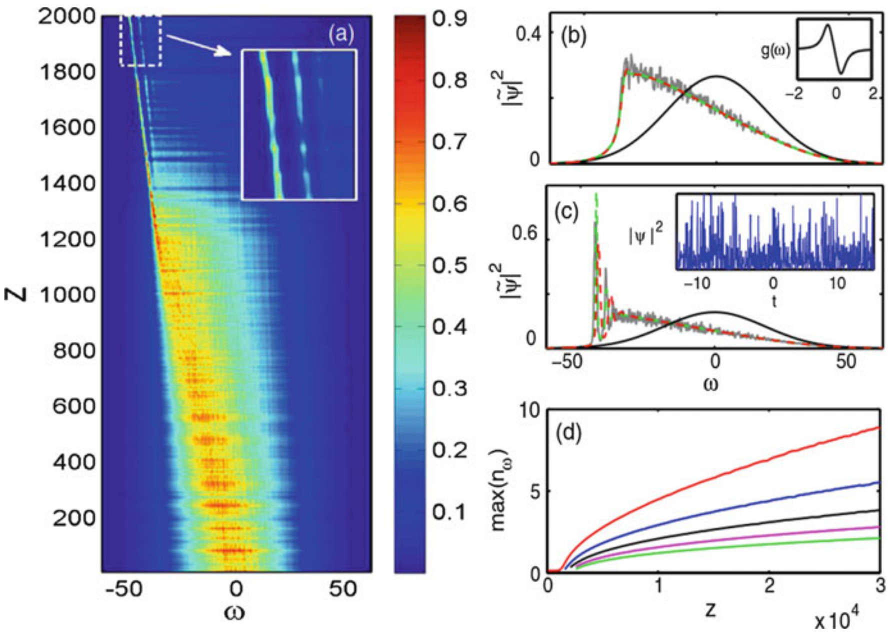

Fig. 8 Incoherent dispersive shock waves with a Raman-like response function: (**a**) Numerical simulation of the NLS equation (33): The stochastic spectrum $|\tilde{\psi}|^2(\omega,z)$ develops an incoherent shock at $z \simeq 1200L_{nl}$ ($\tau_R = 3\tau_0, \eta = 1$). Snapshots at $z = 1040L_{nl}$ (**b**), $z = 1400L_{nl}$ (**c**): NLS (33) (*gray*) is compared with WT Langmuir equation (35) (*green*), singular kinetic equation [Eq. (38)] (*dashed–red*), and initial condition (*solid black*). (**d**) First five maxima of n_ω vs z in the long-term post-shock dynamics: the spectral peaks keep evolving, revealing the non-solitonic nature of the incoherent dispersive shock wave. Insets: (**b**) gain spectrum $g(\omega)$, note that $\Delta\omega_g$ is much smaller than the initial spectral bandwidth of the wave [*black line* in (**b**)]. (**c**) corresponding temporal profile $|\psi(t)|^2$ showing the incoherent wave with stationary statistics. *Source*: from [100]

where the singular operator $\mathscr{H}$ refers to the Hilbert transform,

$$\mathscr{H}f(\omega) = \frac{1}{\pi}\mathscr{P}\int_{-\infty}^{+\infty}\frac{f(\omega-u)}{u}du,$$

where we recall that $\mathscr{P}$ denotes the Cauchy principal value. This kinetic equation describes the essence of incoherent dispersive shock waves: The leading-order Burgers term describes the formation of the shock, which is subsequently regularized by the nonlinear dispersive term involving the Hilbert operator. We remark in Fig. 8 that a quantitative agreement is obtained between the simulations of Eq. (38) and those of the NLS and WT Langmuir equations, without adjustable parameters. Also note that in the presence of a strong spectral background noise, the derived singular equation coincides with the Benjamin-Ono equation, which is a completely integrable equation [100].

3.3.2 Exponential Response: Spectral Collapse Singularity

As described by the general theory reported in [100], the previous scenario of incoherent dispersive shock waves changes in a dramatic way when the response function is not continuous at the origin, as it occurs for a purely exponential response function, $\bar{R}(t) = \exp(-t/\tau_R)/\tau_R$. In this case, considering the limit $\tau_R/\tau_0 \gg 1$, the singular kinetic equation takes the form:

$$\tau_R\partial_z n_\omega = -\gamma n_\omega \mathscr{H} n_\omega - \frac{\gamma}{\tau_R}n_\omega\partial_\omega n_\omega + \frac{\gamma}{2\tau_R^2}n_\omega\mathscr{H}\partial_\omega^2 n_\omega. \tag{39}$$

Interestingly, the first term of (39) was considered as a one-dimensional model of the vorticity formulation of the 3D Euler equation of incompressible fluid flows [102]. In this work, the authors found an explicit analytical solution to the equation $\tau_R\partial_z n_\omega = -\gamma n_\omega\mathscr{H}n_\omega$. For a given initial condition $n_\omega(z=0) = n_\omega^0$ the solution has the form

$$n_\omega(z) = \frac{4n_\omega^0}{\left(2 + (\gamma z/\tau_R)\mathscr{H}n_\omega^0\right)^2 + (\gamma z/\tau_R)^2(n_\omega^0)^2}. \tag{40}$$

There is blow up if and only if there exists ω such that $n_\omega^0 = 0$ and $\mathscr{H}n_\omega^0 < 0$. Then the blow up distance z_c is given by $z_c = -2\tau_R/[\gamma\mathscr{H}n_{\omega=\omega_0}^0]$, where ω_0 is such that $n_{\omega_0}^0 = 0$. It can be shown [100] that, if the initial condition decays faster than a Lorentzian, the spectrum exhibits a collapse-like dynamics, which is ultimately arrested by a small background noise. In this process, the spectrum moves at velocity $\tilde{c}$, while its peak amplitude increases according to $\sim 4\tau_R^2/[\gamma^2 z^2 n^0(\omega = \tilde{c}z)]$. This property is confirmed by the simulations of the NLS equation, as illustrated in Fig. 9.

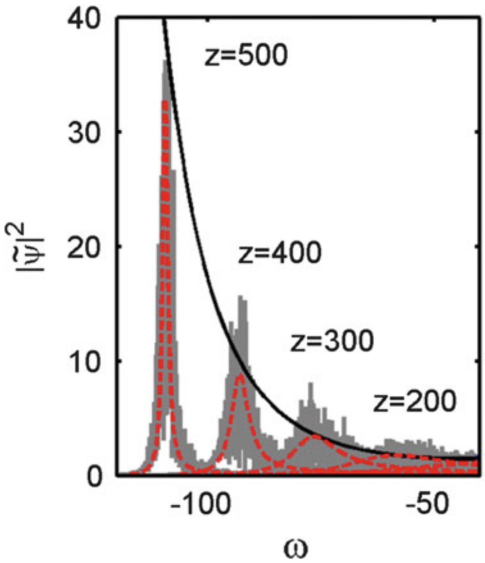

Fig. 9 Inhibition of incoherent shocks with an exponential response function. Without background spectral noise the spectrum exhibits a collapse-like behavior: NLS (33), *gray*; singular kinetic equation (39), *dashed–red* ($\tau_R = 5\tau_0$). The *dark continuous line* denotes the theoretical behavior $\sim 1/[z^2 n^0(\omega = \tilde{c}z)]$, with $\tilde{c} = -\gamma N/\tau_R$, predicted from the first term of equation (39) and the corresponding analytical solution (40). *Source*: from [100]

4 Wave Turbulence Kinetic Equation

In the previous Sects. 2, 3 we considered the Vlasov and WT Langmuir equations which are quadratic nonlinear equations whose derivations refer to a first-order closure of the hierarchy of moments equations. These kinetic equations are formally reversible and describe, in particular, the spontaneous formation of incoherent soliton structures. Let us now consider the following two limits. (1) In the spatial domain the limit of homogeneous statistics of a broadband incoherent wave, so that the Vlasov equation becomes irrelevant, as commented through Fig. 2 in Sect. 1. (2) In the temporal domain the limit of stationary statistics and instantaneous response of the nonlinearity, so that the WT Langmuir equation becomes irrelevant, as commented through Fig. 3. In both limits, we thus need to close the hierarchy of the moments equations to the second-order. The analysis reveals that in this case the appropriate formalism for the description of the random wave is provided by the (Hasselmann) WT kinetic equation, which is a cubic nonlinear equation.

4.1 Kinetic Equation in a Waveguide

4.1.1 Properties of the Kinetic Equation

The WT description of a random wave has been essentially developed in the ideal situation in which the random wave is supposed ‘infinitely extended in space’, an assumption that may be considered as justified when its correlation length is much smaller than the size of the whole beam. However, the propagation of an incoherent localized beam is eventually affected by incoherent diffraction, which inevitably affects the processes of thermalization and condensation. In the following we derive the WT kinetic equation by considering the propagation of the incoherent beam in an optical waveguide. In the guided configuration, incoherent diffraction is compensated by a confining potential, thus allowing to study the thermalization and the condensation of the optical field over large propagation distances. Accordingly, we consider the NLS equation with a confining potential $V(\boldsymbol{x})$ and we formulate a WT description of the random wave into the basis of the eigenmodes of the waveguide (i.e., potential's eigenmodes), instead of the usual plane-wave Fourier basis relevant to statistically homogeneous random waves [$V(\boldsymbol{x}) = 0$] [135].

The NLS equation with a confining potential $V(\boldsymbol{x})$ reads

$$i\partial_z\psi = -\alpha\nabla^2\psi + V(\boldsymbol{x})\psi - \gamma|\psi|^2\psi. \tag{41}$$

Note that in this section we deal essentially with a defocusing nonlinearity, $\gamma < 0$ (so as to ensure the stability of the homogeneous plane-wave solution, i.e., condensate). We recall that this NLS equation conserves the power of the optical field, $N = \int |\psi|^2\, d\boldsymbol{x}$. The NLS equation also conserves the total energy (Hamiltonian) $H = E + U$, which has a linear contribution,

$$E = \int \alpha|\nabla\psi|^2\, d\boldsymbol{x} \; + \int V(\boldsymbol{x})|\psi|^2\, d\boldsymbol{x}, \tag{42}$$

and a nonlinear contribution,

$$U = -\frac{\gamma}{2}\int |\psi|^4\, d\boldsymbol{x}. \tag{43}$$

The potential $V(\boldsymbol{x})$ models the waveguide in which the optical beam propagates. If one considers a multimode optical fiber, the waveguide potential exhibits a revolution symmetry with respect to the axis of propagation of the beam. Then a direct correspondence exists between $V(|\boldsymbol{x}|)$ and the transverse refraction index profile of the waveguide. For a graded-index multimode fiber, we have $V(|\boldsymbol{x}|) = qx^2$ if $|\boldsymbol{x}| \leq a$ and $V(|\boldsymbol{x}|) = V_0$, if $|\boldsymbol{x}| \geq a$, where $q = V_0/a^2$ [135]. This potential is schematically illustrated in Fig. 10. In this way the finite depth of the potential $V_0 < \infty$ introduces an effective frequency cut-off for the classical wave. This is due to the fact that the nonlinear coupling among bounded and unbounded modes is negligible, because of the poor spatial overlap of the corresponding modes.[1]

[1]The efficiency of the generation of unbounded modes ($\omega \leq V_0$) is several orders of magnitude smaller than the conversion efficiency between bounded modes ($\omega \leq V_0$), so that their excitations can be neglected [for details see Appendix 4 in [135]].

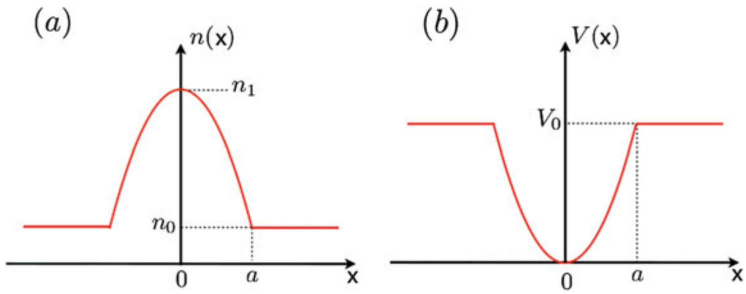

Fig. 10 Refractive index profile $n(x)$ of an optical waveguide (*graded-index fiber*) (**a**), and corresponding confining potential $V(x)$ in the NLS equation (41) (**b**). The finite depth of the potential introduces an effective frequency cut-off for the classical wave problem. The existence of an inhomogeneous (e.g., parabolic) potential reestablishes wave condensation in the thermodynamic limit in 2D, in analogy with quantum Bose-Einstein condensation

4.1.2 Basic Considerations

We assume that the initial random field $\psi(\boldsymbol{x}, z = 0)$ can be expanded into the orthonormal basis of the eigenmodes of the linearized NLS equation [Eq. (41) with $\gamma = 0$],

$$\psi(\boldsymbol{x}, z = 0) = \sum_m c_m(z = 0)\, u_m(\boldsymbol{x}), \tag{44}$$

where the index $\{m\}$ labels the two numbers (m_x, m_y) needed to specify the mode that $u_m(\boldsymbol{x})$ refers to. The modal coefficients are random variables uncorrelated with one another, $\langle c_m(z = 0) c_n^*(z = 0) \rangle = n_m(z = 0)\, \delta^K_{n,m}$, $\delta^K_{n,m}$ being the Kronecker's symbol. We remark that this formalism is also known as the Karhunen-Loeve expansion [118]. The eigenmodes $u_m(\boldsymbol{x})$ are orthonormal, $\int u_m(\boldsymbol{x})\, u_n^*(\boldsymbol{x})\, d\boldsymbol{x} = \delta^K_{n,m}$, and satisfy the 'stationary' (i.e., z-independent) Schrödinger equation

$$\beta_m u_m(\boldsymbol{x}) = -\alpha \nabla^2 u_m(\boldsymbol{x}) + V(\boldsymbol{x}) u_m(\boldsymbol{x}), \tag{45}$$

with the corresponding eigenvalues β_m.

As it propagates through the waveguide the incoherent field $\psi(\boldsymbol{x}, z)$ can be represented as a superposition of modal waves with random coefficients $c_m(z)$, which denotes the respective modal occupancy:

$$\psi(\boldsymbol{x}, z) = \sum_m c_m(z)\, u_m(\boldsymbol{x})\, \exp(-i\beta_m z). \tag{46}$$

In the linear regime of propagation $\gamma = 0$, we have $c_m(z) = c_m(z = 0)$. In the nonlinear regime, we will follow in the next section the procedure of the random phase approximation underlying the WT theory [30, 39]. In particular, the modal occupancies $c_m(z)$ are still random variables uncorrelated with one another, $\langle c_m(z) c_n^*(z) \rangle = n_m(z)\, \delta^K_{n,m}$. The modal occupancies $n_m(z)$ satisfy a coupled system of nonlinear equations that we shall describe below.

The average local power of the field is $\langle |\psi(\boldsymbol{x}, z)|^2 \rangle = \sum_m n_m(z)\, |u_m(\boldsymbol{x})|^2$, and a spatial integration over $\boldsymbol{x}$ gives the total average power of the beam

$$N = \sum_m n_m(z), \tag{47}$$

which is a conserved quantity. The parameter $n_m(z)$ thus denotes the amount of power in the mode $\{m\}$. It can be obtained by projecting the field $\psi(\boldsymbol{x}, z)$ on the corresponding eigenmode $u_m(\boldsymbol{x})$,

$$n_m(z) = \left\langle \left| \int \psi(\boldsymbol{x}, z)\, u_m^*(\boldsymbol{x})\, d\boldsymbol{x} \right|^2 \right\rangle = \langle |c_m(z)|^2 \rangle. \tag{48}$$

Wave condensation takes place when the fundamental mode becomes macroscopically populated, i.e., when $n_0 \gg n_m$ for $m \neq 0$ [136, 137].

In the same way, by substituting the modal expansion of the incoherent field $\psi(\boldsymbol{x}, z)$ into the expression of the linear energy (42), one obtains

$$E(z) = \sum_m E_m(z) = \sum_m n_m(z)\, \beta_m. \tag{49}$$

The total linear energy is the sum of the modal energies weighted by the corresponding modal occupancy $n_m(z)$.

4.1.3 Wave Turbulence Kinetic Equation in a Waveguide

We now study the influence of a weak nonlinear coupling among the modes, so that the modal occupancies defined by (48) depend on z, $n_m(z)$. This weakly nonlinear regime precisely corresponds to the regime investigated numerically in Sect. 4.3.7. Substituting the modal expansion (46) into the NLS equation (41), one obtains

$$i\partial_z a_m = \beta_m a_m - \gamma \sum_{p,q,s} W_{mpqs} a_p a_q^* a_s \tag{50}$$

where $a_m(z) = c_m(z) \exp(-i\beta_m z)$, and the fourth-order tensor is defined by the overlap integral

$$W_{mpqs} = \int u_m^*(\boldsymbol{x}) u_p(\boldsymbol{x}) u_q^*(\boldsymbol{x}) u_s(\boldsymbol{x})\, d\boldsymbol{x}. \tag{51}$$

Equation (50) conserves the total power $N = \sum_m |a_m|^2$ and the Hamiltonian

$$H = \sum_m \beta_m |a_m|^2 - \frac{\gamma}{4} \sum_{m,p,q,s} \left(W_{mpqs} a_m^* a_p a_q^* a_s + W_{mpqs}^* a_m a_p^* a_q a_s^* \right). \tag{52}$$

Starting from Eq. (50) and following the procedure of the random phase approximation [30, 39], we derived in [135] the irreversible kinetic equation governing the nonlinear evolution of the modal occupancies. For this purpose, we take the continuum limit of the discrete sum over the modes $\{m\}$, which is justified when one deals with a large number of modes, i.e., $V_0/\beta_0 \gg 1$. The substitution of the discrete sums by continuous integrals also refers to the so-called 'semiclassical description of the excited states' [137]. Its validity implies that the relevant excitation energies contributing to the discrete sum are much larger than the level spacing β_0, i.e., the spreading of the modal occupancies is much larger than β_0. In [135], the following kinetic equation governing the irreversible evolution of the modal occupancies has been derived:

$$\begin{aligned}
\partial_z \tilde{n}_{\boldsymbol{\kappa}}(z) = \frac{4\pi\gamma^2}{\beta_0^6} & \iiint d\boldsymbol{\kappa}_1 d\boldsymbol{\kappa}_2 d\boldsymbol{\kappa}_3 \delta(\tilde{\beta}_{\kappa_1} + \tilde{\beta}_{\kappa_3} - \tilde{\beta}_{\kappa_2} - \tilde{\beta}_{\kappa}) |\tilde{W}_{\kappa\kappa_1\kappa_2\kappa_3}|^2 \\
& \times \tilde{n}_{\kappa} \tilde{n}_{\kappa_1} \tilde{n}_{\kappa_2} \tilde{n}_{\kappa_3} \left(\tilde{n}_{\kappa}^{-1} + \tilde{n}_{\kappa_2}^{-1} - \tilde{n}_{\kappa_1}^{-1} - \tilde{n}_{\kappa_3}^{-1} \right) \\
& + \frac{8\pi\gamma^2}{\beta_0^2} \int d\boldsymbol{\kappa}_1 \delta(\tilde{\beta}_{\kappa_1} - \tilde{\beta}_{\kappa}) |\tilde{U}_{\kappa\kappa_1}(\tilde{\mathbf{n}})|^2 (\tilde{n}_{\kappa_1} - \tilde{n}_{\kappa}),
\end{aligned} \tag{53}$$

where

$$\tilde{U}_{\kappa\kappa_1}(\tilde{\mathbf{n}}) = \frac{1}{\beta_0^2} \int d\boldsymbol{\kappa}' \, \tilde{W}_{\kappa\kappa_1\kappa'\kappa'} \, \tilde{n}_{\kappa'}. \tag{54}$$

The functions with a tilde refer to the natural continuum extension of the corresponding discrete functions, i.e., $\tilde{n}_{\boldsymbol{k}}(z) = n_{[\boldsymbol{k}/\beta_0]}(z)$, $\tilde{\beta}_{\kappa} = \beta_{[\kappa/\beta_0]}$, $\tilde{W}_{\kappa\kappa_1\kappa_2\kappa_3} = W_{[\kappa/\beta_0][\kappa_1/\beta_0][\kappa_2/\beta_0][\kappa_3/\beta_0]}$ and so on, where $[x]$ denotes the integer part of x.

The kinetic equations (53), (54) differs from the conventional WT kinetic equation in several respects. First, we remark the presence of the new second term in Eq. (53). Note that this term vanishes when the occupation of a mode depends only on its energy $\tilde{\beta}$. Actually, this term enforces an isotropization of the mode occupancies amongst the modes with the same modal energy. Another important property of the kinetic equation (53) is the presence of the function $\tilde{W}_{\kappa\kappa_1\kappa_2\kappa_3}$ in the collision term. We will discuss this term through the analysis of some particular examples of waveguide configurations.

4.1.4 Application to Specific Examples

The kinetic equations (53), (54) is general and, in principle, relevant to different types of waveguide configurations. We briefly comment this aspect by considering different concrete examples.

We first comment the parabolic potential relevant to graded-index multimode fibers. It is also known to play an important role in experiments involving weakly interacting Bose gases [137]. In the ideal parabolic limit ($V_0 \to \infty$), $u_m(\boldsymbol{x})$ refer to the normalized Hermite-Gaussian functions with corresponding eigenvalues $\beta_m = \beta_{m_x,m_y} = \beta_0(m_x + m_y + 1)$,

$$u_{m_x,m_y}(x,y) = \kappa(\pi m_x!\, m_y!\, 2^{m_x+m_y})^{-1/2} H_{m_x}(\kappa x)\, H_{m_y}(\kappa y)\, \exp[-\kappa^2(x^2+y^2)/2], \tag{55}$$

where $\kappa = (q/\alpha)^{1/4}$. In the continuum limit, we have $\tilde{\beta}_{\boldsymbol{\kappa}} = \kappa_x + \kappa_y + \beta_0$. This expression plays the role of a generalized *anisotropic* dispersion relation, whose wave vector reads $\boldsymbol{\kappa} = \beta_0(m_x, m_y)$. The parabolic potential will be discussed in more detail below, in relation with wave condensation in a waveguide in Sect. 4.3.7.

An other example that can easily be illustrated is the circular waveguide of radius R, whose index of refraction is supposed to be constant for $|\boldsymbol{x}| < R$ ('step-index' waveguide). We assume the waveguide to be of infinite depth for simplicity. The field can be expanded into the orthonormal basis of the Bessel functions, $\psi(\boldsymbol{x}, z) = \sum_{l,s} c_{l,s}(z) u_{l,s}(\boldsymbol{x}) \exp(-i\beta_{l,s} z)$, with

$$u_{l,s}(\boldsymbol{x}) = \frac{1}{\sqrt{\pi R^2 J_{l+1}^2(x_{l,s})}} J_l(x_{l,s}|\boldsymbol{x}|/R) \exp(il\theta), \tag{56}$$

where $J_l(x)$ is the Bessel function of the first kind, $x_{l,s}$ is the sth zero of $J_l(x)$, and $(|\boldsymbol{x}|, \theta)$ are the polar coordinates. With these notations, the eigenvalues read $\beta_{l,s} = \alpha x_{l,s}^2/R^2$. In a similar way as above, the passage to the continuum limit can be done by defining the wave vector $\boldsymbol{\kappa} = \beta_{0,1}(l, s)$, which thus leads to the kinetic equation for the evolution of $\tilde{n}_{\boldsymbol{\kappa}}(z)$. Note that with this parametrization of the wave vectors $\boldsymbol{\kappa}$ the density of states $\rho(\beta)$ is uniform.

We finally show that Eq. (53) recovers the traditional WT equation when the field is expanded into the usual plane-wave basis with periodic boundary conditions

$$u_{m_x,m_y}(\boldsymbol{x}) = \frac{1}{L} \exp[2i\pi(m_x x + m_y y)/L], \tag{57}$$

where L stands for the box size and $\boldsymbol{k} = \frac{2\pi}{L}(m_x, m_y)$ the usual wave-vector. This expansion is relevant to the homogeneous problem, i.e., in the absence of the confining potential $[V(x) = 0]$. It models the evolution of the random wave in the presence of a box-shaped confining potential, $V(\boldsymbol{x})$, whose frequency cutoff, $k_c = \pi/dx$ mimics the finite depth of the waveguide, $V_0 \sim \alpha k_c^2$. With this plane-wave modal expansion, one obtains $|\tilde{W}_{\kappa\kappa_1\kappa_2\kappa_3}|^2 = \frac{(2\pi)^2}{L^6}\delta(\boldsymbol{k}_1 + \boldsymbol{k}_3 - \boldsymbol{k}_2 - \boldsymbol{k})$. Because of the Dirac δ-function, the second term in the kinetic equation (53) vanishes, which thus leads to the standard form of the WT kinetic equation

$$\partial_z \tilde{n}_{\boldsymbol{k}}(z) = \mathrm{Coll}[\tilde{n}_{\boldsymbol{k}}], \tag{58}$$

with the collision term

$$\mathrm{Coll}[\tilde{n}_{\boldsymbol{k}}] = \kappa_0\gamma^2 \iiint d\boldsymbol{k}_1 d\boldsymbol{k}_2 d\boldsymbol{k}_3 \delta\left(\omega_{k_1} + \omega_{k_3} - \omega_{k_2} - \omega_k\right) \delta(\boldsymbol{k}_1 + \boldsymbol{k}_3 - \boldsymbol{k}_2 - \boldsymbol{k}) \mathcal{Q}(\tilde{\mathbf{n}}), \tag{59}$$

where $\kappa_0 = 4\pi/(2\pi)^2$, the dispersion relation is $\omega(k) = \alpha k^2$, and

$$\mathcal{Q}(\tilde{\mathbf{n}}) = \tilde{n}_{\boldsymbol{k}}\tilde{n}_{\boldsymbol{k}_1}\tilde{n}_{\boldsymbol{k}_2}\tilde{n}_{\boldsymbol{k}_3}\left(\tilde{n}_{\boldsymbol{k}}^{-1} + \tilde{n}_{\boldsymbol{k}_2}^{-1} - \tilde{n}_{\boldsymbol{k}_1}^{-1} - \tilde{n}_{\boldsymbol{k}_3}^{-1}\right). \tag{60}$$

As discussed in the Introduction, this kinetic equation can be derived by making use of a rigorous mathematical technique based on a multi-scale expansion of the cumulants of the nonlinear wave, as originally formulated in [40–42], and recently studied in more details through the analysis of the probability distribution function of the random field [33].

It is interesting to note that in the 1D case, the degenerate phase-matching conditions lead to a vanishing collision term in Eq. (59). This aspect has been discussed in [138], in relation with integrable turbulence, a subject of growing interest [29, 139]. Notice that the presence of a nonlocal nonlinearity also leads to a vanishing collision term in 1D—though contrary to the integrable NLS case, the hierarchy of the moments equations can be closed to the next order in the presence of nonlocality. Instead of the usual four-wave resonant interaction [Eq. (58)], one obtains in this case a six-wave resonant interaction process. We refer the reader to [68] for a detailed discussion of this interesting six-wave nonlinear dynamics.

4.2 Thermalization and Nonequilibrium Kolmogorov-Zakharov Stationary States

We will describe the essential properties of the WT kinetic equation by considering the standard version of the homogeneous WT kinetic equation, i.e., Eqs. (58)–(60) [with $V(\boldsymbol{x}) = 0$], while the influence of the potential trap will be discussed in Sect. 4.3.7. Note that, to avoid cumbersome notations, in the following we drop the tilde notation adopted here above [in particular we substitute the notation $\tilde{n}_{\boldsymbol{\kappa}}(z)$ with the standard notation $n_{\boldsymbol{k}}(z)$]. We will also generalize the presentation of the results to a spatial dimension $d = 2$ or $d = 3$ in the framework of the dimensionless NLS equation

$$i\partial_z\psi = -\nabla^2\psi + a|\psi|^2\psi. \tag{61}$$

For $d = 2$, the spatial variable has been normalized with respect to the healing length $\Lambda = (\alpha L_{nl})^{1/2}$ (see Sect. 2). In the same way, for $d = 3$ the additional temporal variable has been normalized with respect to the healing time $\tau_0 = (|\beta|L_{nl})^{1/2}$ (see Sect. 3). The variables can be recovered in real units through the transformation: $z \to zL_{nl}, t \to t\tau_0, \boldsymbol{x} \to \boldsymbol{x}\Lambda, \psi \to \psi\sqrt{\rho}$, where we recall that $\rho = N/L^d$ denotes the wave intensity (see Sect. 2). Note that in this section we deal essentially with a defocusing nonlinearity, so as to ensure the stability of the homogeneous plane-wave solution ('condensate'). The parameter $a = -\text{sign}(\gamma)$ then denotes the sign of the nonlinearity, $a > 0$ ($a < 0$) for a defocusing (focusing) nonlinearity. We keep in mind that for $d = 3$ the Laplacian operator in Eq. (61) accounts for both diffraction and dispersion effects, $\nabla^2 = \partial_{xx} + \partial_{yy} + \partial_{tt}$, where we implicitly assumed that the wave propagates in the anomalous dispersion regime, so that chromatic dispersion acts in the same way as diffraction effects, and thus ensures the stability of the monochromatic plane-wave solution in the defocusing regime [140].

4.2.1 Thermodynamic Rayleigh-Jeans Spectrum

The WT kinetic equation has a structure analogous to the celebrated Boltzmann's equation, which is known to describe the evolution of a dilute classical gas far from the equilibrium state [141]. For this reason the kinetic equation (58) exhibits properties similar to those of the Boltzmann's equation. It conserves the total power (or quasi-particle number) of the field

$$N = L^d \int n_{\boldsymbol{k}}(z) d\boldsymbol{k}, \tag{62}$$

the momentum

$$\boldsymbol{P} = L^d \int \boldsymbol{k} n_{\boldsymbol{k}}(z) d\boldsymbol{k}, \tag{63}$$

and the kinetic (linear) energy

$$E = L^d \int \omega(\boldsymbol{k})\, n_{\boldsymbol{k}}(z) d\boldsymbol{k}. \tag{64}$$

Let us remark that Eq. (58) does not conserve the total energy H, but only its linear contribution E. This results from the fact that the nonlinear energy has a negligible contribution in the perturbation expansion procedure of the kinetic theory ($|U/E| \ll 1$).

In analogy with the Boltzmann's equation, the kinetic wave equation is not reversible with respect to the propagation distance z. The irreversible character of Eq. (58) is expressed by the H-theorem of entropy growth, $dS/dz \geq 0$, where the nonequilibrium entropy reads

$$S(z) = L^d \int \log[n_{\boldsymbol{k}}(z)]d\boldsymbol{k}. \tag{65}$$

As in standard statistical mechanics, the thermodynamic equilibrium state is determined from the extremum of entropy, subject to the constraint of conservation of kinetic energy (64), momentum (63) and power (62). The method of the Lagrange multipliers thus gives the thermodynamic Rayleigh-Jeans equilibrium distribution

$$n_{\boldsymbol{k}}^{eq} = \frac{T}{\omega(k) - \boldsymbol{k}.\boldsymbol{v} - \mu}. \tag{66}$$

The parameters T, μ and $\boldsymbol{v}$ are in principle arbitrary and refer to the temperature, chemical potential and mean velocity, by analogy with thermodynamics. We underline that there exist a one-to-one correspondence between $(T, \mu, \boldsymbol{v})$ and the conserved quantities $(E, N, \boldsymbol{P})$. This means that the evolution of the wave is described in the framework of the microcanonical statistical ensemble, in contrast with the conventional canonical treatment using a thermal bath [137]. Note that the equilibrium distribution (66) yields an exactly vanishing collision term (58), $\mathrm{Coll}[n^{eq}] = 0$. This means that once the spectrum has reached the equilibrium distribution (66), it no longer evolves during the propagation, $\partial_z n_{\boldsymbol{k}} = 0$.

In many cases the equilibrium distribution is spherically symmetric and the Rayleigh-Jeans distribution takes the following simplified form

$$n_k^{eq} = \frac{T}{\omega(k) - \mu}. \tag{67}$$

This equilibrium spectrum is Lorentzian-shaped and the chemical potential characterizes the correlation length of the field at equilibrium, $\lambda_c^{eq} \sim 1/\sqrt{-\mu}$. However, we will see that the Langrange multiplier associated to momentum conservation plays an essential role for the study of multiple interacting wave-packets [142], or in the presence of higher-order dispersion effects that lead to an asymmetric supercontinuum equilibrium spectrum, see Sect. 5.2.

4.2.2 Nonequilibrium Kolmogorov-Zakharov Stationary Spectra

As discussed in the introduction, the process of thermalization is physically relevant when one considers a Hamiltonian wave system, which can be considered as an 'isolated' system. Conversely, when one considers a dissipative system which is driven far from equilibrium by an external source, then it no longer relaxes toward the Rayleigh-Jeans equilibrium distribution (66). A typical physical example of forced system could be the excitation of hydrodynamic surface waves by the wind. In general, the frequency-scales of forcing and damping differ significantly. The nonlinear interaction leads to an energy redistribution among the frequencies and an important problem is to find the stationary spectra of the system.

V.E. Zakharov was the first to realize that the kinetic equation of weak-turbulence theory also admits nonequilibrium stationary solutions [30, 143]. Contrary to the Rayleigh-Jeans equilibrium distribution, these stationary solutions carry a non-vanishing flux of conserved quantities, i.e., the energy and the particle fluxes. Such nonequilibrium stationary distributions are the analogue of the Kolmogorov spectra of hydrodynamic turbulence proposed by Kolmogorov in his theory in 1941. Zakharov used a clever set of 'conformal transformations' to show that the kinetic equation admits finite flux spectra as exact stationary solutions.

The formation of these nonequilibrium stationary solutions requires the existence of a permanent forcing or damping in the system, a feature that has been widely studied theoretically [30, 32, 33] (also see [144, 145]), and experimentally in different circumstances (e.g., surface waves, spin waves, surface tension waves, capillary waves, elastic waves). In optics, an experiment aimed at observing these nonequilibrium stationary spectra has been reported in [67] and reviewed in [68]. In this case, the optical system is forced at the entry of the nonlinear medium ($z = 0$), and the formation of the nonstationary spectrum was observed in the transient propagation of the optical wave. Actually, in optics the propagation length z plays the role of time, so that the observation of a permanent nonequilibrium stationary state would require a forcing and a damping at any z. This situation is rather artificial in optics, so that, so far, Kolmogorov-Zakharov spectra did not play a major role in nonlinear optics experiments. For this reason, we will not discuss such nonequilibrium stationary states and refer the reader to [30, 33, 43] for details. For concreteness, we just give here the expressions of the nonequilibrium stationary solutions

$$n_{\boldsymbol{k}}^{Q} = C_Q \frac{Q^{1/3}}{k^{\alpha_Q}} \tag{68}$$

$$n_{\boldsymbol{k}}^{P} = C_P \frac{P^{1/3}}{k^{\alpha_P}} \tag{69}$$

where Q and P are the particle and energy fluxes in frequency space and C_P, C_Q are prefactors. These solutions are exact stationary solutions of the WT kinetic equation (58). The exponents α_Q and α_P depend on the scaling of the dispersion relation and on the explicit nonlinearities. Considering the particular example of the NLS equation (61), one obtains $\alpha_Q = d - 2/3$ and $\alpha_P = d$, where d denotes the spatial dimension.

It is interesting to note that the process of relaxation to a stationary spectrum can be described by means of self-similar solutions of the WT kinetic equation. In substance, the non-stationary solution describes a self-similar front that propagates in frequency-space and which leaves a quasi-stationary state in its wake. This self-similar relaxation solution can be obtained for both equilibrium and nonequilibrium Kolmogorov-Zakharov stationary solutions of the kinetic equation. We refer the reader to [38, 146–148] for more details concerning the properties of these self-similar solutions. So far, these non-stationary solutions have not been exploited in the context of optical waves.

4.3 Wave Condensation

The phenomenon of wave thermalization can be characterized by a self-organization process, in the sense that it is thermodynamically advantageous for the system to generate a large-scale coherent structure in order to reach the most disordered equilibrium state. A remarkable example of this counterintuitive phenomenon is provided by wave condensation [33, 53, 55, 57, 135, 149], whose thermodynamic equilibrium properties are analogous to those of quantum Bose-Einstein condensation [55]. Classical wave condensation can be interpreted as a redistribution of energy among different modes, in which the (kinetic) energy is transferred to small scales fluctuations, while an inverse process increases the power (i.e., number of 'particles') into the lowest allowed mode, thus leading to the emergence of a large scale coherent structure [55, 57, 149, 150]. It is important to note that the phenomenon of wave condensation has been extended in this last decade to optical cavity systems [58–61, 64, 65, 151], which raises interesting questions on the relation between laser operation and the Bose-Einstein condensation of photons [66, 152–154]. These aspects will be discussed in more details in Sect. 5.

4.3.1 Wave Condensation in the Cubic NLS Equation

4.3.2 3D: Condensation in the Thermodynamic Limit

To describe the thermodynamic equilibrium properties of the condensation process in three dimensions it is important to point out some preliminary observations. We remark that the distribution (67) realizes the maximum of the entropy $S[n_{\mathbf{k}}]$ and vanishes exactly the collision term, $\mathrm{Coll}[n_k^{eq}] = 0$. However, note that Eq. (67) is only a *formal* solution, because it does not lead to converging expressions for the energy E and the power N in the limits $k \to \infty$, a feature which is usually termed 'ultraviolet catastrophe'. The usual way to regularize such unphysical divergence is to introduce an ultraviolet cut-off k_c. Note that a frequency cut-off appears naturally in the numerical simulation through the spatial discretization (dx) of the NLS equation (61), $k_c = \pi/dx$. As will be discussed in detail in Sect. 4.3.7, an effective physical frequency cut-off arises naturally in the guided wave configuration of the optical field.

Following the procedure of [55], one can combine Eqs. (62)–(64) and (67), which gives the expression for the power of the field at equilibrium

$$\frac{N}{L^3} = 4\pi\, Tk_c \left[1 - \frac{\sqrt{-\mu}}{k_c} \arctan\left(\frac{k_c}{\sqrt{-\mu}}\right)\right], \tag{70}$$

$$\frac{E}{L^3} = \frac{4\pi\, Tk_c^3}{3} \left[1 + 3\frac{\mu}{k_c^2} + 3\left(\frac{-\mu}{k_c^2}\right)^{\frac{3}{2}} \arctan\left(\frac{k_c}{\sqrt{-\mu}}\right)\right]. \tag{71}$$

An inspection of Eq. (70) reveals that μ tends to 0^- for a non-vanishing temperature T, keeping a constant power density N/L^3. This means that the correlation length λ_c diverge to infinity [see Eq. (67)]. By analogy with the Bose-Einstein transition in quantum systems, such a divergence of the equilibrium distribution at $\boldsymbol{k} = 0$ reveals the existence of a condensation process.

As in standard Bose-Einstein condensation, the fraction of condensed power N_0/N vs the temperature T (or the energy E), may be calculated by setting $\mu = 0$ in the equilibrium distribution (67). Note that the assumption $\mu = 0$ for $T \le T_c$ can be justified rigorously in the thermodynamic limit (i.e., $L \to \infty$, $N \to \infty$, keeping N/L^3 constant). One readily obtains $(N - N_0)/L^3 = 4\pi Tk_c$ and $E/L^3 = 4\pi Tk_c^3/3$, which gives

$$N_0/N = 1 - E/E_c, \tag{72}$$

where the critical energy reads $E_c = Nk_c^2/3$. Alternatively, the fraction of condensed power may be expressed as a function of the temperature,

$$N_0/N = 1 - T/T_c, \tag{73}$$

where $T_c = 3E_c/(4\pi L^3 k_c^3)$. As in standard Bose-Einstein condensation, N_0 vanishes at the critical temperature T_c, and N_0 becomes the total number of particles as T tends to 0.

4.3.3 Weakly Nonlinear Regime: Weak Condensate Amplitude

The linear behavior of n_0 vs E in Eq. (72) is consistent with the results of numerical simulations. However note that Eq. (72) is derived for a spherically symmetric continuous distribution of $n_{\boldsymbol{k}}$, while in the numerics the integration is discretized. A discretization of Eq. (72) leads to a better agreement between the theory and the numerical simulations of Eq. (61) [55]. More precisely, making use of wave turbulence theory, one may express the averaged total energy of the field $\langle H\rangle$ in terms of the condensed particles n_0, which gives [57]

$$\frac{\langle H\rangle}{L^3} = (n - n_0)\frac{\sum_{\boldsymbol{k}}' 1}{\sum_{\boldsymbol{k}}' \frac{1}{k^2}} + a\left(n^2 - \frac{1}{2}n_0^2\right), \tag{74}$$

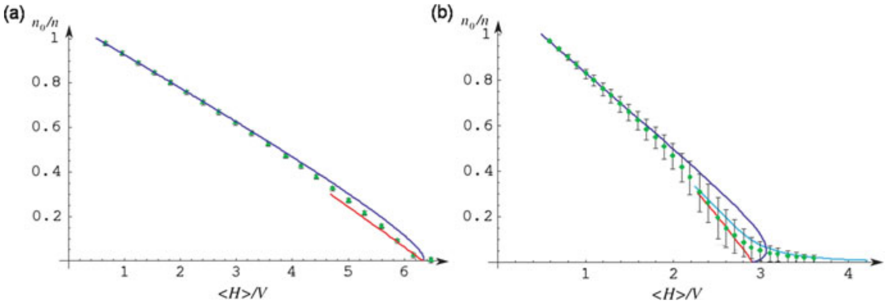

Fig. 11 Condensate fraction n_0/n vs total energy density $\langle H\rangle/L^d$. Points (*diamond*) refer to numerical simulations of the normalized NLS Eq. (61) for $d = 3, N_* = 32^3$ modes (**a**), and $d = 2, N_* = 32^2$ modes (**b**) $[N/L^d = 1, dx = 1\ (k_c = \pi)]$. Each numerical point corresponds to a time average over 3000 time units once the equilibrium state is reached. The *red line* corresponds to the condensation curve in the presence of a small condensate amplitude [WT regime, Eq. (74)], while the *blue line* in the presence of a high-condensate amplitude [Bogoliubov regime, Eq. (75)]. The *green line* in (**b**) refers to the condensation curve for a non-vanishing chemical potential, [Eq. (76), (77)]. The bars denote the amplitude of the fluctuations of n_0/n at equilibrium. *Source*: from [57]

where $\sum_{\boldsymbol{k}}'$ denotes the sum over the whole frequency space which excludes the mode $\boldsymbol{k} = 0$ ($n_0 \equiv N_0/L^d$, $n \equiv N/L^d$). This expression is plotted in Fig. 11 (red line), and it is in good agreement with the numerical simulations in the regime of weak condensation (typically $n_0 < 0.3$).

4.3.4 Bogoliubov Regime: Strong Condensate Amplitude

To describe the regime of strong condensation, one has to take into account the "interactions between the quasi-particles". To include the nonlinear (interaction) contribution, the Bogoliubov's expansion procedure of a weakly interacting Bose gas has been adapted to the classical wave problem. The interested reader may find the details of the analysis in [55, 57]. One obtains the following closed relation between the total energy and the fraction of condensed power

$$\frac{\langle H\rangle}{L^3} = (n - n_0)\frac{\sum_{\boldsymbol{k}}' 1}{\sum_{\boldsymbol{k}}' \frac{k^2 + an_0}{k^4 + 2an_0k^2}} + \frac{a}{2}\left[n^2 + (n - n_0)^2\right]. \tag{75}$$

In the presence of high-condensate amplitudes, this expression is in quantitative agreement with the numerical simulations of the NLS equation (61), without any adjustable parameter (see Fig. 11).

4.3.5 2D: Condensation Beyond the Thermodynamic Limit

Let us now consider the condensation process in two dimensions. The analysis exposed above in 3D may readily be applied to 2D, which gives $N/L^2 = \pi T \log(1 - k_c^2/\mu)$. It becomes apparent from this expression that, for a fixed power density N/L^2, μ reaches zero for a vanishing temperature T. In complete analogy with the Bose-Einstein condensation, this indicates that condensation no longer takes place in 2D. In other terms, the critical temperature T_c tends to zero because of the infrared divergence of the equilibrium distribution $n_{\boldsymbol{k}}^{eq}$. Actually, this result is rigorously correct in the thermodynamic limit (i.e., $L \to \infty$, $N \to \infty$, keeping $n \equiv N/L^2$ constant). Nevertheless, for situations of physical interest in which N and L are finite, wave condensation is re-established in two dimensions, a property confirmed by the numerical simulations [57]. Indeed, one can calculate the critical temperature for condensation in two dimensions, $T_c = nL^2/\sum_{\boldsymbol{k}}' 1/k^2$ [150]. This expression reveals that the discrete sum in frequency space provides a non-vanishing value of T_c, while T_c tends to zero in the thermodynamic limit, because of the (infrared) logarithmic divergence of the continuous integral $\int d\boldsymbol{k}/k^2$.

In complete analogy with quantum Bose-Einstein condensation, for a finite surface of the optical beam, wave condensation occurs for a non-vanishing value of the chemical potential, $\mu \neq 0$. The condensation curve may thus be derived without the implicit assumption $\mu = 0$. The interested reader may find the details in [57]. One obtains

$$\frac{\langle H\rangle(\mu)}{L^2} = (n - n_0)\frac{\sum_{\boldsymbol{k}}' \frac{k^2}{k^2-\mu}}{\sum_{\boldsymbol{k}}' \frac{1}{k^2-\mu}} + a\left(n^2 - \frac{1}{2}n_0^2\right), \tag{76}$$

$$\frac{n_0(\mu)}{n} = \frac{1}{-\mu}\frac{1}{\sum_{\boldsymbol{k}} \frac{1}{k^2-\mu}}. \tag{77}$$

We plotted in Fig. 11b the condensate fraction n_0/n [Eq. (77)] vs the energy density $\langle H\rangle/L^2$ [Eq. (76)], as a parametric function of μ. It reveals that a non-vanishing chemical potential makes the transition to condensation "smoother", with the appearance of a characteristic "tail" in the condensation curve. Such a "tail" progressively disappears as the surface L^2 increases, so that the condensation curve n_0/n vs $\langle H\rangle/L^2$ tends to the expression derived in the thermodynamic limit, i.e., Eq. (76) with $\mu = 0$ recovers Eq. (74). Let us remark that the theory is in quantitative agreement with the numerical simulations of the NLS equation (61), as illustrated in Fig. 11.

It results that the critical behaviour of the two-dimensional condensation curve looks similar to that of a genuine "phase transition". Note however that, strictly speaking, "phase transitions" only occur in the thermodynamic limit, so that such terminology is not appropriate for the two dimensional problem considered here. Nevertheless, if one considers the macroscopic occupation of the fundamental mode $\boldsymbol{k} = 0$ as the essential characteristic of condensation, one may say that wave condensation do occur in 2D. It is important to note that for $d = 2$, nearby the transition to condensation some clear evidence of a Berezinskii-Kosterlitz-Thouless transition has been provided, with an algebraic decay of the correlation function of the field [155].

4.3.6 Condensation Beyond the Cubic NLS Equation: Nonlocal and Saturable Nonlinearities

The phenomenon of classical wave condensation has been essentially studied in the framework of the NLS equation in the presence of a pure cubic Kerr nonlinearity. In many cases, however, realistic optical experiments are not modelled by a cubic Kerr nonlinearity. In a recent work [149], it has been shown that wave condensation can take place with more complex nonlinearities. The examples of the nonlocal nonlinearity and of the saturable nonlinearity were considered in [149], which refer to natural extensions of the cubic nonlinearity [140]. It was shown that the generalized NLS equation accounting either for a nonlocal or a saturable nonlinearity describes a process of wave condensation completely analogous to that described in the framework of the cubic Kerr nonlinearity. Following the procedure of the previous Sect. 4.3.1, analytical expressions of the condensate fraction are derived in both the weakly and the strongly nonlinear regimes of propagation, and a quantitative agreement is obtained with the simulations [149].

4.3.7 Condensation in a Waveguide

In the previous Sect. 4.3.1 we have considered wave condensation in the ideal limit in which the incoherent wave is expanded in the plane-wave Fourier basis with periodic boundary conditions. As discussed above, this approach of wave condensation requires the introduction of a frequency cut-off in the theory [55, 57], so as to regularize the ultraviolet catastrophe inherent to classical nonlinear waves. From the physical point of view, such a frequency cut-off is not properly justified for classical waves. We will see that an effective frequency cut-off arises naturally in the guided-wave configuration of the optical beam. This frequency cut-off plays a key role in wave condensation (see Sect. 4.3.1), since it prevents the divergence of the critical energy for condensation [135] [see Eq. (72)]. Moreover, we have also seen that in 2D, wave condensation does not occur in the thermodynamic limit [55, 57]. We will see that a parabolic waveguide configuration reestablishes wave condensation in two dimensions, in analogy with quantum Bose-Einstein condensation [137]. Accordingly, wave condensation and thermalization can be studied accurately through the analysis of the two-dimensional spatial evolution of a guided optical beam.

4.3.8 Rayleigh-Jeans Distribution in a Waveguide

The starting point is the WT kinetic derived in Sect. 4.1 into the basis of the eigenfunctions of the potential $V(\boldsymbol{x})$. Here we follow [135] to describe wave condensation in an optical waveguide. The kinetic equations (53), (54) conserves the power $N = \beta_0^{-2} \int d\boldsymbol{\kappa} n_{\boldsymbol{\kappa}}$ and the energy $E = \beta_0^{-2} \int d\boldsymbol{\kappa} \beta_{\boldsymbol{\kappa}} n_{\boldsymbol{\kappa}}$, where we recall that $\beta_{\boldsymbol{\kappa}} = \kappa_x + \kappa_y + \beta_0$. Contrarily to the homogeneous WT kinetic equation (58), the kinetic equation (53), (54) does not conserve the momentum, a feature which is consistent with the fact that the potential $V(\boldsymbol{x})$ prevents momentum conservation in the NLS equation (41). The kinetic equations (53), (54) exhibits a H-theorem of entropy growth, $d\mathscr{S}/dz \geq 0$, where the nonequilibrium entropy reads $\mathscr{S}(z) = \beta_0^{-2} \int d\boldsymbol{\kappa} \ln(n_{\boldsymbol{\kappa}})$. The Rayleigh-Jeans equilibrium state $n_{\boldsymbol{\kappa}}^{eq}$ realizing the maximum of entropy, subject to the constraints of conservation of E and N, is obtained by introducing the corresponding Lagrange's multipliers,

$$n_{\boldsymbol{\kappa}}^{eq} = \frac{T}{\beta_{\boldsymbol{\kappa}} - \mu}. \tag{78}$$

Note that, in a way akin to the usual Rayleigh-Jeans distribution (67), the temperature denotes the amount of energy $\mathscr{E}_{\boldsymbol{\kappa}}$ that is equipartitioned among the modes of the waveguide. Indeed, in the tails of the equilibrium distribution (78), i.e., $\beta_{\boldsymbol{\kappa}} \gg |\mu|$, we have $\mathscr{E}_{\boldsymbol{\kappa}} = \beta_{\boldsymbol{\kappa}}\, n_{\boldsymbol{\kappa}}^{eq} \sim T$ [see Eq. (49)]. Also note that the equilibrium state (78) cancels both collisions terms of the kinetic Eqs. (53), (54).

This equilibrium property of energy equipartition has been confirmed by the numerical simulations of the NLS equation (41) with a truncated parabolic potential, as illustrated in Fig. 12. To be concrete, in the numerical simulations we considered a realistic graded-index multimode optical fiber, with a radium of 15 µm and an index difference of $n_1 - n_0 = 10^{-3}$ (see Fig. 10), and a refractive index of reference $n_0 = 1.45$. With these parameters the number of modes is $N_* = 66$. It is important to note that silica fibers exhibit a focusing nonlinearity, $\gamma < 0$ in Eq. (41). The incoherent beam may thus exhibit filamentation effects (i.e., speckle beam fragmentation) during its propagation in the fiber. However, as revealed by the numerical simulations, the beam does not exhibit filamentation effects because we consider the weakly nonlinear regime of propagation, in which the linear energy dominates the nonlinear energy, $U/E \ll 1$. The weakly nonlinear condition can easily be satisfied in the framework of the considered optical fiber system, since the nonlinearity of silica fibers is known to be relatively small as compared to other types of commonly used nonlinear optical media. In the numerical simulations, the following standard value of the nonlinear silica coefficient was considered $n_2 = -2 \times 10^{-8}\,\mu\text{m}^2/\text{W}$, together with a power of the beam of 94 kW.

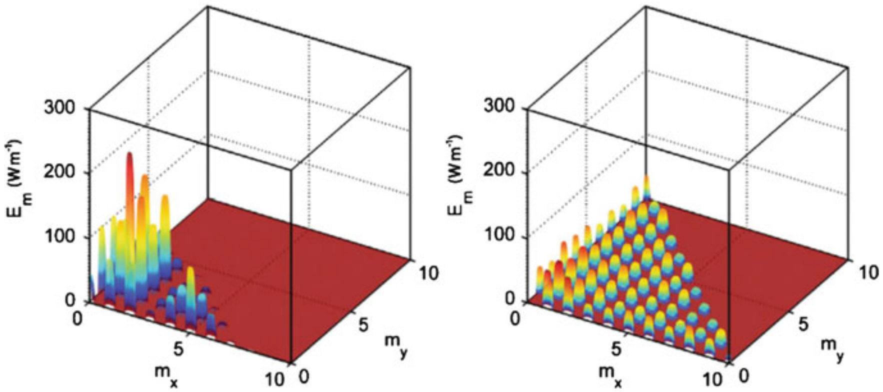

Fig. 12 Condensation and thermalization in a trap: Numerical simulation of the NLS equation (41) with a parabolic potential $V(\boldsymbol{x})$, showing the establishment of energy equipartition among the modes of the waveguide: Energy per mode, $\mathscr{E}_m = \beta_m n_m$ [see Eq. (49)] vs the mode $m = (m_x, m_y)$, in the initial condition (**a**), and averaged over the propagation once the equilibrium state is reached, i.e., $\partial_z \mathscr{S} \simeq 0$ (**b**). The amount of power n_m in the mode $m = (m_x, m_y)$ is calculated by projecting the field amplitude into the corresponding eigenmode [see Eq. (48)]. Energy almost reaches an equipartition among all modes, except the fundamental condensed mode $m_x = m_y = 0$ which is macroscopically populated [not shown in (**a**), (**b**)]. In particular, we considered a truncated parabolic potential (Fig. 10), so that $\beta_{m_x,m_y} \simeq \beta_0(m_x + m_y + 1)$ and only modes whose eigenvalue verifies $\beta_{m_x,m_y} \le V_0$ are guided. *Source*: from [135]

4.3.9 Frequency Cut-Off, Density of States and Thermodynamic Limit

The number of modes involved in the dynamics with a trap $V(\boldsymbol{x})$ is finite because of the truncation of the potential (see Fig. 10, $V_0 < \infty$). In this way the truncated potential introduces an effective frequency cut-off for the classical nonlinear wave, because modes whose eigenvalues exceed the potential depth, $\beta_{\boldsymbol{\kappa}} > V_0$, are not guided during the propagation. A more rigorous justification of this aspect is given in the Appendix of [135]. Note that this is in contrast with the homogeneous problem [$V(\boldsymbol{x}) = 0$ in Eq. (41)], as discussed in Sect. 4.3.1. In this case, the frequency cut-off k_c is introduced by the spatial discretization (dx) of the NLS equation, i.e., $k_c = \pi/dx$, so that in the continuous limit $k_c \to \infty$ (see, e.g., [55]).

Let us discuss the importance of the truncation of the potential ($V_0 < \infty$) through the example of a parabolic potential considered in the numerical simulations (see Figs. 12, 13). Considering the constraint, $\beta_0 \le \beta(\boldsymbol{\kappa}) \le V_0$, as well as the assumption $\beta_0 \ll V_0$ (i.e., large number of modes $N_* \gg 1$), the power of the field at equilibrium reads $N = (T/\beta_0^2) \int_0^{V_0} d\kappa_x \int_0^{V_0-\kappa_x} (\kappa_x + \kappa_y + \beta_0 - \mu)^{-1} \, d\kappa_y$, which gives

$$N = \frac{T}{\beta_0^2} \left[V_0 - \tilde{\mu} \ln \left(\frac{-\tilde{\mu}}{V_0 - \tilde{\mu}} \right) \right], \tag{79}$$

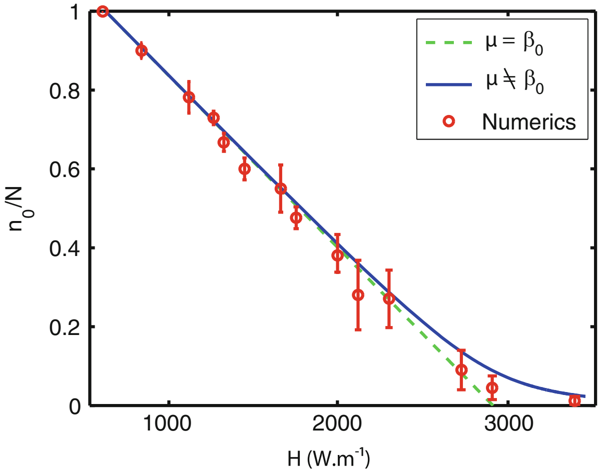

Fig. 13 Wave condensation in a trap: Fraction of power condensed in the fundamental mode at equilibrium, n_0/N, vs the energy of the field, H, for a truncated parabolic potential (parameters are given in Sect. 4.3.7). The *red points* refer to the results of the numerical simulations of the NLS equation (41) with a parabolic potential $V(\boldsymbol{x})$. They have been obtained by averaging n_0/N over the propagation distance once the equilibrium state is reached, i.e., $\partial_z \mathscr{S} \simeq 0$. The '*error-bars*' denote the amount of fluctuations (standard deviation) of n_0/N once equilibrium is reached. The *continuous blue line* refers to the theoretical condensation curve given in Eqs. (82)–(83), while the *dashed green line* refers to the corresponding thermodynamic limit [$\tilde{\mu} \to 0$ in Eqs. (82)–(83)]. In these plots the eigenvalues β_m and eigenmodes $u_m(\boldsymbol{x})$ in Eqs. (82)–(83) account for the truncation of the potential ($V_0 < \infty$). *Source*: from [135]

where we defined $\tilde{\mu} = \mu - \beta_0$. In order to comment expression (79), we recall that in the homogeneous problem [$V(\boldsymbol{x}) = 0$ in Eq. (41)] wave condensation was shown to only occur in 3D, while in 2D the chemical potential was shown to reach zero for a vanishing temperature [55, 57, 150]. In analogy with Bose-Einstein condensation in quantum gases, this means that wave condensation does not occur in the thermodynamic limit in 2D. Conversely, Eq. (79) reveals that $\tilde{\mu} \to 0$ for a non-vanishing critical temperature, $T_c = 4\alpha Nq/V_0$, which indicates that the presence of a parabolic potential $V(\boldsymbol{x})$ reestablishes wave condensation in the thermodynamic limit in 2D. Indeed, the thermodynamic limit for a parabolic potential corresponds to taking $N \to \infty$ and $q \to 0$, keeping constant the product Nq [137]. This result is in complete analogy with the well-known fact that a parabolic potential reestablishes Bose-Einstein condensation in 2D [137]. There is however a difference with quantum condensation. Bose-Einstein condensation is known to be reestablished in a parabolic potential of infinite depth, $V_0 \to \infty$, while here T_c tends to zero in the limit $V_0 \to \infty$. Contrary to the quantum case, one also needs to introduce a finite depth of the potential, $V_0 < \infty$, to get wave condensation in 2D. This condition is satisfied for any optical waveguide configuration.

4.3.10 Condensate Fraction in the Waveguide

We now look for a relation between the fraction of condensed power n_0/N and the temperature T or the energy E, in a way completely analogous to what has been done for the homogeneous problem ($V(\boldsymbol{x}) = 0$) in Sect. 4.3.1. As in the usual interpretation of Bose-Einstein condensation in a trap, we set $\mu = \beta_0$ in the equilibrium distribution (78). Note that the assumption $\tilde{\mu} = \mu - \beta_0 = 0$ for $T \leq T_c$ can be justified rigorously in the 2D thermodynamic limit. Isolating the fundamental mode, one has $N - n_0 = (T/\beta_0^2) \iint_{\mathscr{D}} 1/(\kappa_x + \kappa_y)\, d^2\boldsymbol{\kappa}$, where $n_0 = T/[\beta_0^2(\beta_0 - \mu)]$. We thus readily obtain $N - n_0 = TV_0/\beta_0^2$. Proceeding in a similar way for the energy, one obtains $E - n_0\beta_0 = \frac{TV_0^2}{2\beta_0^2}(1 + 2\beta_0/V_0)$. Eliminating the temperature from the expressions for E and N gives the following expression of the condensate fraction

$$\frac{n_0}{N} = 1 - \frac{E - E_0}{NV_0/2}, \tag{80}$$

where $E_0 = N\beta_0$ refers to the minimum energy, i.e. the energy of the field when all the power is condensed, $n_0/N = 1$. The condensate amplitude n_0/N increases as the energy E decreases, and condensation arises below the critical energy

$$E_c = E_0 + NV_0/2 = \frac{NV_0}{2}\left(1 + \frac{2\beta_0}{V_0}\right). \tag{81}$$

This expression deserves to be commented in two respects. First, because of the truncation of the waveguide potential ($V_0 < \infty$), the value of E_c does not diverge to infinity. This is in contrast with the homogeneous problem [$V(\boldsymbol{x}) = 0$ in Eq. (41)], as discussed above in 2D in Sect. 4.3.1. In this case the critical value of the energy behaves as $E_c \sim Nk_c^2/\ln(k_c)$, where $k_c = \pi/dx$ is the arbitrary frequency cut-off. In the continuous limit in which the spatial discretization of the NLS equation tends to zero, $dx \to 0$, the critical value of the energy E_c diverges to infinity (see, e.g., [55, 57]). A second point that could be remarked in Eq. (81) is that wave condensation is reestablished in the thermodynamic limit in 2D. Indeed, writing Eq. (81) in the following form, $E_c/S = Nq(1 + 2\beta_0/V_0)/(2\pi)$, where $S = \pi a^2$ is the waveguide surface, it becomes apparent that the energy density E_c/S does not tend to zero in the thermodynamic limit ($N \to \infty, q \to 0$, keeping Nq constant). As discussed in the previous Sect. 4.3.9, this is again in contrast with the homogeneous problem and the plane-wave expansion of the field, in which E_c/S tends to zero logarithmically in the thermodynamic limit [57, 150].

The simple analysis of Eqs. (80), (81) outlined above provides physical insight into the process of wave condensation. However, a direct quantitative comparison with the numerical simulations requires the derivation of the condensation curve relating the condensate fraction to the Hamiltonian, as discussed above in Sect. 4.3.1 for the homogeneous problem, $V(\boldsymbol{x}) = 0$. For this purpose, we note that Eq. (80) can be improved along three lines. (1) The continuous integrals by a discrete sum over the modes of the waveguide. One obtains $n_0/N = 1 - (E - E_0)\sum'(m_x + m_y)^{-1}/\left(E_0(N_* - 1)\right)$, where we recall that N_* is the number of modes of the waveguide, and $\sum'$ denotes the sum over all modes $\{m = (m_x, m_y)\}$ excluding the fundamental mode $m = 0$. In the continuous limit we have $\sum' \frac{1}{m_x+m_y} \rightarrow \beta_0^{-1} \iint_{\mathscr{D}} \frac{d^2\boldsymbol{\kappa}}{\kappa_x+\kappa_y} = V_0/\beta_0$ and the number of modes $N_* = \beta_0^{-2} \iint_{\mathscr{D}} d^2\boldsymbol{\kappa} = V_0^2/(2\beta_0^2)$, so that the above equation recovers Eq. (80). (2) A generalization of the expression of the condensate fraction, n_0/N vs E, can be done beyond the thermodynamic limit [57, 150], i.e., without the implicit assumption $\tilde{\mu} = 0$ for $T \leq T_c$. From the physical point of view, this means that we take into account the finite size of the optical waveguide. (3) We include the contribution of the nonlinear energy U into the expression of the condensation curve. We split the contribution of the fundamental mode into the modal expansion of the field, $\psi(\boldsymbol{x}, z) = \psi_0(\boldsymbol{x}, z) + \varepsilon(\boldsymbol{x}, z)$, where $\psi_0(\boldsymbol{x}, z) = c_0(z)u_0(\boldsymbol{x})\exp(-i\beta_0 z)$ is the coherent condensate contribution and $\varepsilon(\boldsymbol{x}, z) = \sum_{m\neq 0} c_m(z)u_m(\boldsymbol{x})\exp(-i\beta_m z)$ is the incoherent contribution. This expansion can be substituted into the expression of U in Eq. (43), and then computed in explicit form by making use of the random phase approximation [135]. The generalizations (1)–(3) finally lead to the following expression of the condensation curve beyond the thermodynamic limit, including the nonlinear contribution of the energy

$$\frac{n_0}{N}(\tilde{\mu}) = \frac{1}{-\tilde{\mu}\sum_m \frac{1}{\beta_m - \beta_0 - \tilde{\mu}}} \tag{82}$$

$$\langle H\rangle(\tilde{\mu}) = N\frac{\sum_m \frac{\beta_m}{\beta_m - \beta_0 - \tilde{\mu}}}{\sum_m \frac{1}{\beta_m - \beta_0 - \tilde{\mu}}} + \langle U\rangle(\tilde{\mu}), \tag{83}$$

where $\langle U\rangle(\tilde{\mu})$ is a cumbersome expression given in [135]. The fraction of condensed power n_0/N is thus coupled to the total energy $\langle H\rangle$ through the non-vanishing chemical potential, $\tilde{\mu} = \mu - \beta_0 \neq 0$. The parametric plot of (82), (83) with respect to $\tilde{\mu}$ is reported in Fig. 13 (continuous line). As for the homogeneous problem [$V(\boldsymbol{x}) = 0$], the long tail in the condensation curve at high energies H is due to the non-vanishing chemical potential, $\tilde{\mu} \neq 0$. In the thermodynamic limit $\tilde{\mu} \rightarrow 0$, the condensation curve (82), (83) recovers the straight line discussed above through Eqs. (80), (81) (see the dashed line in Fig. 13). Let us remark the good agreement between the theoretical condensation curve and the simulations, without using adjustable parameters. We finally note that Eqs. (82), (83) are valid for various different types of waveguide index profiles, provided one makes use of the appropriate eigenvalues β_m and eigenmodes $u_m(\boldsymbol{x})$ (see [135]).

5 Generalizations and Perspectives

5.1 Turbulence in Optical Cavities

The phenomenon of condensation discussed above in Sect. 4.3 has been recently interpreted within a broader perspective in different active and passive optical cavity configurations [58–65]. This raises important questions, such as e.g., the relation between laser operation and the phenomenon of Bose-Einstein condensation. As a matter of fact, these questions are still the subject of vivid debate—we refer the reader to [66, 152, 154, 156] for some recent discussions on this important problem.

An important analogy with condensation has been also discussed in the dynamics of active mode-locked laser systems in the presence of additive noise source [60, 154, 157]. On the basis of their previous works [158, 159], the authors showed that the formation of coherent pulses in actively mode-locked lasers exhibits in certain conditions a transition of the laser mode system to a light pulse state that is similar to Bose-Einstein condensation, in the sense that it is characterized by a macroscopic occupation of the fundamental mode as the laser power is increased. The analysis is based on statistical light-mode dynamics with a mapping between the distribution of the laser eigenmodes to the equilibrium statistical physics of noninteracting bosons in an external potential.

5.1.1 Wave Turbulence in Raman Fiber Lasers

The dynamics of Raman fiber lasers has been also shown to exhibit some interesting analogies with condensation-like phenomena [59, 64, 65]. Here we discuss in more detail these systems in light of the WT theory that has been developed to describe their turbulent dynamics. For more details, we refer the interested reader to [63] for an overview on the WT description of Raman fiber lasers (also see the more recent work [160]).

In [161], the Raman fiber laser is modelled as a turbulent system whose optical power spectrum results from a weakly nonlinear interaction among the multiple modes of the cavity. Performing a mean field approach in which the Raman Stokes field does not evolve significantly over one cavity round trip, the authors of [161] first establish a differential equation for the evolution of the complex amplitude E_n of the nth longitudinal mode

$$\tau_{rt}\frac{dE_n}{dt} - \frac{1}{2}(g-\delta_n)E_n(t) = -\frac{i}{2}\gamma L \sum_{l\neq 0} E_{n-l}(t) \times \sum_{m\neq 0} E_{n-m}(t)E^*_{n-m-l}(t)\exp(2i\beta\, ml\Delta^2\, c\, t). \quad (84)$$

In their approach, the time evolution of E_n is determined by the Raman gain g, the dispersion of the fiber, the losses δ_n of the fiber and of the cavity mirrors, and the four-wave mixing process. γ is the Kerr coupling coefficient and β represents the second-order dispersion coefficient of the cavity fiber. $\Delta = 1/\tau_{rt} = c/2L$ is the free spectral range of the Fabry-Perot cavity that has a length L. Gain, losses and dispersive effects occurring inside the whole laser cavity are supposed to influence the formation of the optical power spectrum through their dependence in frequency-space. In particular fiber Bragg grating mirrors are considered as spectral filters introducing parabolic losses in frequency space ($\delta_n = \delta_0 + \delta_2(n\Delta)^2$). Dispersive effects occurring inside the laser cavity are supposed to be dominantly governed by the second-order dispersion β of the cavity fiber. It must be emphasized that Eq. (84) refers to the discretized version of the one-dimensional NLS equation, in which gain and losses terms have been added [162]. In other words, the approach developed by the authors of [161] amounts to apply a WT treatment to a one-dimensional NLS equation, whose integrability is broken by the presence of gain and loss terms.

Assuming an exponential decay for the correlation function among the modes, $\langle E_n(t)E_n^*(t')\rangle = I_n \exp(-|t-t'|/\tau)$, the following WT kinetic equation that governs the temporal evolution of the intracavity spectrum was derived [161]

$$\tau_{rt}\frac{dI(\Omega)}{dt} = (g - \delta(\Omega))I(\Omega) + S_{\mathrm{FWM}}(\Omega), \tag{85}$$

where $I(\Omega) = \langle E_n E_n^*\rangle/\Delta$. The mathematical expression of the collision term $S_{\mathrm{FWM}}(\Omega)$ can be separated into two parts

$$S_{\mathrm{FWM}}(\Omega) = -\delta_{\mathrm{NL}} I(\Omega) + (\gamma L)^2 \int \frac{\mathscr{F}[I]\, d\Omega_1\, d\Omega_2}{(3\tau_{rt}/\tau)[1 + (4\tau L\beta/3\tau_{rt})^2\Omega_1^2\Omega_2^2]}, \tag{86}$$

where the functional reads $\mathscr{F}[I] = I(\Omega-\Omega_1)I(\Omega-\Omega_2)I(\Omega-\Omega_1-\Omega_2)$, while the nonlinear term responsible for four-wave-mixing-induced losses δ_{NL} reads

$$\delta_{\mathrm{NL}} = (\gamma L)^2 \int \frac{\mathscr{G}[I]\, d\Omega_1\, d\Omega_2}{(3\tau_{rt}/\tau)[1 + (4\tau L\beta/3\tau_{rt})^2\Omega_1^2\Omega_2^2]}, \tag{87}$$

where $\mathscr{G}[I] = [I(\Omega-\Omega_1) + I(\Omega-\Omega_2)]I(\Omega-\Omega_1-\Omega_2) - I(\Omega-\Omega_1)I(\Omega-\Omega_1)$. A stationary solution of the WT kinetic equation (85) has been obtained by Babin et al. in [161], which exhibits the following hyperbolic-secant structure, $I(\Omega) = 2I/\big(\pi\Gamma \cosh(2\Omega/\Gamma)\big)$, where Γ is the width of the intracavity laser power spectrum. This analytical solution is in very good agreement with spectra recorded in experiments in which the fiber laser operates well above threshold, in various different configurations, even in regimes in which the mean field approximation should no longer hold [163]. Although the WT approach developed in [161] has undoubtedly provided a new insight into the physics of Raman fiber lasers, some other numerical and experimental works have raised some interesting questions concerning the applicability of the WT approach to the description of the spectral broadening phenomenon. In particular, numerical simulations of the mean field equations introduced in [161] revealed that the shape of the laser optical power spectrum strongly depends on the sign of the second-order dispersion coefficient [59]. This cannot be captured by the WT theory, which is inherently insensitive to the sign of the second-order dispersion parameter. As pointed out in [162, 164], the formation of the Stokes spectrum is also deeply influenced both by dispersive effects and by the spectral shape of the fiber Bragg grating mirrors used to close the laser cavity.

5.1.2 Laminar-Turbulent Transition in Raman Fiber Lasers

Fast recording techniques have been recently exploited for the experimental characterization of a laminar-turbulent transition in Raman fiber lasers [65]. The fiber laser used in the these experiments has been specifically designed. It is made with dispersion-free ultra-wideband super-Gaussian fiber grating mirrors. Slightly changing the pump power, an abrupt transition with a sharp increase in the width of laser spectrum has been observed, together with an abrupt change of the statistical properties of the Stokes radiation. The laminar state observed before the transition is associated to a multimode Stokes emission with a relatively narrow linewidth and relatively weak fluctuations of the Stokes power. On the other hand, the turbulent state corresponds to a high multimode operation with a wider spectrum and stronger fluctuations of the Stokes power. The laminar-turbulent transition has been also studied by means of intensive numerical simulations (see Fig. 14) [59, 64, 65]. The simulations reveal that, by increasing the pump power, the mechanism underlying the laminar-turbulent transition relies on the generation of an increasing number of

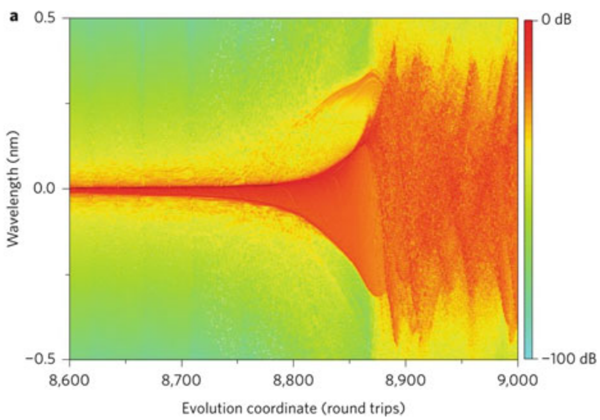

Fig. 14 Numerical simulations evidencing the laminar-turbulent transition in a Raman fiber laser. The evolution of the laser optical power spectrum is plotted as a function of number of round trips inside the laser cavity. *Source*: from [65]

dark (or grey) solitons. This experimental work opens new fields of investigations, in particular as regard the impact of phase-defects on the turbulent dynamics of purely 1D wave systems.

5.1.3 Wave Kinetics of Random Fiber Lasers

Random lasers are a rapidly growing field of research, with implications in soft-matter physics, light localization, and photonic devices [26, 165, 166]. Considering a different perspective, the authors of [160] described the cyclic wave dynamics inherent to laser systems by considering weakly dissipative modifications of the integrable NLS equation. In this way, a 'local kinetic equation' describing the turbulent dynamics of a random fiber laser system is derived [160]. The key property of this kinetic equation is that the δ-function reflecting energy conservation at each elementary four-wave interaction is substituted by an effective Lorentzian function that involves a frequency dependent gain. As a remarkable result, the collision term of the local kinetic equation does not vanish in spite of the trivial resonant conditions inherent to the 1D four-wave interaction with a purely quadratic dispersion relation [138]. From this point of view, the local kinetic equation exhibits properties reminiscent of those considered in [38, 167], although the equations are different, e.g., as regard the renormalization of the dispersion relation by the nonlinearity and the additional nonlinear damping. Then at variance with the purely conservative (Hamiltonian) system, in active cyclic laser systems, the interactions are mediated by a non-homogenous gain, which leads to an effective interaction over the finite interval of the evolution coordinate. We also note that the local kinetic equation is derived under a double separation of scales, i.e., the turbulent regime is dominated by dispersive effects as compared to gain effects, and the gain itself if much larger than gain variation over the typical spectral width of the radiation. Furthermore, the authors confirm their theoretical work by means of direct experimental measurements in random fibre lasers: In the high-power regime, the equilibrium spectrum of the random laser measured experimentally is found in good agreement with the nonequilibrium stationary solution of the local kinetic equation, see Fig. 15. Finally, the theory is also completed by means of a generalization of the linear kinetic Schawlow-Townes theory. For more details on these aspects we refer the reader to [160].

5.1.4 Turbulent Dynamics in Passive Optical Cavities

As commented above, a classical wave can exhibit a genuine process of wave condensation as it propagates in a 2D conservative Kerr material, [33, 55, 135]. Actually, a phenomenon completely analogous to such conservative condensation process can occur in an incoherently pumped passive optical cavity, despite the fact that the system is inherently dissipative [62]. For this purpose, let consider a *passive optical cavity* pumped by an incoherent optical wave, whose time correlation, t_c,

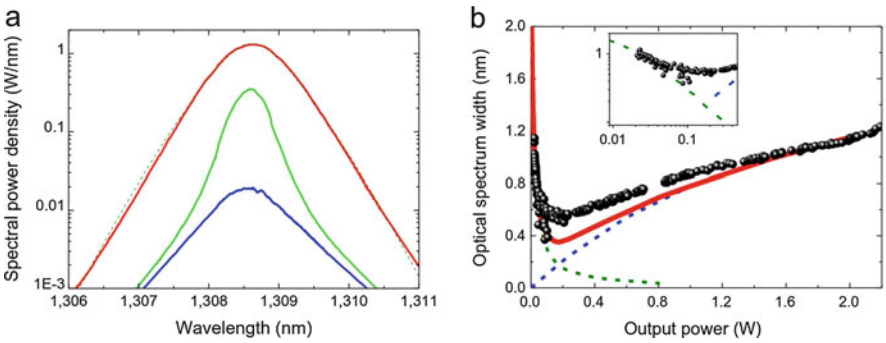

Fig. 15 Nonlinear kinetic description of the random fiber laser optical spectrum. (**a**) Optical spectrum measured experimentally: near the generation threshold (*blue curve*, laser power = 0.025 W), slightly above the generation threshold (*green curve*, 0.2W) and well above the generation threshold (red curve, 1.5 W). The optical spectrum predicted by the local wave kinetic equation, for laser power 1.5 W is shown by *dashed red line*. (**b**) Spectrum width as a function of the laser's output power in theory and experiment. Experimental data are shown by *black circles*. The prediction for the spectrum broadening from the nonlinear kinetic theory based on the local wave kinetic equation (*blue dashed line*). The prediction for the spectral narrowing from the modified linear kinetic Schawlow-Townes theory (*dashed green line*). The *red line* denotes the sum of nonlinear and linear contributions. The inset shows the spectral narrowing near the threshold in log-scale. For more details see [160]. *Source*: from [160]

is much smaller than the round trip time, $t_c \ll \tau_{rt}$. In this way, the optical field from different cycles are mutually incoherent with one another, which makes the optical cavity *non-resonant*. Because of this property, the cavity does not exhibit the widely studied dynamics of pattern formation [168, 169]. Instead, the dynamics of the cavity exhibits a turbulent behavior that can be characterized by an irreversible process of thermalization toward energy equipartition. A mean-field WT equation was derived in [62], which accounts for the incoherent pumping, the nonlinear interaction and both the cavity losses and propagation losses. In spite of the dissipative nature of the cavity dynamics, the intracavity field undergoes a condensation process below a critical value of the incoherence (kinetic energy) of the pump. This phenomenon is illustrated in Fig. 16a, which shows the temporal evolution of the condensate fraction in the intracavity field: After a transient, the fraction of power condensed in the fundamental transverse mode of the cavity saturates to a constant value, which is found in agreement with the theory. Figure 16b reports the condensation curve, i.e., the fraction of condensed power at equilibrium vs the kinetic energy of the injected pump wave. This latter quantity reflects the degree of coherence of the pump wave and plays the role of the control parameter of the transition to wave condensation in the cavity configuration. We remark in Fig. 16b that the condensate fraction in this dissipative optical cavity is found in agreement with the theory inherited from the conservative Hamiltonian NLS equation, without using adjustable parameters. For more details on the simulations and the theory, we refer the reader to [62].

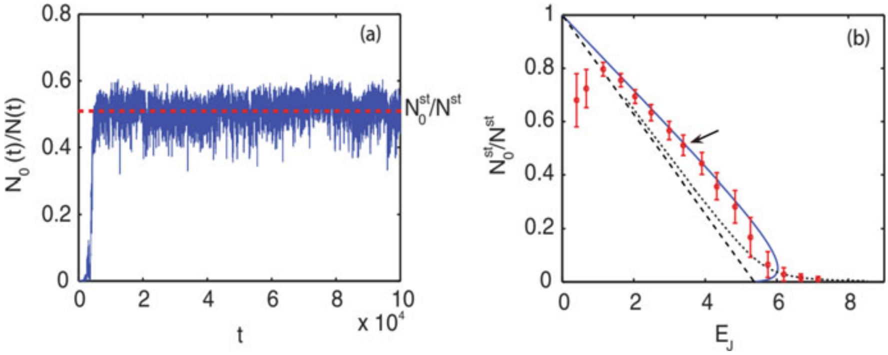

Fig. 16 Wave condensation in an incoherently pumped passive optical cavity. (**a**) Evolution of the fraction of condensed power $N_0(t)/N(t)$ vs time t: The condensate growth saturates to a constant value N_0^{st}/N^{st}, which is in agreement with the theory [62]. (**b**) *Condensation curve*: fraction of condensed power in the stationary equilibrium state N_0^{st}/N^{st} vs the kinetic energy of the pump E_J. The *condensation curve* is computed for a fixed value of the pump intensity J_0, while E_J is varied by modifying the degree of coherence of the pump (i.e., its spectral width). The *blue solid line* refers to the (Bogoliubov) strong condensation regime. The *black dotted line* refers to the weak condensation regime beyond the thermodynamic limit ($\mu \neq 0$), while the *dashed black line* refers to the thermodynamic limit ($\mu \to 0$). The *red points* correspond to the NLS numerical simulations with the cavity boundary conditions. For more details, see [62]. *Source*: from [62]

Let us note an important difference that distinguishes the thermalization and condensation processes discussed here with those reported in the quantum photon context in [61, 170]. In these works the thermalization process is achieved thanks to the presence of dye molecules, which thus play the role of an external thermostat. Conversely, in the passive cavity configuration considered here, the process of thermalization solely results from the four-wave interaction mediated by the intracavity Kerr medium, while the 'temperature' is controlled by varying the kinetic energy (degree of coherence) of the injected pump.

In a recent experimental work [171], the incoherently pumped passive cavity has been implemented in a fully integrated optical fiber system, nearby the zero-dispersion wavelength of the fiber. The dynamics of the cavity exhibits a quasi-soliton turbulent behavior which is reminiscent of the turbulent dynamics of the purely Hamiltonian wave system considered in [172, 173]. The analysis reveals that, as the coherence of the injected pump wave is degraded, the cavity undergoes a transition from the coherent quasi-soliton regime toward the highly incoherent (weakly nonlinear) turbulent regime characterized by short-lived and extreme rogue wave events. This transition can then be interpreted in analogy with a phenomenon of quasi-soliton condensation. The experiments realized in the incoherently pumped passive optical cavity have been characterized by means of complementary spectral and temporal PDF measurements [171].

An unexpected result of [171] is that quasi-soliton condensation can take place efficiently, even in the presence of a low cavity finesse, in contrast with wave-condensation in 2D defocusing media discussed here above, which requires a high finesse [62]. This can be interpreted as a consequence of the fact that the process of thermalization of an optical wave constitutes a prerequisite for the phenomenon of wave-condensation in a defocusing medium, while wave thermalization is known to require a high cavity finesse. There is another important difference which distinguishes wave-condensation and (quasi-)soliton condensation. Wave-condensation is known to exhibit a property of long-range order and coherence, in the sense that the correlation function of the field amplitude does not decay at infinity, $\lim_{|\mathbf{r}-\mathbf{r}'|\to\infty} \langle A(\mathbf{r})\, A^*(\mathbf{r}')\rangle \neq 0$, a property consistent with the idea that the coherence length of a plane-wave diverges to infinity [55]. This is in contrast with the spatial localized character of a (quasi-)soliton, which naturally limits the range of coherence to the characteristic spatial width of the (quasi-)soliton structure. Wave-condensation then appears to be more sensitive to the "boundary conditions" of the system, and thus results less robust than (quasi-)soliton condensation when considered in an optical cavity system.

5.2 Optical Wave Thermalization Through Supercontinuum Generation

The phenomenon of SC generation is characterized by a dramatic spectral broadening of the optical field during its propagation [24, 174]. As a rather general rule, the process of spectral broadening is interpreted through the analysis of the following main nonlinear effects: the four-wave mixing effect, the soliton fission, the Raman self-frequency shift and the generation of dispersive waves [174]. Due to such a multitude of nonlinear effects involved in the process, a complete and satisfactory theoretical description of SC generation is still lacking. However, there is a growing interest in developing new theoretical tools aimed at describing SC generation in more details, see e.g., [175].

The general physical picture of SC generation in PCFs can be summarized as follows. When the PCF is pumped with long pulses in the anomalous dispersion regime, MI is known to lead to the generation of a train of soliton-like pulses, which in turn lead to the emission of Cherenkov radiation in the form of spectrally shifted dispersive waves. These optical solitons are known to exhibit a self-frequency shift towards longer wavelengths as a result of the Raman effect. One encounters the same picture if the PCF is characterized by two zero dispersion wavelengths. In this case the Raman frequency shift of the solitons is eventually arrested in the vicinity of the second zero dispersion wavelengths. The SC spectrum then results to be essentially bounded by the corresponding dispersive waves [24, 176]. The important aspect to underline here is that in all these regimes *the existence of coherent soliton structures plays a fundamental role into the process of SC generation*.

This physical picture of SC generation changes in a significant way when one considers the regime in which long and intense pump pulses are injected into the PCF. Indeed, in this highly nonlinear regime, the spectral broadening process is essentially dominated by the combined effects of the Kerr nonlinearity and higher-order dispersion, i.e., by four-wave mixing processes [177]. In this regime the optical field exhibits rapid and random temporal fluctuations, which prevent the formation of robust and persistent coherent soliton structures. It turns out that the optical field exhibits an incoherent turbulent dynamics, in which coherent soliton structures do not play any significant role. In the following we shall term this regime the 'incoherent regime of SC generation' [178].

In these last years a nonequilibrium thermodynamic interpretation of this incoherent regime of SC generation has been formulated [23, 50, 51, 99, 178] on the basis of the WT theory. In the following we remind the main aspect of optical wave thermalization through SC generation. For more details we refer the interested reader to the short review article [179]. The generalized NLS equation is known to describe the main properties of SC generation in a PCF [123, 174]. In its simplest form that neglects the Raman effect, the shock term, the generalized NLS equation takes the form:

$$i\frac{\partial \psi}{\partial z} + \sum_{j\geq 2}^{m} \frac{i^j \beta_j}{j!}\frac{\partial^j \psi}{\partial t^j} + \gamma|\psi|^2\psi = 0, \tag{88}$$

with the corresponding dispersion relation:

$$k(\omega) = \sum_{j\geq 2}^{m} \frac{\beta_j \omega^j}{j!}. \tag{89}$$

In the following we consider dispersion curves of PCFs characterized by two zero dispersion wavelengths, whose accurate description requires a high-order Taylor expansion of the dispersion relation ($m > 4$ and even). Starting from the high-order dispersion NLS equation (88), one can derive the irreversible WT kinetic equation governing the evolution of the averaged spectrum of the field $n(z,\omega)$ $[\langle \tilde{\psi}(z,\omega_1)\tilde{\psi}^*(z,\omega_2)\rangle = n(z,\omega_1)\,\delta(\omega_1-\omega_2)]$:

$$\partial_z n(z,\omega_1) = Coll[n], \tag{90}$$

with the collision term

$$\begin{aligned} Coll[n] = \iiint d\omega_2\, d\omega_3\, d\omega_4\; n(\omega_1)n(\omega_2)n(\omega_3)n(\omega_4) \\ \times\, W\left[n^{-1}(\omega_1) + n^{-1}(\omega_2) - n^{-1}(\omega_3) - n^{-1}(\omega_4)\right] \end{aligned} \tag{91}$$

where '$n(\omega)$' stands for '$n(z,\omega)$' in Eq. (91). As usual in the WT kinetic equation, the phase-matching conditions of energy and momentum conservation are expressed by the presence of Dirac δ-functions in $W = \frac{\gamma^2}{\pi}\,\delta(\omega_1+\omega_2-\omega_3-\omega_4)\,\delta[k(\omega_1) + k(\omega_2) - k(\omega_3) - k(\omega_4)]$, where $k(\omega)$ refers to the linear dispersion relation.

Equation (90) conserves the power density $N/T_0 = \int n(z,\omega)\,d\omega$, the density of kinetic energy $E/T_0 = \int k(\omega)\,n(z,\omega)\,d\omega$ and the density of momentum $P/T_0 = \int \omega\,n(z,\omega)\,d\omega$, where T_0 refers to the considered numerical time window. It also exhibits a H-theorem of entropy growth, $\partial_z \mathscr{S} \geq 0$, where the nonequilibrium entropy reads $\mathscr{S}(z) = \int \log[n(z,\omega)]\,d\omega$. The Rayleigh-Jeans equilibrium distribution is obtained by maximising the entropy under the constraints imposed by the conservation of the energy, momentum and power, which gives

$$n^{eq}(\omega) = \frac{T}{k(\omega) + \lambda\omega - \mu}, \tag{92}$$

where T and μ are by analogy with thermodynamics the temperature and the chemical potential of the incoherent wave at equilibrium.

The meaning of the parameter λ becomes apparent through the analysis of the group-velocity v_g of the optical field $[k'(\omega) \equiv \partial k/\partial\omega = 1/v_g(\omega)]$. Indeed, recalling the definition of an average, $\langle \mathscr{A} \rangle_{eq} = \int \mathscr{A}\, n^{eq}(\omega)\,d\omega / \int n^{eq}(\omega)\,d\omega$ and making use of the equilibrium spectrum (92), one readily obtains

$$\langle k'(\omega) \rangle_{eq} = -\lambda. \tag{93}$$

The parameter λ then denotes the average of the inverse of the group-velocity of the optical field at equilibrium. We report in Fig. 17c the comparison of the theoretical prediction (92) with the results of the numerical simulations of the high-order NLS equation (88). A quantitative agreement is obtained between the simulations and the theory (92), without using adjustable parameters [51]. The Rayleigh-Jeans spectrum is characterized by a double-peaked structure, which results from the presence of two zero dispersion wavelengths in the dispersion curve of the PCF. The relaxation toward thermal equilibrium is also corroborated by the saturation of the process of entropy production illustrated in Fig. 17b. Note however that a notable discrepancy is visible in the tails of the spectrum in Fig. 17c, as if the thermalization process were not achieved in a complete fashion. Actually, the simulations reveal that the tails of the spectrum exhibits a very slow process of spectral broadening, which apparently tends to evolve toward the expected Rayleigh-Jeans tails—though the required propagation length is extremely large. This aspect will be discussed in more detail in Sect. 5.3. Note that the good agreement between the theory and the simulations has been obtained in a variety of configurations, e.g., under cw or incoherent pumping, as discussed in detail in [50, 51].

5.2.1 Thermodynamic Phase-Matching

The thermodynamic equilibrium spectrum given in Eq. (92) is characterized by a double peak structure, which originates from the two zero dispersion wavelengths that characterize the PCF dispersion curve. It is important to underline, however, that the frequencies (ω_1, ω_2) of the two peaks of $n^{eq}(\omega)$ do not simply correspond to the

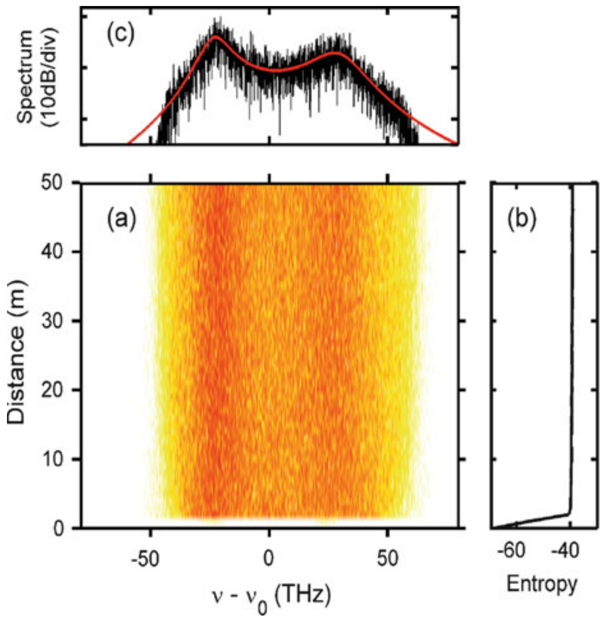

Fig. 17 Optical wave thermalization through SC generation. (**a**) Simulation of the instantaneous NLS equation (88) with a dispersion curve featured by two zero-dispersion wavelengths (for more details see [179]). (**b**) Optical wave thermalization is characterized by a process of entropy production, which saturates to a constant level once the equilibrium state is reached, as described by the H-theorem of entropy growth. (**c**) Comparison of the thermodynamic Rayleigh-Jeans equilibrium spectrum $n^{eq}(\omega)$ [Eq. (92)] (*red line*), and the numerical spectrum corresponding to an averaging over the last 20 m of propagation. A good agreement is obtained without adjustable parameters—note however a discrepancy in the tails of the spectrum (see the text for discussion)

minima of the dispersion relation, i.e. $k'(\omega_{1,2}) \neq 0$. To further analyze this aspect, let us write the thermodynamic equilibrium spectrum in the form $n^{eq}(\omega) = T/\mathscr{F}(\omega)$, with $\mathscr{F}(\omega) = k(\omega) + \lambda\omega - \mu$. The two frequencies (ω_1, ω_2) which maximize the equilibrium spectrum (92) satisfy $\mathscr{F}'(\omega_1) = \mathscr{F}'(\omega_2) = 0$, i.e., $k'(\omega_1) = k'(\omega_2) = -\lambda$. This observation reveals that *the two frequencies* (ω_1, ω_2) *of the double peaked equilibrium spectrum (92) are selected in such a way that the corresponding group-velocities coincide with the average group-velocity of the optical wave*,

$$v_g(\omega_1) = v_g(\omega_2) = 1/\left\langle k'(\omega)\right\rangle_{eq} = -1/\lambda. \tag{94}$$

It can be shown that there exists, in principle, a unique pair of frequencies (ω_1, ω_2) satisfying the conditions given by Eqs. (94). In other terms, for a given thermodynamic equilibrium spectrum (92), there exists a *unique* pair of frequencies (ω_1, ω_2) that leads to a matched group-velocity of the double peaked spectrum [51]. In this sense, Eq. (94) can be regarded as a thermodynamic phase-matching condition.

The thermodynamic phase-matching given by Eq. (94) then imposes a matching of the group-velocities of the two spectral peaks of the SC spectrum. The fact that different wave-packets naturally tend to propagate with the same group-velocity was discussed in [142]. This can be interpreted in analogy with basic equilibrium thermodynamic properties, namely that an isolated system can only exhibit a uniform motion of translation (and rotation) as a whole, while any macroscopic internal motion is not possible at thermodynamic equilibrium [180]. In this way, it was shown that a velocity locking is required, in the sense that it prevents "a macroscopic internal motion in the wave system." We refer the interested reader to [51, 118] for more details on this aspect.

5.3 Breakdown of Thermalization

As discussed in the introduction section in relation with the Fermi-Pasta-Ulam problem, thermalization does not necessarily in nonlinear systems. By considering the one-dimensional NLS equation, we present in this section two different mechanisms that inhibit the process of optical wave thermalization toward the Rayleigh-Jeans distribution. Depending on whether the dispersion relation is truncated up to the third, or fourth-order, the wave system exhibits different types of relaxation processes. Provided that the interaction occurs in the weakly nonlinear regime, the WT theory provides an accurate description of such mechanisms of breakdown of thermalization.

5.3.1 Truncated Thermalization

We consider here the 1D NLS equation in which the dispersion relation is truncated to the fourth-order. In this case, the WT theory reveals the existence of an irreversible evolution toward a Rayleigh-Jeans equilibrium state characterized by a compactly supported spectral shape [52]. This phenomenon of truncated thermalization may explain the physical origin of the abrupt SC spectral edges discussed above in Sect. 5.2. Besides its relevance in the context of SC generation, this phenomenon is also important from a fundamental point of view. Indeed, *it unveils the existence of a genuine frequency cut-off that arises in a system of classical waves described by the generalized NLS equation*, a feature of importance considering the well-known ultraviolet catastrophe of ensemble of classical waves [118].

The starting point is the NLS equation (88) accounting for third- and fourth-orders dispersion effects, as well as the corresponding WT kinetic equation (90). The kinetic theory reported in [52] reveals that the process of thermalization to the Rayleigh-Jeans spectrum (92) is not achieved in a complete way, but turns out to be truncated within a specific frequency interval defined by the bounds, $\omega \in [\omega_-, \omega_+]$, with

$$\omega_\pm = -\frac{\tilde{\alpha}}{4\tilde{\beta}\tau_0} \pm \frac{\sqrt{21}}{12\tilde{\beta}\tau_0}\sqrt{3\tilde{\alpha}^2 + 8\tilde{\beta}}, \tag{95}$$

where $\tilde{\alpha}$ and $\tilde{\beta}$ refer to the normalized third- and fourth-orders dispersion parameters, namely $\tilde{\alpha} = L_{nl}\beta_3/(6\tau_0^3)$, and $\tilde{\beta} = L_{nl}\beta_4/(24\tau_0^4)$, where $\tau_0 = \sqrt{\beta_2 L_{nl}/2}$ is the corresponding healing time, i.e., the characteristic time for which linear and nonlinear effects are of the same order of magnitude [118].

The confirmation of this process of truncated thermalization by the numerical simulations has not been a trivial task. This is due to the fact that in the usual configurations of SC generation discussed above, the cascade of MI side-bands generated by the cw pump in the early stage of propagation spreads beyond the frequency interval predicted by the theory. As already discussed, the MI process is inherently a coherent nonlinear phase-matching effect which is not described by the WT kinetic equation [Eqs. (90), (91)]. This explains why the numerical simulations reported above (or in [50, 51]) did not evidence a precise signature of this phenomenon of truncated thermalization.

In order to analyze the theoretical predictions in more detail, one needs to decrease the injected pump power so as to maintain the (cascaded) MI side-bands within the frequency interval (95). Intensive numerical simulations of the NLS equation in this regime of reduced pump power have been performed in [52]. This study reveals that the nonlinear dynamics slows down in a dramatic way, so that the expected process of thermalization requires huge nonlinear propagation lengths. This results from the fact that the normalized parameters $\tilde{\alpha}$ and $\tilde{\beta}$ decrease as the pump power decreases, so that the NLSE approaches the integrable limit, which does not exhibit thermalization [138]. We report in Fig. 18 the wave spectra at different propagation lengths obtained by solving the NLS equation with $\tilde{\alpha} = 0.1$ and $\tilde{\beta} = 0.02$. In the early stage of propagation, $z \sim 200$, the spectrum remains confined within the frequency interval $[\omega_-, \omega_+]$ predicted by the theory [Eq. (95)], although the spectrum exhibits a completely different spectral profile than the expected Rayleigh-Jeans distribution. As a matter of fact, the process of thermalization requires enormous propagation lengths, as illustrated in Fig. 18d, which shows that the wave spectrum eventually relaxes toward a truncated Rayleigh-Jeans distribution. For more details on these numerical simulations, we refer the reader to [118].

5.3.2 Anomalous Thermalization

Here we discuss another mechanism that inhibits the natural process of thermalization. We consider the 1D NLS equation by truncating the dispersion relation up to the third order. We will see that the incoherent wave exhibits an irreversible

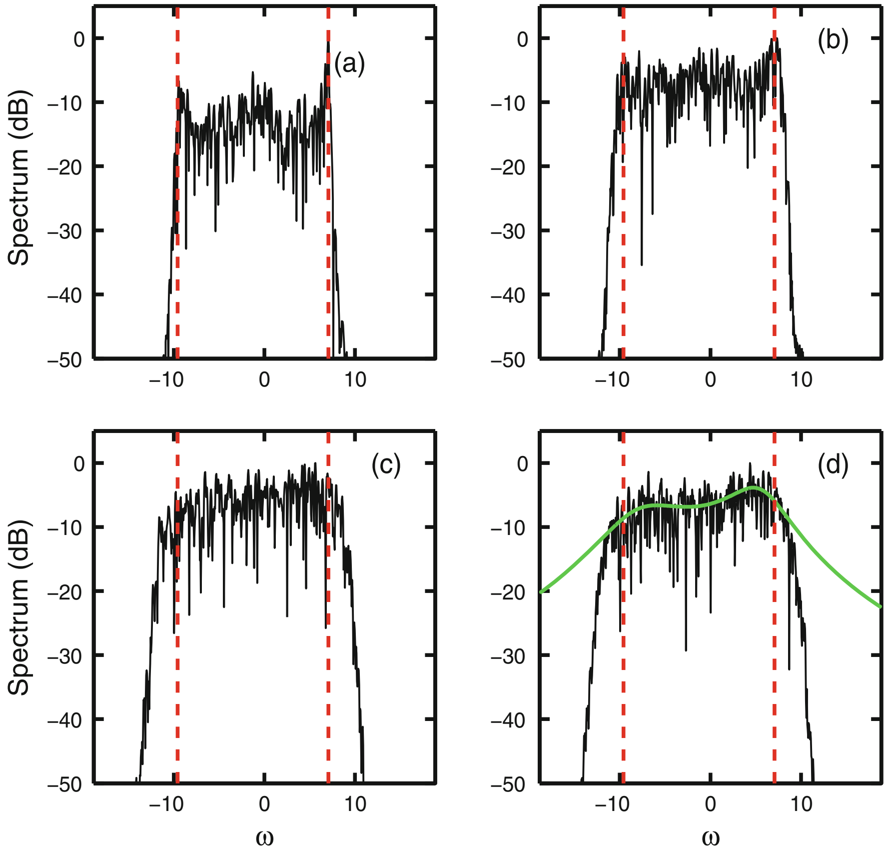

Fig. 18 Truncated thermalization of incoherent waves: Spectra $|\tilde{\psi}|^2(\omega, z)$ obtained by solving the NLS equation (88) with solely third and fourth-order dispersion effects ($\tilde{\alpha} = 0.1$, $\tilde{\beta} = 0.02$): (**a**) $z = 200$, (**b**) $z = 10^4$, (**c**) $z = 5 \times 10^5$, (**d**) $z = 10^6$. After a long transient, the wave relaxes toward a truncated Rayleigh-Jeans distribution [Eq. (92), *green line*] (**d**). The *dashed red lines* denote the frequencies $\omega_\pm$ in Eq. (95)—ω is here in units of τ_0^{-1}. *Source*: from [52]

evolution toward an equilibrium state of a different nature than the conventional Rayleigh-Jeans equilibrium state. The WT kinetic equation reveals that this effect of anomalous thermalization is due to the existence of a local invariant in frequency space J_ω, which originates in degenerate resonances of the system [112, 113]. In contrast to conventional integral invariants that lead to a generalized Rayleigh-Jeans distribution, here, it is the local nature of the invariant J_ω that makes the new equilibrium states different than the usual Rayleigh-Jeans equilibrium states. We remark that local invariants and the associated process of anomalous thermalization have been also identified in the 1D vector NLS equation, a configuration in which optical fiber experiments have been also performed, see [112].

The starting point is the NLS equation (88) accounting for third-order dispersion effects, as well as the corresponding WT kinetic equation (90). A refined analysis of the WT kinetic equation reveals a remarkable property, namely the existence of a local invariant in frequency space:

$$J(\omega) = n(\omega, z) - n(q - \omega, z), \tag{96}$$

where $q = 2s\omega_*$, ω_* being the zero-dispersion angular frequency, and $s = \text{sign}(\beta_2)$ [112, 113]. This invariant is 'local' in the sense that it is verified for each frequency ω individually, $\partial_z J(\omega) = 0$. It means that the subtraction of the spectrum by the reverse of itself translated by q, remains invariant during the whole evolution of the wave. The invariant (96) finds its origin in the following degenerate resonance of the phase-matching conditions: a pair of frequencies $(\omega, q - \omega)$ may resonate with any pair of frequencies $(\omega', q - \omega')$, because $k(\omega) + k(q - \omega) = sq^2/3$ does not depend on ω. Because of the existence of this local invariant, the incoherent wave relaxes toward an equilibrium state of fundamental different nature than the expected thermodynamic Rayleigh-Jeans spectrum:

$$n^{loc}(\omega) = \frac{J_\omega}{2} + \frac{1}{\lambda}\left(1 + \sqrt{1 + \left(\frac{\lambda J_\omega}{2}\right)^2}\right). \tag{97}$$

Here, the parameter λ is determined from the initial condition through the conservation of the power. We remark that the equilibrium distribution (97) vanishes exactly the collision term of the kinetic equation, i.e., it is a stationary solution. The equilibrium distribution is characterized by a remarkable property: it exhibits a constant spectral pedestal, $n^{loc}(\omega) \to 2/\lambda$ for $|\omega| \gg |\omega_*|$. We remark in this respect that in the tails of the spectrum ($|\omega| \gg |\omega_*|$), the invariant J_ω vanishes, so that a constant spectrum ($n_\omega = const$) turns out to be a stationary solution of the WT kinetic equation. The existence of the process of anomalous thermalization has been confirmed by the numerical simulations of both the NLS equation and the WT kinetic equation, as illustrated in Fig. 19. For more details on theoretical and numerical simulations of anomalous thermalization, we refer the reader to [113, 118, 181].

5.3.3 Local vs Integral Invariants

The equilibrium distribution (97) is of a fundamental different nature than the conventional Rayleigh-Jeans distribution. In particular, as discussed just above, $n^{loc}(\omega)$ is characterized by a constant spectral pedestal in the tails of the spectrum. The kinetic theory reveals that the difference between $n^{loc}(\omega)$ and $n^{eq}(\omega)$ is due to the existence of the local invariant J_ω. Let us briefly discuss the 'local' nature of the invariant J_ω in regard to the *integral* invariants investigated in [182–185] in line with the problem of integrability. First of all, one may note that the possible existence of

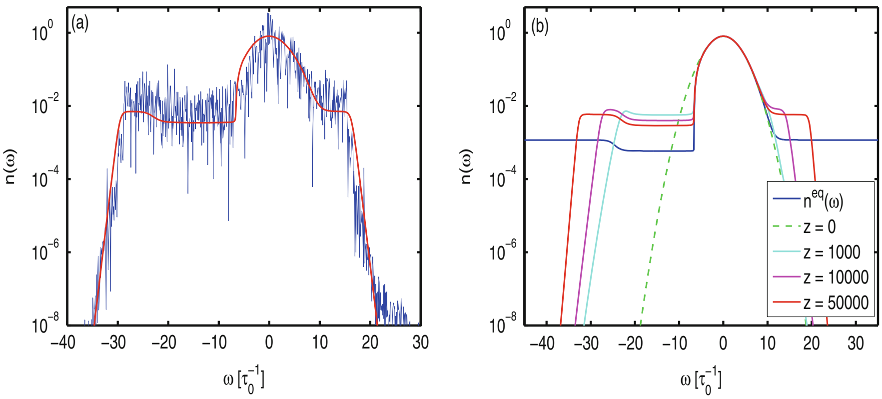

Fig. 19 Anomalous thermalization of incoherent waves: (**a**) Spectral evolution obtained by integrating numerically the NLSE with third-order dispersion (*blue*) and the corresponding WT kinetic equation (*red*) at $z = 20,000$ for $\tilde{\alpha} = 0.05$ (**a**). (**b**) Numerical simulations of the WT kinetic equation showing the spectral profile $n(z, \omega)$ at different propagation lengths z: a constant spectral pedestal emerges in the tails of the spectrum ($\tilde{\alpha} = 0.05$). The spectrum slowly relaxes toward the equilibrium state $n^{loc}(\omega)$ given by Eq. (97) (*blue*). *Source*: from [181]

a set of additional *integral* invariants, $Q_j = \int \phi_j(\omega)\, n_\omega(z)\, d\omega$, would still lead to a (generalized) Rayleigh-Jeans distribution,

$$n^{eq}(\omega) = \frac{T}{k(\omega) + \sum_j \lambda_j \phi_j(\omega) - \mu}, \tag{98}$$

where λ_j refer to the Lagrangian multipliers associated to the conservation of Q_j [185]. The *local* invariant J_ω thus leads to an equilibrium spectrum $n^{loc}(\omega)$ of a different nature than the generalized Rayleigh-Jeans spectrum (98).

One may wonder whether the local invariant J_ω may generate the existence of integral invariants of the kinetic equation (i.e., Eqs. (90), (91) with $m = 3$). We can easily verify that $Q = \int \phi_\omega\, n_\omega(z)\, d\omega$ is a conserved quantity of the kinetic equation whenever ϕ_ω satisfies the following relation

$$\phi_{\omega_1} + \phi_{q-\omega_1} = \phi_{\omega_2} + \phi_{q-\omega_2}, \tag{99}$$

for any couple of frequencies (ω_1, ω_2). In other terms, it is sufficient that $\phi_\omega + \phi_{q-\omega}$ does not depend on ω for Q to be a conserved quantity of the kinetic equation. A simple way to satisfy this condition is to construct ϕ_ω as follows, $\phi_\omega = \varphi_\omega - \varphi_{q-\omega}$. In this way, regardless of the particular choice of the function φ_ω,

$$Q = \int \left(\varphi_\omega - \varphi_{q-\omega}\right)\, n_\omega(z)\, d\omega, \tag{100}$$

is a conserved quantity of the kinetic equation. This shows that the existence of a local invariant (J_ω) can generate an infinite set of integral invariants Q.

5.4 Emergence of Rogue Waves from Optical Turbulence

In this section we briefly comment some open interesting issues related to optical wave turbulence in fibers. An interesting problem concerns a proper description of the emergence of extreme rogue waves (RW) from a turbulent environment. A rather commonly accepted opinion is that RWs can be conveniently interpreted in the light of exact analytical solutions of integrable nonlinear wave equations, the so-called Akhmediev breathers, or more specifically their limiting cases of infinite spatial and temporal periods, the rational soliton solutions, such as Peregrine and higher-order solutions of the integrable 1D NLSE—see the recent reviews [27, 28]. Rational soliton solutions can be regarded as a coherent and deterministic approach to the understanding of RW phenomena. On the other hand, RWs are known to spontaneously emerge from an incoherent turbulent state [29, 139, 186–190]. This raises a difficult problem, since the description of the turbulent system requires a statistical WT approach, whereas rational soliton solutions are inherently coherent deterministic structures. This problem was addressed in the optical fiber context in [172, 173] by considering a specific NLSE model that exhibits a quasi-soliton turbulence scenario, a feature that can be interpreted in analogy with wave condensation, see Sect. 5.1.4. It was shown that the deterministic description of rogue wave events in terms of rational soliton solutions is not inconsistent with the corresponding statistical WT description of the turbulent system [173]. It is important to stress that the emergence of RW events was shown to solely occur near by the transition to (quasi-)soliton condensation. From a different perspective, the fluctuations of the condensate fraction in 2D wave condensation have been recently computed theoretically, revealing that large fluctuations solely occur near by the transition to condensation, while they are significantly quenched in the strongly condensed Bogoliubov regime (small 'temperature'), and almost completely suppressed in the weakly nonlinear turbulent regime (high 'temperature'). This result is consistent with the general idea that nearby second-order phase-transitions, physical systems are inherently sensitive to perturbations and thus exhibit large fluctuations. One can then address a possible alternative point of view on the question of the spontaneous emergence of rogue waves from a conservative turbulent environment: Is it possible to interpret the sporadic emergence of RW events as the natural large fluctuations inherent to the phase transition to soliton condensation? This issue may pave the way for a statistical mechanics approach based on the idea of scaling and universal theory of critical phenomena to the description of RWs.

Acknowledgements The authors are grateful to many collaborators for fruitful discussions: P. Aschieri, S.A. Babin, J. Barré, B. Barviau, P. Béjot, F. Biancalana, D. Christodoulides, S. Coen, C. Conti, D. Faccio, C. Finot, M. Guasoni, R. Kaiser, B. Kibler, M. Haelterman, K. Hammani, T.

Hansson, H.R. Jauslin, M. Lisak, C. Michel, G. Millot, C. Montes, S. Nazarenko, M. Onorato, S. Pitois, E.V. Podivilov, S. Residori, M. Segev, S. Trillo, S. Wabnitz, V.E. Zakharov. The authors also acknowledge P. Suret, S. Randoux, D. Churkin and S. Turitsyn for their deep insights and valuable contributions in the understanding of optical turbulence, in particular in dissipative laser systems or near by the limit of integrability. A.P. is especially grateful to T. Dauxois and S. Ruffo for their introduction into the physics of long-range interactions. It is also a pleasure for A.P. to thank M. Onorato, S. Residori and F. Baronio for their fantastic work in organizing the conference "Rogue and Shock Waves in Nonlinear Dispersive Media," held in Cargese (France, July 2015), where I had a chance to participate. A.P. acknowledges support from the French National Research Agency (ANR-12-BS04-0011 OPTIROC), as well as from the Labex ACTION (ANR-11-LABX-01-01) program. A.P. also acknowledges support from the European Research Council under the European Community's Seventh Framework Programme (FP7/20072013 Grant Agreement No. 306633, PETAL project).

References

1. Mitchell, M., Chen, Z., Shih, M., Segev, M.: Self-trapping of partially spatially incoherent light. Phys. Rev. Lett. **77**, 490 (1996)
2. Mitchell, M., Segev, M.: Self-trapping of incoherent white light. Nature (London) **387**, 880 (1997)
3. Segev, M., Christodoulides, D.: Incoherent solitons. In: Trillo, S., Torruellas, W. (eds.) Spatial Solitons. Springer, Berlin (2001)
4. Kivshar, Y., Agrawal, G.: Optical Solitons: From Fibers to Photonic Crystals. Academic, New York (2003)
5. Pasmanik, G.A.: Self-interaction of incoherent light beams. Sov. Phys. JETP **39**, 234 (1974)
6. Mitchell, M., Segev, M., Coskun, M.T., Christodoulides, D.: Theory of self-trapped spatially incoherent light beams. Phys. Rev. Lett. **79**, 4990 (1997)
7. Christodoulides, D., Coskun, T., Mitchell, M., Segev, M.: Theory of incoherent self-focusing in biased photorefractive media. Phys. Rev. Lett. **78**, 646 (1997)
8. Hall, B., Lisak, M., Anderson, D., Fedele, R., Semenov, V.E.: Statistical theory for incoherent light propagation in nonlinear media. Phys. Rev. E **65**, 035602 (2002)
9. Christodoulides, D.N., Eugenieva, E.D., Coskun, T.H., Segev, M., Mitchell, M.: Equivalence of three approaches describing partially incoherent wave propagation in inertial nonlinear media. Phys. Rev. E **63**, 035601 (2001)
10. Lisak, M., Helczynski, L., Anderson, D.: Relation between different formalisms describing partially incoherent wave propagation in nonlinear optical media. Opt. Commun. **220**, 321 (2003)
11. Christodoulides, D.N., Coskun, T.H., Mitchell, M., Chen, Z., Segev, M.: Theory of incoherent dark solitons. Phys. Rev. Lett. **80**, 5113 (1998)
12. Chen, Z., Mitchell, M., Segev, M., Coskun, T.H., Christodoulides, D.N.: Self-trapping of dark incoherent light beams. Science **280**, 889 (1998)
13. Soljacic, M., Segev, M., Coskun, T., Christodoulides, D., Vishwanath, A.: Modulation instability of incoherent beams in noninstantaneous nonlinear media. Phys. Rev. Lett. **84**, 467 (2000)
14. Kip, D., Soljacic, M., Segev, M., Eugenieva, E., Christodoulides, D.: Modulation instability and pattern formation in spatially incoherent light beams. Science **290**, 495–498 (2000)
15. Kibler, B., Michel, C., Garnier, J., Picozzi, A.: Temporal dynamics of incoherent waves in noninstantaneous response nonlinear Kerr media. Opt. Lett. **37**, 2472 (2012)
16. Picozzi, A., Haelterman, M.: Parametric three-wave soliton generated from incoherent light. Phys. Rev. Lett. **86**, 2010–2013 (2001)

17. Picozzi, A., Haelterman, M., Pitois, S., Millot, G.: Incoherent solitons in instantaneous response nonlinear media. Phys. Rev. Lett. **92**, 143906 (2004)
18. Peccianti, M., Assanto, G.: Incoherent spatial solitary waves in nematic liquid crystals. Opt. Lett. **26**(22), 1791–1793 (2001)
19. Rotschild, C., Schwartz, T., Cohen, O., Segev, M.: Incoherent spatial solitons in effectively-instantaneous nonlocal nonlinear media. Nat. Photonics **2**, 371 (2008)
20. Picozzi, A., Garnier, J.: Incoherent soliton turbulence in nonlocal nonlinear media. Phys. Rev. Lett. **107**(23), 233901 (2011)
21. Wu, M., Krivosik, P., Kalinikos, B., Patton, C.: Random generation of coherent solitary waves from incoherent waves. Phys. Rev. Lett. **96**, 227202 (2006)
22. Picozzi, A., Pitois, S., Millot, G.: Spectral incoherent solitons: a localized soliton behavior in frequency space. Phys. Rev. Lett. **101**, 093901 (2008)
23. Kibler, B., Michel, C., Kudlinski, A., Barviau, B., Millot, G., Picozzi, A.: Emergence of spectral incoherent solitons through supercontinuum generation in a photonic crystal fiber. Phys. Rev. E **84**, 066605 (2011)
24. Dudley, J.M., Taylor, J.R.: Supercontinuum Generation in Optical Fibers. Cambridge University Press, Cambridge (2010)
25. Couairon, A., Mysyrowicz, A.: Femtosecond filamentation in transparent media. Phys. Rep. **441**(2), 47–189 (2007)
26. Wiersma, D.S.: The physics and applications of random lasers. Nat. Phys. **4**(5), 359–367 (2008)
27. Onorato, M., Residori, S., Bortolozzo, U., Montina, A., Arecchi, F.: Rogue waves and their generating mechanisms in different physical contexts. Phys. Rep. (2013)
28. Dudley, J.M., Dias, F., Erkintalo, M., Genty, G.: Instabilities, breathers and rogue waves in optics. Nat. Photonics **8**(10), 755–764 (2014)
29. Walczak, P., Randoux, S., Suret, P.: Optical rogue waves in integrable turbulence. Phys. Rev. Lett. **114**, 143903 (2015)
30. Zakharov, V.E., L'vov, V.S., Falkovich, G.: Kolmogorov Spectra of Turbulence I. Springer, Berlin (1992)
31. Frisch, U.: Turbulence. The Legacy of A. N. Kolmogorov. Cambridge University Press, Cambridge (1995)
32. Newell, A.C., Rumpf, R.: Wave turbulence. Annu. Rev. Fluid Mech. **43**, 59–78 (2011)
33. Nazarenko, S.: Wave Turbulence. Lecture Notes in Physics, vol. 825. Springer, Berlin (2011)
34. Newell, A.C., Rumpf, B., Zakharov, V.E.: Spontaneous breaking of the spatial homogeneity symmetry in wave turbulence. Phys. Rev. Lett. **108**, 194502 (2012)
35. Tsytovich, V.N.: Nonlinear Effects in Plasma. Plenum, New York (1970)
36. Hasselmann, K.: On the non-linear energy transfer in a gravity-wave spectrum. Part 1. General theory. J. Fluid Mech. **12**, 481–500 (1962)
37. Hasselmann, K.: On the non-linear energy transfer in a gravity-wave spectrum. Part 2. Conservation theorems, wave-particle analogy, irreversibility. J. Fluid Mech. **15**, 273–281 (1963)
38. Dyachenko, S., Newell, A.C., Pushkarev, A., Zakharov, V.E.: Optical turbulence: weak turbulence, condensates and collapsing filaments in the nonlinear Schrödinger equation. Phys. D **57**, 96 (1992)
39. Zakharov, V., Dias, F., Pushkarev, A.: One-dimensional wave turbulence, Phys. Rep. **398**, 1 (2004)
40. Benney, D.J., Saffman, P.G.: Nonlinear interactions of random waves in dispersive medium. Proc. R. Soc. London Ser. A **289**, 301 (1966)
41. Newell, A.: The closure problem in a system of random gravity waves. Rev. Geophys. **6**, 1 (1968)
42. Benney, D.J., Newell, A.: Random wave closure. Stud. Appl. Math. **48**, 29 (1969)
43. Newell, A.C., Nazarenko, S., Biven, L.: Wave turbulence and intermittency. Phys. D **152-153**, 520–550 (2001)

44. Rasmussen, K., Cretegny, T., Kevrekidis, P.G., Gronbech-Jensen, N.: Statistical mechanics of a discrete nonlinear system. Phys. Rev. Lett. **84**, 3740 (2000)
45. Jordan, R., Turkington, B., Zirbel, C.L.: A mean-field statistical theory for the nonlinear Schrödinger equation. Phys. D **137**, 353 (2000)
46. Rumpf, R., Newell, A.C.: Coherent structures and entropy in constrained, modulationally unstable, nonintegrable systems. Phys. Rev. Lett. **87**, 054102 (2001)
47. Rumpf, B.: Simple statistical explanation for the localization of energy in nonlinear lattices with two conserved quantities. Phys. Rev. E **69**, 016618 (2004)
48. Derevyanko, S.A.: Thermalized polarization dynamics of a discrete optical-waveguide system with four-wave mixing. Phys. Rev. A **88**, 033851 (2013)
49. Antenucci, F., Ibáñez Berganza, M., Leuzzi, L.: Statistical physics of nonlinear wave interaction. Phys. Rev. B **92**, 014204 (2015)
50. Barviau, B., Kibler, B., Kudlinski, A., Mussot, A., Millot, G., Picozzi, A.: Experimental signature of optical wave thermalization through supercontinuum generation in photonic crystal fiber. Opt. Express **17**, 7392 (2009)
51. Barviau, B., Kibler, B., Picozzi, A.: Wave turbulence description of supercontinuum generation: influence of self-steepening and higher-order dispersion. Phys. Rev. A **79**, 063840 (2009)
52. Barviau, B., Garnier, J., Xu, G., Kibler, B., Millot, G., Picozzi, A.: Truncated thermalization of incoherent optical waves through supercontinuum generation in photonic crystal fibers. Phys. Rev. A **87**(3), 035803 (2013)
53. Davis, M., Morgan, S., Burnett, K.: Simulations of Bose fields at finite temperature. Phys. Rev. Lett. **87**, 160402 (2001)
54. Davis, M., Morgan, S., Burnett, K.: Simulations of thermal Bose fields in the classical limit. Phys. Rev. A **66**, 053618 (2002)
55. Connaughton, C., Josserand, C., Picozzi, A., Pomeau, Y., Rica, S.: Condensation of classical nonlinear waves. Phys. Rev. Lett. **95**, 263901 (2005)
56. Zakharov, V., Nazarenko, S.: Dynamics of the Bose-Einstein condensation. Phys. D **201**, 203 (2005)
57. During, G., Picozzi, A., Rica, S.: Breakdown of weak-turbulence and nonlinear wave condensation. Phys. D **238**, 1524 (2009)
58. Conti, C., Leonetti, M., Fratalocchi, A., Angelani, L., Ruocco, G.: Condensation in disordered lasers: theory, 3d+1 simulations, and experiments. Phys. Rev. Lett. **101**, 143901 (2008)
59. Turitsyna, E., Falkovich, G., Mezentsev, V., Turitsyn, S.: Optical turbulence and spectral condensate in long-fiber lasers. Phys. Rev. A **80**, 031804 (2009)
60. Weill, R., Fischer, B., Gat, O.: Light-mode condensation in actively-mode-locked lasers. Phys. Rev. Lett. **104**(17), 173901 (2010)
61. Klaers, J., Schmitt, J., Vewinger, F., Weitz, M.: Bose-Einstein condensation of photons in an optical microcavity. Nature **468**, 545 (2010)
62. Michel, C., Haelterman, M., Suret, P., Randoux, S., Kaiser, R., Picozzi, A.: Thermalization and condensation in an incoherently pumped passive optical cavity. Phys. Rev. A **84**, 033848 (2011)
63. Turitsyn, S.K., Babin, S.A., Turitsyna, E.G., Falkovich, G.E., Podivilov, E., Churkin, D.: Optical wave turbulence. In: Shira, V., Nazarenko, S. (eds.) Wave Turbulence. World Scientific Series on Nonlinear Science Series A, vol. 83. World Scientific, Singapore (2013)
64. Turitsyna, E., Falkovich, G., El-Taher, A., Shu, X., Harper, P., Turitsyn, S.: Optical turbulence and spectral condensate in long fibre lasers. Proc. R. Soc. A **468**, 2145 (2012)
65. Turitsyna, E., Smirnov, S., Sugavanam, S., Tarasov, N., Shu, X., Babin, S., Podivilov, E., Churkin, D., Falkovich, G., Turitsyn, S.: The laminar-turbulent transition in a fibre laser. Nat. Photonics **7**(10), 783–786 (2013)
66. Carusotto, I., Ciuti, C.: Quantum fluids of light. Rev. Mod. Phys. **85**, 299–366 (2013)
67. Bortolozzo, U., Laurie, J., Nazarenko, S., Residori, S.: Optical wave turbulence and the condensation of light. J. Opt. Soc. Am. B **26**, 2280 (2009)

68. Laurie, J., Bortolozzo, U., Nazarenko, S., Residori, S.: One-dimensional optical wave turbulence: experiment and theory. Phys. Rep. **514**, 121 (2012)
69. Bernstein, I., Green, J., Kruskal, M.: Exact nonlinear plasma oscillations. Phys. Rev. **108**, 546 (1957)
70. Hasegawa, A.: Dynamics of an ensemble of plane waves in nonlinear dispersive media. Phys. Fluids **18**, 77 (1975)
71. Hasegawa, A.: Envelope soliton of random phase waves. Phys. Fluids **20**, 2155 (1977)
72. Marklund, M., Shukla, P.K.: Nonlinear collective effects in photon-photon and photon-plasma interactions. Rev. Mod. Phys. **78**, 591–640 (2006)
73. Dylov, D., Fleischer, J.: Observation of all-optical bump-on-tail instability. Phys. Rev. Lett. **100**, 103903 (2008)
74. Garnier, J., Picozzi, A.: Unified kinetic formulation of incoherent waves propagating in nonlinear media with noninstantaneous response. Phys. Rev. A **81**, 033831 (2010)
75. Mendonça, J.T., Tsintsadze, N.L.: Analog of the Wigner-Moyal equation for the electromagnetic field. Phys. Rev. E **62**, 4276–4282 (2000)
76. Lahaye, T., Menotti, C., Santos, L., Lewenstein, M., Pfau, T.: The physics of dipolar bosonic quantum gases. Rep. Prog. Phys. **72**, 126401 (2009)
77. Skupin, S., Saffman, M., Krolikowski, K.: Nonlocal stabilization of nonlinear beams in a self-focusing atomic vapor. Phys. Rev. Lett. **98**, 263902 (2007)
78. Conti, C., Peccianti, M., Assanto, G.: Route to nonlocality and observation of accessible solitons. Phys. Rev. Lett. **91**, 073901 (2003)
79. Conti, C., Peccianti, M., Assanto, G.: Observation of optical spatial solitons in a highly nonlocal medium. Phys. Rev. Lett. **92**, 113902 (2004)
80. Ghofraniha, N., Conti, C., Ruocco, G., Trillo, S.: Shocks in nonlocal media. Phys. Rev. Lett. **99**, 043903 (2007)
81. Conti, C., Fratalocchi, A., Peccianti, M., Ruocco, G., Trillo, S.: Observation of a gradient catastrophe generating solitons. Phys. Rev. Lett. **102**, 083902 (2009)
82. Segev, M., Crosignani, B., Yariv, A., Fischer, B.: Spatial solitons in photorefractive media. Phys. Rev. Lett. **68**, 923–926 (1992)
83. Litvak, A., Sergeev, A.: One dimensional collapse of plasma waves. JETP Lett. **27**, 517 (1978)
84. Wyller, J., Krolikowski, W., Bang, O., Rasmussen, J.J.: Generic features of modulational instability in nonlocal Kerr media. Phys. Rev. E **66**, 066615 (2002)
85. Turitsyn, S.: Spatial dispersion of nonlinearity and stability of multidimensional solitons. Theor. Math. Phys. **64**, 226 (1985)
86. Bang, O., Krolikowski, W., Wyller, J., Rasmussen, J.J.: Collapse arrest and soliton stabilization in nonlocal nonlinear media. Phys. Rev. E **66**, 046619 (2002)
87. Dreischuh, A., Neshev, D.N., Petersen, D.E., Bang, O., Krolikowski, W.: Observation of attraction between dark solitons. Phys. Rev. Lett. **96**, 043901 (2006)
88. Krolikowski, W., Bang, O., Nikolov, N., Neshev, D., Wyller, J., Rasmussen, J., Edmundson, D.: Modulational instability, solitons and beam propagation in spatially nonlocal nonlinear media. J. Opt. B: Quantum Semiclassical Opt. **6**, S288 (2004)
89. Snyder, A., Mitchell, D.: Accessible solitons. Science **276**, 1538 (1997)
90. Cohen, O., Buljan, H., Schwartz, T., Fleischer, J., Segev, M.: Incoherent solitons in instantaneous nonlocal nonlinear media. Phys. Rev. E **73**, 015601 (2006)
91. Zakharov, V., Pushkarev, A., Shvets, V., Yan'kov, V.: Soliton turbulence. JETP Lett. **48**, 83 (1988)
92. Jordan, R., Josserand, C.: Self-organization in nonlinear wave turbulence. Phys. Rev. E **61**, 1527 (2000)
93. Rumpf, R., Newell, A.C.: Localization and coherence in nonintegrable systems. Phys. D **184**, 162 (2003)
94. Zakharov, V.E., Musher, S.L., Rubenchik, A.M.: Hamiltonian approach to the description of non-linear plasma phenomena. Phys. Rep. **129**, 285 (1985)
95. Onorato, M., Osborne, A., Fedele, R., Serio, M.: Landau damping and coherent structures in narrow-banded $1 + 1$ deep water gravity waves. Phys. Rev. E **67**, 046305 (2003)

96. Garnier, J., Ayanides, J.-P., Morice, O.: Propagation of partially coherent light with the maxwell-debye equation. J. Opt. Soc. Am. B **20**, 1409 (2003)
97. Campa, A., Dauxois, T., Ruffo, S.: Statistical mechanics and dynamics of solvable models with long-range interactions. Phys. Rep. **480**, 57–159 (2009)
98. Musher, S., Rubenchik, A., Zakharov, V.: Weak Langmuir turbulence. Phys. Rep. **252**, 177 (1995)
99. Michel, C., Kibler, B., Picozzi, A.: Discrete spectral incoherent solitons in nonlinear media with noninstantaneous response. Phys. Rev. A **83**, 023806 (2011)
100. Garnier, J., Xu, G., Trillo, S., Picozzi, A.: Incoherent dispersive shocks in the spectral evolution of random waves. Phys. Rev. Lett. **111**(11), 113902 (2013)
101. Whitham, G.: Linear and Nonlinear Waves. Wiley, New York (1974)
102. Constantin, P., Lax, P., Majda, A.: A simple one-dimensional model for the three-dimensional vorticity equation. Commun. Pure Appl. Math. **38**, 715–724 (1985)
103. Fokas, A., Ablowitz, M.: The inverse scattering transform for the benjamin-ono equation – a pivot to multidimensional problems. Stud. Appl. Math. **68**, 1 (1983)
104. Coifman, R., Wickerhauser, V.: The scattering transform for the benjamin-ono equation. Stud. Appl. Math. **6**, 825 (1990)
105. Benjamin, T.: Internal waves of permanent form in fluids of great depth. J. Fluid Mech. **29**, 559 (1967)
106. Ono, H.: Algebraic solitary waves in stratified fluids. J. Phys. Soc. Japan **39**, 1082 (1975)
107. Gallavotti, G.E.: The Fermi-Pasta-Ulam Problem: A Status Report. Lecture Notes in Physics. Springer, Berlin (2007)
108. Onorato, M., Vozella, L., Proment, D., Lvov, Y.V.: Route to thermalization in the α-fermi–pasta–ulam system. Proc. Natl. Acad. Sci. **112**(14), 4208–4213 (2015)
109. Lake, B., Yuen, H., Rundgaldier, H., Ferguson, W.: Nonlinear deep-water waves: theory and experiment. part 2. evolution of a continuous wave train. J. Fluid Mech. **83**, 49 (1977)
110. Simaeys, G., Emplit, P., Haelterman, M.: Experimental demonstration of the Fermi-Pasta-Ulam recurrence in a modulationally unstable optical wave. Phys. Rev. Lett. **87**, 033902 (2001)
111. Mussot, A., Kudlinski, A., Droques, M., Szriftgiser, P., Akhmediev, N.: Fermi-pasta-ulam recurrence in nonlinear fiber optics: the role of reversible and irreversible losses. Phys. Rev. X **4**, 011054 (2014)
112. Suret, P., Randoux, S., Jauslin, H., Picozzi, A.: Anomalous thermalization of nonlinear wave systems. Phys. Rev. Lett. **104**, 054101 (2010)
113. Michel, C., Suret, P., Randoux, S., Jauslin, H., Picozzi, A.: Influence of third-order dispersion on the propagation of incoherent light in optical fibers. Opt. Lett. **35**, 2367 (2010)
114. Peccianti, M., Assanto, G.: Nematicons. Phys. Rep. **516**(4), 147–208 (2012)
115. Rotschild, C., Cohen, O., Manela, O., Segev, M., Carmon, T.: Solitons in nonlinear media with an infinite range of nonlocality: first observation of coherent elliptic solitons and of vortex-ring solitons. Phys. Rev. Lett. **95**(21), 213904 (2005)
116. Babenko, V., Zel'dovich, B.Y., Malyshev, V., Sychev, A.A.: Spectrum of a giant laser pulse under frequency self-modulation conditions. Quantum Electron. **3**(2), 97–99 (1973)
117. Manassah, J.T.: Self-phase modulation of incoherent light revisited. Opt. Lett. **16**, 1638 (1991)
118. Picozzi, A., Garnier, J., Hansson, T., Suret, P., Randoux, S., Millot, G., Christodoulides, D.: Optical wave turbulence: towards a unified nonequilibrium thermodynamic formulation of statistical nonlinear optics. Phys. Rep. **542**(1), 1–132 (2014)
119. Levin, Y., Pakter, R., Rizzato, F.B., Teles, T.N., Benetti, F.P.: Nonequilibrium statistical mechanics of systems with long-range interactions. Phys. Rep. **535**(1), 1–60 (2014)
120. Xu, G., Vocke, D., Faccio, D., Garnier, J., Roger, T., Trillo, S., Picozzi, A.: From coherent shocklets to giant collective incoherent shock waves in nonlocal turbulent flows. Nat. Commun. **6**, 8131 (2015)
121. Snyder, A., Mitchell, D.: Big incoherent solitons. Phys. Rev. Lett. **80**, 1422 (1998)
122. Mouhot, C., Villani, C.: On Landau damping. Acta Math. **207**, 29 (2011)
123. Agrawal, G.: Nonlinear Fiber Optics, 5th edn. Academic, New York (2012)

124. Xu, G., Garnier, J., Trillo, S., Picozzi, A.: Spectral dynamics of incoherent waves with a noninstantaneous nonlinear response. Opt. Lett. **38**, 2972–2975 (2013)
125. Montes, C.: Photon soliton and fine structure due to nonlinear compton scattering. Phys. Rev. A **20**, 1081 (1979)
126. Xu, G., Garnier, J., Conforti, M., Picozzi, A.: Generalized description of spectral incoherent solitons. Opt. Lett. **39**, 4192–4195 (2014)
127. Musher, S., Rubenchik, A., Zakharov, V.: Weak Langmuir turbulence of an isothermal plasma. JETP **42**, 80 (1976)
128. Xu, G., Garnier, J., Trillo, S., Picozzi, A.: Impact of self-steepening on incoherent dispersive spectral shocks and collapselike spectral singularities. Phys. Rev. A **90**, 013828 (2014)
129. Gurevich, A., Pitaevskii, L.: Nonstationary structure of a collisionless shock wave. Sov. Phys. JETP **38**, 291 (1974)
130. Taylor, R., Baker, D., Ikezi, H.: Observation of collisionless electrostatic shocks. Phys. Rev. Lett. **24**, 206 (1970)
131. Hoefer, M.A., Ablowitz, M.J., Coddington, I., Cornell, E.A., Engels, P., Schweikhard, V.: Dispersive and classical shock waves in Bose-Einstein condensates and gas dynamics. Phys. Rev. A **74**, 023623 (2006)
132. Chang, J.J., Engels, P., Hoefer, M.A.: Formation of dispersive shock waves by merging and splitting Bose-Einstein condensates. Phys. Rev. Lett. **101**, 170404 (2008)
133. Ghofraniha, N., Gentilini, S., Folli, V., DelRe, E., Conti, C.: Shock waves in disordered media. Phys. Rev. Lett. **109**, 243902 (2012)
134. Ghofraniha, N., Amato, L.S., Folli, V., Trillo, S., DelRe, E., Conti, C.: Measurement of scaling laws for shock waves in thermal nonlocal media. Opt. Lett. **37**, 2325–2327 (2012)
135. Aschieri, P., Garnier, J., Michel, C., Doya, V., Picozzi, A.: Condensation and thermalization of classsical optical waves in a waveguide. Phys. Rev. A **83**, 033838 (2011)
136. Leggett, A.: Quantum Liquids. Oxford University Press, Oxford (2006)
137. Pitaevskii, S., Stringari, L.: Bose-Einstein Condensation. Oxford Science Publications, Oxford (2003)
138. Suret, P., Picozzi, A., Randoux, S.: Wave turbulence in integrable systems: nonlinear propagation of incoherent optical waves in single-mode fibers. Opt. Express **19**, 17852 (2011)
139. Randoux, S., Walczak, P., Onorato, M., Suret, P.: Intermittency in integrable turbulence. Phys. Rev. Lett. **113**, 113902 (2014)
140. Boyd, R.: Nonlinear Optics, 3rd edn. Academic, New York (2008)
141. Huang, K.: Statistical Mechanics. Wiley, New York (1963)
142. Pitois, S., Lagrange, S., Jauslin, H.R., Picozzi, A.: Velocity locking of incoherent nonlinear wave packets. Phys. Rev. Lett. **97**, 033902 (2006)
143. Zakharov, V.: Weak turbulence spectrum in a plasma without a magnetic field. Sov. Phts. JETP **24**, 455 (1967)
144. Annenkov, S.Y., Shrira, V.I.: Evolution of wave turbulence under gusty forcing. Phys. Rev. Lett. **107**, 114502 (2011)
145. Annenkov, S.Y., Shrira, V.I.: Fast nonlinear evolution in wave turbulence. Phys. Rev. Lett. **102**, 024502 (2009)
146. Connaughton, C., Newell, A.C., Pomeau, Y.: Non–stationary spectra of local wave turbulence. Phys. D **184**(1–4), 64–85 (2003). Complexity and Nonlinearity in Physical Systems – A Special Issue to Honor Alan Newell
147. Lacaze, R., Lallemand, P., Pomeau, Y., Rica, S.: Dynamical formation of a Bose-Einstein condensate. Phys. D **152**, 779 (2001)
148. Escobedo, M., Valle, M.A.: Instability of the rayleigh-jeans spectrum in weak wave turbulence theory. Phys. Rev. E **79**, 061122 (2009)
149. Picozzi, A., Rica, S.: Condensation of classical optical waves beyond the cubic nonlinear Schrödinger equation. Opt. Commun. **285**, 5440 (2012)
150. Picozzi, A.: Towards a nonequilibrium thermodynamic description of incoherent nonlinear optics. Opt. Express **15**, 9063 (2007)

151. Assémat, E., Picozzi, A., Jauslin, H.R., Sugny, D.: Instabilities of optical solitons and Hamiltonian singular solutions in a medium of finite extension. Phys. Rev. A **84**, 013809 (2011)
152. Kirton, P., Keeling, J.: Nonequilibrium model of photon condensation. Phys. Rev. Lett. **111**, 100404 (2013)
153. Sob'yanin, D.N.: Bose-Einstein condensation of light: general theory. Phys. Rev. E **88**, 022132 (2013)
154. Fischer, B., Weill, R.: When does single-mode lasing become a condensation phenomenon? Opt. Express **20**, 26704–26713 (2012)
155. Nazarenko, S., Onorato, M., Proment, D.: Bose-einstein condensation and berezinskii-kosterlitz-thouless transition in the two-dimensional nonlinear schrödinger model. Phys. Rev. A **90**, 013624 (2014)
156. Kirton, P., Keeling, J.: Thermalization and breakdown of thermalization in photon condensates. Phys. Rev. A **91**, 033826 (2015)
157. Weill, R., Levit, B., Bekker, A., Gat, O., Fischer, B.: Laser light condensate: experimental demonstration of light-mode condensation in actively mode locked laser. Opt. Express **18**(16), 16520–16525 (2010)
158. Gordon, A., Fischer, B.: Phase transition theory of many-mode ordering and pulse formation in lasers. Phys. Rev. Lett. **89**, 103901 (2002)
159. Weill, R., Rosen, A., Gordon, A., Gat, O., Fischer, B.: Critical behavior of light in mode-locked lasers. Phys. Rev. Lett. **95**, 013903 (2005)
160. Churkin, D.V., Kolokolov, I.V., Podivilov, E.V., Vatnik, I.D., Nikulin, M.A., Vergeles, S.S., Terekhov, I.S., Lebedev, V.V., Falkovich, G., Babin, S.A., et al.: Wave kinetics of random fibre lasers. Nat. Commun. **2**, 6214 (2015)
161. Babin, S.A., Churkin, D.V., Ismagulov, A.E., Kablukov, S.I., Podivilov, E.V.: Four-wave-mixing-induced turbulent spectral broadening in a long Raman fiber laser. J. Opt. Soc. Am. B **24**, 1729 (2007)
162. Dalloz, N., Randoux, S., Suret, P.: Influence of dispersion of fiber bragg grating mirrors on formation of optical power spectrum in Raman fiber lasers. Opt. Lett. **35**, 2505–2507 (2010)
163. Randoux, S., Dalloz, N., Suret, P.: Intracavity changes in the field statistics of Raman fiber lasers. Opt. Lett. **36**(6), 790–792 (2011)
164. Turitsyna, E.G., Turitsyn, S.K., Mezentsev, V.K.: Numerical investigation of the impact of reflectors on spectral performance of Raman fibre laser. Opt. Express **18**, 4469 (2010)
165. Turitsyn, S.K., Babin, S.A., El-Taher, A.E., Harper, P., Churkin, D.V., Kablukov, S.I., Ania-Castanon, J.D., Karalekas, V., Podivilov, E.V.: Random distributed feedback fibre laser. Nat. Photonics **4**, 231 (2010)
166. Turitsyn, S.K., Babin, S.A., Churkin, D.V., Vatnik, I.D., Nikulin, M., Podivilov, E.V.: Random distributed feedback fibre lasers. Phys. Rep. **542**(2), 133–193 (2014). Random Distributed Feedback Fibre Lasers
167. L'vov, V.S., L'vov, Y., Newell, A.C., Zakharov, V.: Statistical description of acoustic turbulence. Phys. Rev. E **56**, 390–405 (1997)
168. Leo, F., Coen, S., Kockaert, P., Gorza, S.-P., Emplit, P., Haelterman, M.: Temporal cavity solitons in one-dimensional Kerr media as bits in an all-optical buffer. Nat. Photonics **4**, 471 (2010)
169. Arecchi, T., Boccalettic, S., Ramazza, P.: Pattern formation and competition in nonlinear optics. Phys. Rep. **318**, 1 (1999)
170. Klaers, J., Vewinger, F., Weitz, M.: Thermalization of a two-dimensional photonic gas in a white wall photon box. Nat. Phys. **6**(7), 512–515 (2010)
171. Conforti, M., Mussot, A., Fatome, J., Picozzi, A., Pitois, S., Finot, C., Haelterman, M., Kibler, B., Michel, C., Millot, G.: Turbulent dynamics of an incoherently pumped passive optical fiber cavity: quasisolitons, dispersive waves, and extreme events. Phys. Rev. A **91**, 023823 (2015)
172. Hammani, K., Kibler, B., Finot, C., Picozzi, A.: Emergence of rogue waves from optical turbulence. Phys. Lett. A **374**, 3585 (2010)

173. Kibler, B., Hammani, K., Finot, C., Picozzi, A.: Rogue waves, rational solitons and wave turbulence theory. Phys. Lett. A **375**, 3149 (2011)
174. Dudley, J.M., Genty, G., Coen, S.: Supercontinuum generation in photonic crystal fiber. Rev. Mod. Phys. **78**, 1135 (2006)
175. Korhonen, M., Friberg, A.T., Turunen, J., Genty, G.: Elementary field representation of supercontinuum. J. Opt. Soc. Am. B **30**, 21–26 (2013)
176. Mussot, A., Beaugeois, M., Bouazaoui, M., Sylvestre, T.: Tailoring cw supercontinuum generation in microstructured fibers with two-zero dispersion wavelengths. Opt. Express **15**, 11553–11563 (2007)
177. Wadsworth, W., Joly, N., Knight, J., Birks, T., Biancalana, F., Russell, P.: Supercontinuum and four-wave mixing with q-switched pulses in endlessly single-mode photonic crystal fibres. Opt. Express **12**, 299–309 (2004)
178. Barviau, B., Kibler, B., Coen, S., Picozzi, A.: Towards a thermodynamic description of supercontinuum generation. Opt. Lett. **33**, 2833 (2008)
179. Kibler, B., Michel, C., Barviau, B., Millot, G., Picozzi, A.: Thermodynamic approach of supercontinuum generation. Opt. Fiber Technol. **18**, 257 (2012)
180. Landau, L., Lifchitz, E.: Statistical Physics, Part 1. Pergamon Press, New York (1980)
181. Michel, C., Garnier, J., Suret, P., Randoux, S., Picozzi, A.: Kinetic description of random optical waves and anomalous thermalization of a nearly integrable wave system. Lett. Math. Phys. **96**(1), 415–447 (2011)
182. Zakharov, V., Schulman, E.: Degenerative dispersion laws, motion invariants and kinetic equations. Physica **4D**, 192 (1980)
183. Zakharov, V., Schulman, E.: To the integrability of the system of two coupled nonlinear Schrödinger equations. Physica **4D**, 270 (1982)
184. Zakharov, V., Schulman, E.: On additional motion invariants of classical Hamiltonian wave systems. Physica **29D**, 283 (1988)
185. Balk, A., Ferapontov, E.: In: Zakharov, V. (ed.) Nonlinear Waves and Weak Turbulence. American Mathematical Society Translations. American Mathematical Society, Providence, RI (1998)
186. Onorato, M., Osborne, A., Serio, M., Cavaleri, L., Brandini, C., Stansberg, C.: Extreme waves, modulational instability and second order theory: wave flume experiments on irregular waves. European Journal of Mechanics-B/Fluids **25**(5), 586–601 (2006)
187. Akhmediev, N., Soto-Crespo, J., Ankiewicz, A.: Extreme waves that appear from nowhere: on the nature of rogue waves. Phys. Lett. A **373**(25), 2137–2145 (2009)
188. Janssen, P.A.E.M.: The Interaction of Ocean Waves and Wind. Cambridge University Press, Cambridge (2004)
189. Ankiewicz, A., Soto-Crespo, J., Akhmediev, N.: Rogue waves and rational solutions of the Hirota equation. Phys. Rev. E **81**(4), 046602 (2010)
190. Viotti, C., Dutykh, D., Dudley, J.M., Dias, F.: Emergence of coherent wave groups in deep-water random sea. Phys. Rev. E **87**, 063001 (2013)